Guided Wave Optics Laboratory

Report No. 60

Characterization of Optical Polymers for Multi-layered Electro-optic Devices

Lori Ellen Rohlev

October 1994

Department of Electrical and Computer Engineering

University of Colorado at Boulder

Boulder, Colorado

Report No. 60

Characterization of Optical Polymers for Multi-layered Electro-optic Devices

Lori Ellen Rohlev

October 1994

Guided Wave Optics Laboratory
Department of Electrical and Computer Engineering
University of Colorado at Boulder
Boulder, Colorado 80309-0425

This work was supported by the Army Research Office under Grant #DAAL-03-92-G-0289 and by the Office of Naval Research under Grant #DOD-ONRN00014-92-J-1190.

REPORT DOCUMENTATION PAGE

Form Approved
OMB No. 0704-0188

1a. REPORT SECURITY CLASSIFICATION: unclassified	1b. RESTRICTIVE MARKINGS: none
2a. SECURITY CLASSIFICATION AUTHORITY: DISCASS	3. DISTRIBUTION/AVAILABILITY OF REPORT: unrestricted
2b. DECLASSIFICATION/DOWNGRADING SCHEDULE: N/A	
4. PERFORMING ORGANIZATION REPORT NUMBER(S): ECE/GWOL/60	5. MONITORING ORGANIZATION REPORT NUMBER(S): DOD-ONRN00014-92-J-1190
6a. NAME OF PERFORMING ORGANIZATION: University of Colorado; 6b. OFFICE SYMBOL (If applicable):	7a. NAME OF MONITORING ORGANIZATION: Office of Naval Research, Attn: Dr. Arthur Jordan, Code 1114 SE
6c. ADDRESS (City, State, and ZIP Code): Electrical & Computer Engineering Dept., Boulder, CO 80309-0425	7b. ADDRESS (City, State, and ZIP Code): 800 N. Quincy Avenue, Arlington, VA 22217-5000
8a. NAME OF FUNDING/SPONSORING ORGANIZATION: Office of Naval Research; 8b. OFFICE SYMBOL (If applicable):	9. PROCUREMENT INSTRUMENT IDENTIFICATION NUMBER
8c. ADDRESS (City, State, and ZIP Code): 800 N. Quincy Avenue, Arlington, VA 22217-5000	10. SOURCE OF FUNDING NUMBERS: PROGRAM ELEMENT NO. / PROJECT NO. / TASK NO. / WORK UNIT ACCESSION NO.

11. TITLE (Include Security Classification)

(u) Characterization of Optical Polymers for Multilayered Electrooptic Devices

12. PERSONAL AUTHOR(S): Lori Ellen Rohlev

13a. TYPE OF REPORT	13b. TIME COVERED	14. DATE OF REPORT (Year, Month, Day)	15. PAGE COUNT
technical (PhD thesis)	FROM _____ TO _____	October 1994	148

16. SUPPLEMENTARY NOTATION

17. COSATI CODES			18. SUBJECT TERMS (Continue on reverse if necessary and identify by block number)
FIELD	GROUP	SUB-GROUP	

19. ABSTRACT (Continue on reverse if necessary and identify by block number)

Nonlinear optical (NLO) polymers could potentially replace standard inorganic electrooptic materials, such as LiNbO3 and GaAs, in integrated optoelectronic devices and systems. The large electrooptic coefficients and the low dielectric constants of poled polymers make them ideal for high-speed electrooptic applications. Electrooptic devices can be easily fabricated by spin coating the polymer onto a substrate, forming optical channels by bleaching and making material electrooptic by poling the channels. This simple fabrication procedure makes polymers ideal for multilayered applications. As new materials are developed and used in new configurations and applications, they must be characterized for optimum device design and performance.

20. DISTRIBUTION/AVAILABILITY OF ABSTRACT: ☒ UNCLASSIFIED/UNLIMITED ☐ SAME AS RPT ☐ DTIC USERS	21. ABSTRACT SECURITY CLASSIFICATION: unclassified
22a. NAME OF RESPONSIBLE INDIVIDUAL: Alan R. Mickelson	22b. TELEPHONE (Include Area Code): 303/492-7539; 22c. OFFICE SYMBOL:

CHARACTERIZATION OF OPTICAL POLYMERS FOR MULTI-LAYERED ELECTRO-OPTIC DEVICES

by

LORI ELLEN ROHLEV

B.S., University of New Mexico, 1986

M.S., University of Southern California, 1989

A thesis submitted to the

Faculty of the Graduate School of the

University of Colorado in partial fulfillment

of the requirement for the degree of

Doctor of Philosophy

Department of Electrical Engineering

1994

This thesis for the Doctor of Philosophy degree by

Lori Ellen Rohlev

has been approved for the

Department of

Electrical and Computer Engineering

by

_____

Alan R. Mickelson

_____

Christian V. Radehaus

Date _____

Rohlev, Lori Ellen (Ph.D., Electrical Engineering)

Characterization of Optical Polymers for Multi-layered Electro-Optic Devices

Thesis directed by Alan R. Mickelson

Nonlinear optical (NLO) polymers could potentially replace standard inorganic electro-optic materials, such as $LiNbO_3$ and GaAs, in integrated optoelectronic devices and systems. The large electro-optic coefficients and the low dielectric constants of poled polymers, make them ideal for high speed electro-optic applications. Electro-optic devices can be easily fabricated by spin-coating the polymer onto a substrate, forming optical channels by bleaching and making the material electro-optic by poling the channels. This simple fabrication procedure makes polymers ideal for multi-layered applications. As new materials are developed and used in new configuration and applications, they must be characterized for optimum device design and performance.

Several new modeling tools and measurement techniques have been developed to aid in the characterization of NLO polymers as they are used in high speed electro-optic applications. A model was developed to determine the electric field distribution of a structure consisting of thick coplanar waveguide (CPW) electrodes buried beneath several anisotropic dielectric layers. This configuration can be used to model electro-optic devices made from bleached and poled polymers. The capacitance, impedance and effective dielectric constant of the multi-layered structure were determined from the electric field distribution for different electrode

dimensions and dielectric materials. A TRL calibration was performed on a CPW structure coated with a thin polymer layer. The resulting propagation constants were used to calculate the equivalent distributed circuit elements of the structure. The dielectric constant of the polymer layer was then extracted from the capacitance of the structure and found to have a flat frequency response over the frequency range of 0.5 GHz to 40 GHz. A fiber optic Mach-Zehnder interferometer, with electronic phase stabilization, was used to measure the electro-optic coefficient of a poled polymer waveguide. The measurement setup can be used to monitor the electro-optic coefficient during poling.

ACKNOWLEDGEMENTS

I would like to acknowledge Alan Mickelson and Christian Radehaus of the University of Colorado at Boulder for their technical guidance throughout the course of my work. I would also like to thank Marc Stiller of Roitech for his hints and suggestions on endface preparation with the wafer saw, Franz Jahoda for his technical support concerning the fiber Mach-Zehnder interferometer, Jack Griffith and Slav Rohlev of Hewlett Packard for their help in solving numerous fabrication problems, John Schlager of NIST for letting me use his fiber optic fusion splicer, Dylan Williams of NIST for his contributions to the dielectric measurements and the group at IBM Almaden Research Center, including Bill Fleming, John Thackara, Don Burland and Jerry Swalen, for the material that made this work possible and their technical support. I especially wish to thank my husband, Tony Rohlev, for doing everything in his power to make my research fun, exciting and successful. His influence, support and never-ending optimism are greatly appreciated. Thanks, also to my parents, Dave and Mary Carole Primas, and my in-laws, Slav and Natasha Rohlev, for their support and encouragement in every aspect.

CONTENTS

CHAPTER

TABLES

FIGURES

FIGURE

Chapter 1

INTRODUCTION

1.1 Statement of Purpose

The aim of this dissertation is to describe a theoretical model and several experimental techniques that have been developed for the purpose of characterizing nonlinear poled polymers as they are used in high speed electro-optic applications. The approach of the work described in this dissertation was to characterize these nonlinear optical (NLO) polymers, not as bulk materials, but as thin film materials, as they are used in actual device configurations. Although the techniques developed in this work are general, they have been tested on multi-layered device configurations incorporating coplanar waveguide (CPW) electrodes and single mode optical waveguides. The CPW electrodes are used for both modulating and poling and the optical waveguides are formed by UV bleaching.

The information gained from the characterization of optical polymers can be used by chemists in the search for polymeric materials that are optimized for passive optical waveguides and electro-optic devices. Materials which have high electro-optic coefficients, high glass transition temperatures and are thermally stable are being investigated. Results from the material characterization, including dielectric and electro-optic properties, can also be helpful to device designers in determining the

optimum device performance. By relating the material and fabrication parameters to the device performance, a CAD tool can be developed to aid in the design of these devices [1]. The desired electrical properties include low loss electrodes, high speed modulation and optimum electric field distribution for poling and switching. The desired optical properties include low loss channels and single mode operation at the desired operating wavelength. By characterizing the electrical and optical properties of a polymeric structure, electro-optic devices with low switching voltages, that are capable of high speed modulation and are fiber compatible can be realized.

1.2 Motivation and Applications

As the semiconductor industry moves towards higher chip packing densities, higher speed operation and increased complexity, the packaging of semiconductor chips becomes crucial to the future of the industry. A multi-chip package must provide the interconnections, powering, cooling and protection of many semiconductor chips without sacrificing performance [2]. A multi-chip module (MCM) is a structure used to interconnect and power multiple bare chips through several layers of metallization separated by interlayer dielectrics [3], [4]. Polymers are often used as the interlayer dielectric or insulating materials because they can be processed into thin films and have been optimized for use in multi-layer applications [5].

One way to meet the demands of multi-chip packaging is to extend the role of the interlayer polymers from insulating materials, to materials used for optical signal

distribution. The polymers used in packaging have been well characterized in terms of their electrical, chemical, thermal and mechanical properties. Polymers, having the same basic properties as those used for packaging, can also be used for optical chip-to-chip interconnects if low loss optical channels can be formed in them [6], [7]. Passive integrated optical waveguides are ideal for such applications because they can transmit high bandwidth signals, which are immune to EMI and RFI and can be closely spaced with minimal optical coupling.

As previously mentioned, polymers that were once used only as insulating layers, have been modified to be used for passive optical waveguides. In recent years, these polymers have again been modified to make them electro-optic. Polymers with large electro-optic coefficients have already been developed and have the potential of becoming an important material in the optoelectronics industry [8], [9]. Electro-optic devices fabricated in polymers can be incorporated with other optical and electronic components [10]. Components including lasers, electro-optic modulators, integrated optical waveguides and detectors are needed for such applications as optical control of phased-array radar [11], [12], [13], optical storage and optical computing [14], [15]. Polymers can be used in optical MCMs for discrete integrated electro-optic devices, optical vias and passive optical waveguides for chip-to-chip interconnects or signal routing in computer back planes as shown in Figure 1-1.

Whereas the material properties of inorganic crystals are fixed, the properties of the polymers can be chemically optimized for applications requiring materials with low optical loss and large electro-optic coefficients [16], [17], [18], [19]. The electro-

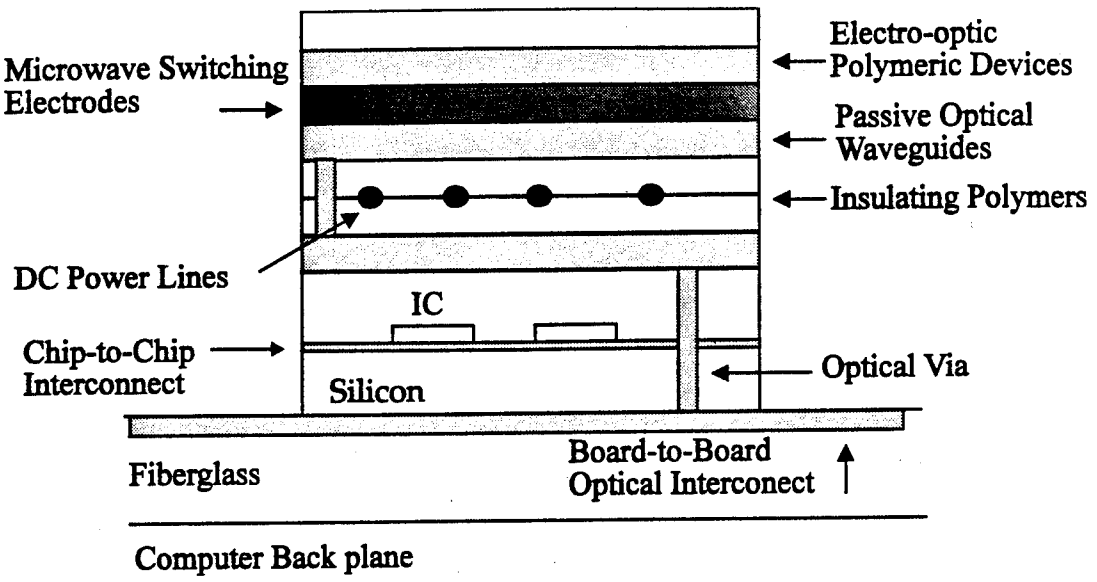

Figure 1-1 Potential uses of polymers in optical MCMs.

optic mechanism in NLO polymers does not limit the speed of a polymeric device because the mechanism is related to the displacement of electrons, resulting in subpicosecond response times. The speed of the device, built with traveling wave electrodes, is limited by the difference in microwave index ($\sqrt{\varepsilon}$) and the optical index of refraction (n). The small dielectric constant of polymers results in high speed operation and lower capacitive losses. Table 1-1 compares some of the properties of $LiNbO_3$ and a NLO polymer.

NLO polymers offer many advantages over inorganic crystals for electro-optic applications, due to the flexibility in the material parameters and the fabrication techniques. Electro-optic modulators built from poled polymers are very attractive because the devices can be fabricated using standard semiconductor processing techniques into multi-layer devices [20]. The processing steps are all done at low-

Table 1-1 Comparison of the properties of $LiNbO_3$ and NLO polymers when used in electro-optic applications.

	Lithium Niobate	NLO Polymers
Possibility of Multi-layers	NO	YES
Dielectric constant	$\varepsilon_x = 43$, $\varepsilon_y = 28$	$\varepsilon = 3.5$
Optical Index	$n_o = 2.2$	$n_o = 1.67$
Space-Bandwidth Product	5 GHz-cm	100 GHz-cm
Electro-optic coefficient	$r_{33} = 31$ pm / V	$r_{33} = 10$-50 pm / V
Loss	0.1 dB/cm @ 1.3 μm	0.2-0.5 dB/cm @ 1.3 μm
Fabrication of waveguides	Ti:indiffusion or Proton exchange	Spin on substrate Bleach channels

temperatures and the spun-on layers are compatible with a wide range of materials [21]. The device performance can be optimized by varying the fabrication parameters. High speed electro-optic devices have been designed and tested with many different materials, electrode configurations and fabrication techniques [22], [23], [24], [25]. Because this is a new field, the materials and fabrications techniques have not been standardized. Not only are NLO polymers being considered as replacements for standard inorganic crystals, but their flexibility leads to novel applications such as flat panel displays [26], optical sources or detectors, grating couplers [27] and optical amplifiers [28].

Some of the properties of poled polymers that must be investigated as new materials and configurations are developed include the optical index of refraction, the dielectric constant, the dielectric loss and the electro-optic coefficient [29]. Most techniques either characterize the bulk material or use indirect measurement techniques. For example, the dielectric constant is usually measured at discrete

frequencies using resonant techniques. The electro-optic coefficient is often measured by looking at second harmonic signals, rather than directly at the electro-optic effect. Measurement techniques that characterize polymer waveguides as they will be used in high speed electro-optic applications will help advance the field of NLO polymers and the novel applications that result.

1.3 Outline of Dissertation

Chapter 2 begins with a general description of the electro-optic effect in NLO materials followed by a description of the origin and behavior of the electro-optic effect as it applies to NLO polymers. The material properties of polymers used for VLSI interconnects are compared to the desired material properties of polymers used for electro-optic applications. As mentioned earlier, one of the biggest advantages of using polymers for electro-optic applications is that devices can be easily fabricated in multiple thin film layers using standard clean room equipment. The device configuration used for the work described in this thesis is presented along with the fabrication steps involved. The final section describes some of the design considerations for high speed electro-optic devices.

A model was developed to determine the electric field distribution of a multi-layered dielectric structure with CPW electrodes and is described in Chapter 3. The structure used in the model consists of five anisotropic dielectric layers and thick metal electrodes, simulating a polymeric device with several dielectric layers and poled optical waveguides. Results from this model have been used to compute the

effect of the dielectric layers and metal thickness on the capacitance, impedance and effective dielectric constant of the structure.

Chapter 4 presents a technique that was developed to determine the dielectric constant of a thin film material. The technique is based on determining the propagation constants of CPW structures with and without a top dielectric layer. This technique was applied to the measurement of several different polymers over the frequency range of 0.5 GHz to 40 GHz. Results from the model developed in Chapter 3 are used to extract the dielectric constant from the change in capacitance of the structure.

In Chapter 5, a measurement technique for determining the electro-optic coefficient of a poled optical channel is described. The technique consists of placing a poled polymer waveguide one arm of a fiber optic Mach-Zehnder interferometer. A feedback stabilization circuit is used eliminate slow phase drifts between the two arms. The intensity fringes due to modulation of the waveguide can then be used to determine the electro-optic coefficient of the poled polymer. The setup for this measurement can be used to monitor the electro-optic coefficient while the sample is being poled.

Chapter 6 will summarize the contributions that this work has made towards the field of NLO polymers in electro-optic applications. Possible extensions and future directions to this work will also be discussed.

Chapter 2

THEORY OF POLYMERIC ELECTRO-OPTIC DEVICES

2.1 Introduction

Electro-optic devices are fabricated from a wide variety of materials including both inorganic crystals and organic polymers. The basic operation of the electro-optic device is the same, regardless of the material. There are two ways in which light propagating through an electro-optic material can be altered by the applied electric field. In one case, the input polarization state is altered by the applied field. In the other case, the phase of the input light, polarized along one of the birefringent axes, will be altered by the electric field across the device. Electro-optic devices fabricated from organic polymers look very promising for high speed switches due to the potentially high nonlinear coefficients, low dielectric constants and the ease of fabrication of both single and multi-layer devices. Organic nonlinear materials are ideal for high speed electro-optic devices because the mechanism for modulation is electronic. Because the electronic resonances are well into the optical, the speed of the device is not limited by the electronic mechanisms. In addition, the low dielectric constant of organic materials allows the velocities of the light and the modulation signal to be closely matched, permitting high speed modulation.

The electro-optic effect can be used in many different optical applications,

using either bulk modulators or integrated optical modulators. When using bulk modulators, light is usually coupled into and out of the device using free space optics. By integrating the optical waveguides directly in the electro-optic material, light can be coupled into the device from an optical fiber, resulting in a lower insertion loss. Because the length of an integrated electro-optic device can be made shorter than a bulk modulator, the switching voltages will be smaller. Integrated optical components can also be extended to multiple layers when using planar circuit technology.

This chapter will begin with a brief description of the electro-optic effect in nonlinear materials and the theory of operation of two basic electro-optic devices, the directional coupler and the Mach-Zehnder interferometer. The electro-optic effect as it relates to the molecular optical nonlinearity of the polymeric materials will then be presented. Although most of the material properties that are required for interlevel dielectrics used in VLSI interconnects are identical to the desired material properties for electro-optic polymers, the polymers used in electro-optic applications must also meet certain other requirements, as will be described. Several of the measurement techniques that are currently being used to characterize the optical properties of these materials, including the index of refraction and optical loss of the polymers, will be presented. Because one of the key advantages of using NLO polymers is the ease of fabrication, a brief description of the device configuration and the fabrication steps used in this work will be presented. Some of the information specific to the materials used for this research will be presented in Appendix A. The final section will present

some of the tradeoffs and considerations used to design high speed electro-optic that are compatible with single mode optical fibers from NLO polymers.

2.2 The Electro-Optic Effect In Nonlinear Optical Materials

For a nonlinear optical material, the induced polarization density in the presence of an electric field is given by,

$$\begin{aligned} P_I(\omega) = P_I^o + & \\ & \chi_{IJ}^{(1)}(-\omega;\omega_1)E_J(\omega_1) + \\ & \chi_{IJK}^{(2)}(-\omega;\omega_1,\omega_2)E_J(\omega_1)E_K(\omega_2) + \\ & \chi_{IJKL}^{(3)}(-\omega;\omega_1,\omega_2,\omega_3)E_J(\omega_1)E_K(\omega_2)E_L(\omega_3) + \cdots \quad , \end{aligned} \tag{2-1}$$

where the linear and nonlinear susceptibility tensors are given by the χ's, E_I is the applied electric field and P_I^o represents the permanent polarization density. A summation over the indices is assumed, where I, J, and K correspond to x, y, and z in the macroscopic reference frame. In order for the even-order terms ($\chi^{(2)}$, $\chi^{(4)}$, etc.) not to vanish, the material must be noncentrosymmetric, or not possess an inversion center. The dominant nonlinear term is usually the $\chi^{(2)}$ term and is responsible for such effects as frequency doubling $\chi^{(2)}(-2\omega;\omega,\omega)$ and the Pockels effect $\chi^{(2)}(-\omega;\omega,0)$ [30], [31].

The Pockels effect is also referred to as the electro-optic effect and is the mechanism used in electro-optic devices. The polarization density due to the electro-optic effect is given by,

$$P_I^{(2)}(\omega) = 2\chi_{IJK}^{(2)}(-\omega;\omega,0)E_J(\omega)E_K(0). \tag{2-2}$$

The factor of 2 is present because optical detectors cannot distinguish between

modulation sidebands including both sum and difference frequencies.

The index of refraction ellipsoid is used to describe the polarization of light and the index of refraction seen by the various polarizations of light propagating in an anisotropic material. The index ellipsoid is given by,

$$\frac{x^2}{n_x^2}+\frac{y^2}{n_y^2}+\frac{z^2}{n_z^2}=1 \ , \tag{2-3}$$

where x, y and z are the principal axes and n_x, n_y and n_z are the indices of refraction along the principal axes [32]. If an electric field is applied across the material, the index ellipsoid is altered and the resulting index change is given by,

$$\Delta\left|\frac{1}{n^2}\right|_I = \sum_{K=1}^{3} r_{IK}E_K \ \text{ or } \ (\Delta n)_I = -\frac{n_I^3}{2}\sum_{K=1}^{3} r_{IK}E_K \ , \tag{2-4}$$

where I=1..6, and K =1 corresponds to the x-direction, K=2 corresponds to the y-direction and K=3 corresponds to the z-direction. The index of refraction in this equation is either the ordinary index, n_o, or the extraordinary index, n_e, depending on the orientation of the light. The electro-optic tensor (r_{IK}) is a 6 X 3 matrix [33].

Equation (2-4), describing the index ellipsoid of an electro-optic field with an applied electric field, can also be written as,

$$\left(\frac{1}{n_x^2}+r_{1K}E_K\right)x^2+\left(\frac{1}{n_y^2}+r_{2K}E_K\right)y^2+\left(\frac{1}{n_z^2}+r_{3K}E_K\right)z^2+ \\ 2yzr_{4K}E_K+2xzr_{5K}E_K+2xyr_{6K}E_K=1 \ . \tag{2-5}$$

In Equation (2-5), E_K is the applied electric field, where K corresponds to the direction of the electric field as defined earlier. If the field contains more than one component, a summation over K is assumed. The general result of applying an electric field across an electro-optic material is to change the magnitude of the

refractive index along the principal axes and rotate the principal axes. The electro-optic tensor is usually quite sparse, so that the index ellipsoid resulting from a general electric field is straight-forward to calculate.

The second order susceptibility is related to the electro-optic coefficient by,

$$\chi_{IK}^{(2)} = -\frac{n_I^4 r_{IK}}{2}. \tag{2-6}$$

The index change resulting from an applied electric field is related to the second order susceptibility by,

$$\Delta n_I = \left(\frac{\chi_{IJK}^{(2)}}{n_I}\right) E_K. \tag{2-7}$$

An electro-optic material can either be characterized in terms of χ or r.

The electro-optic modulation resulting from using an electric field to change the index ellipsoid can be categorized into two main types [34]. The first type uses the relative change in index between the slow and fast indices of refraction to alter the polarization of the incoming light. The phase retardation resulting over the length of the material (L) for light traveling in the z-direction (having x and y components) is given by,

$$\Gamma = \frac{2\pi}{\lambda}\left(n'_y - n'_x\right)L \cong \frac{2\pi}{\lambda}\left[\frac{n_y r_{2K} E_K}{2} - \frac{n_x r_{1K} E_K}{2}\right] . \tag{2-8}$$

By placing the electro-optic device between crossed polarizers, the intensity of the incoming light can be modulated by a modulation voltage $[V_m \sin(\omega_m t)]$ resulting in,

$$\frac{I_{out}}{I_{in}} \cong \frac{1}{2}\left[1 + \Gamma \sin(\omega_m t)\right] , \tag{2-9}$$

where Γ is the total retardation. By requiring Γ to be much less than 1, the intensity variation will replicate the modulating voltage and not be distorted by higher order harmonics.

The second type of modulation changes the optical index of the material and results in a change in the output phase of the optical signal proportional to the applied electric field. If the incident beam is polarized parallel to one of the axes, the resulting phase change along that axis is,

$$\Delta\phi = \frac{2\pi}{\lambda}\Delta n \cdot L = \frac{2\pi}{\lambda}\frac{n^3 rE}{2}\cdot L \quad . \tag{2-10}$$

If the optical field of the incident beam is given by $E_{in} = E_o\cos(\omega_o t)$, and the electric modulation field is given by $E_m\sin(\omega_m t)$, then the output optical field is given by,

$$E_{out} = E_o\cos\left(\omega_o t + \Delta\phi(t)\right) = E_{ol}\cos\left(\omega_o t + \frac{2\pi}{\lambda}\cdot\frac{n^3 rE_m}{2}\cdot L\cdot\sin(\omega_m t)\right) \quad . \tag{2-11}$$

The phase modulation index (m) is then given by,

$$m = \frac{2\pi}{\lambda}\cdot\frac{n^3 rE_m}{2}\cdot L. \tag{2-12}$$

The phase modulation can then be used to create intensity modulation by placing the phase modulator in one arm of a Mach-Zehnder interferometer.

As mentioned earlier, integrated electro-optic devices are advantageous because they have low loss, low switching voltages and are compatible with single mode optical fibers. The first step in building an integrated electro-optic device is to form single mode optical waveguides. By making the optical channels single mode, the integrated channels can be easily coupled to single mode fibers with minimal

coupling loss. Optical modulation or switching is also much easier with a single mode rather than multi-modes. Depending on whether the waveguides are made in inorganic crystals or organic polymers, different techniques are used to form the optical waveguides. The technique used to form the optical guide defines a unique index distribution for optical guiding. The specific index distribution can contribute to the optical loss of the waveguide. The loss is generally due either to scattering in the guide or absorption in the material [35]. The index distribution and physical roughness of the side-wall of a channel depends on the technique used to fabricate the waveguides. Because the mode of the optical fiber cannot be identical to the mode of the optical waveguide, there is also a loss associated with coupling fibers to optical waveguides. Electro-optic devices require the optical channels to be routed within the devices using bends in the waveguides. The three types of channels that are used in electro-optic devices are straight channels, S-bends, and y-junctions [36]. The bends must be optimized so that the light remains coupled in the waveguide and does not radiate out at the bends [37]. This requires determining the minimum radius of curvature for the bend and the lateral offset between the input and output waveguides for a minimum optical loss at the bend. The typical radius of curvatures are greater than 2 mm.

Once single mode waveguides with low loss in straight channels, bends and y-junctions can be formed in the material, integrated electro-optic devices can be fabricated. The two basic building blocks of electro-optic switches and modulators are the directional coupler [38], [39], [40], and the Mach-Zehnder interferometer. In

the directional coupler, shown in Figure 2-1, the electric field changes the relative phase constants of the symmetric and anti-symmetric modes over the coupling region. The coupling region is the region where the two waveguides are brought close together so that the light can couple from one channel to the other. The waveguides are usually separated by the width of the channels. Coupling lengths vary from 100's of μm to 1 cm , depending on the index change. By varying the voltage on the electrodes, the intensity of the light is switched between the two output arms.

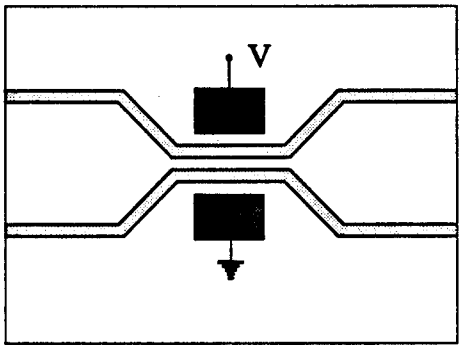

Figure 2-1 An integrated directional coupler designed from S-bends and lumped electrodes.

In the Mach-Zehnder interferometers shown in Figure 2-2, the electric field changes the relative phase delay between the two arms of the structure, so that when they are recombined, the output intensity at each output is modulated. The Mach-Zehnder interferometer can either be fabricated from two directional couplers or from two y-junctions.

Along with designing devices that are fiber compatible and have low loss, the devices should have low insertion loss and a high extinction ratios. As will be described later this thesis, the electrode configuration is crucial in the design of high

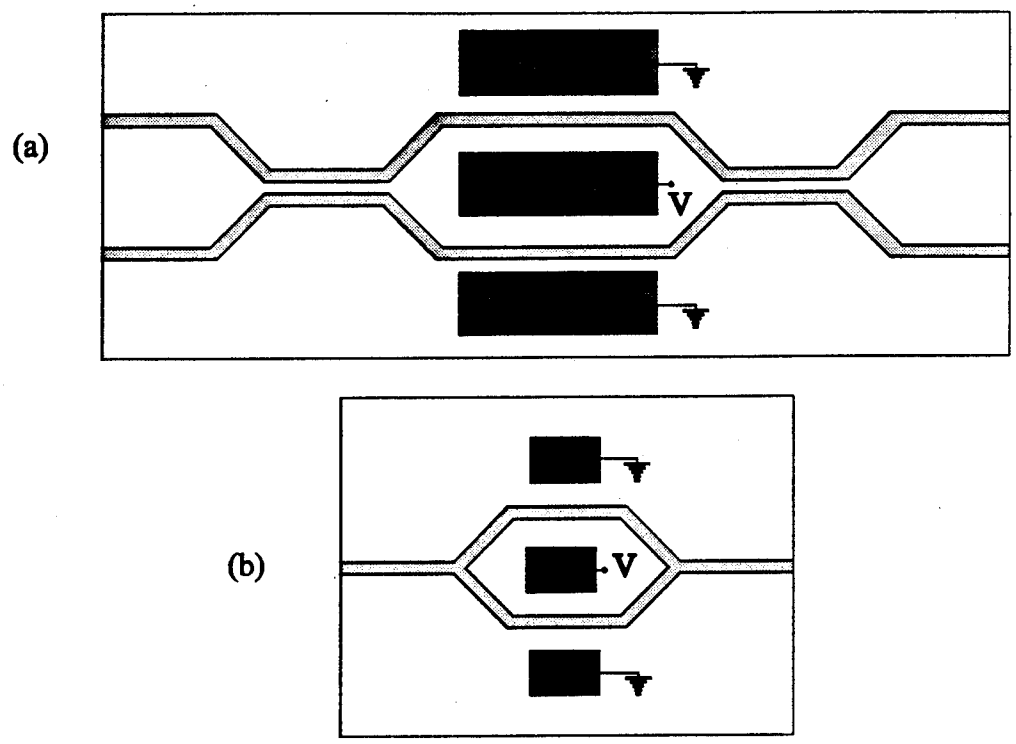

Figure 2-2 An integrated Mach Zehnder interferometer with bulk electrodes (a) fabricated from two optical couplers and (b) fabricated from two y-junctions.

speed devices with low switching voltages and large overlap between the optical and electrical signals. An additional design goal is to make the device as insensitive to temperature and wavelength variations as possible.

2.3 Polymer Materials For Electro-Optic Devices

This section will describe the contribution of molecular polarizability to the bulk nonlinearity of a polymeric material. The electro-optic polymers consist of a polymer host material containing nonlinear optical molecules or dye molecules. The three types of polymeric materials are guest host, side-chain and crosslinked. In guest

host systems, the dye molecules are suspended in the polymer, but are not covalently attached. In side-chain systems the dye molecules are covalently attached to the polymer backbone at one end of the dye molecule. In cross-linked systems, the dye molecules are covalently attached to the polymers at both ends of the dye molecule. In all cases, the material is noncentrosymmetric.

Analogous to the case of the bulk material, the total dipole moment of an individual dye molecule is given by,

$$\begin{aligned} p_i(\omega) = p_i^{\circ} + & \\ & \alpha_{ij}(-\omega;\omega_1)E'_j(\omega_1) + \\ & \beta_{ijk}(-\omega;\omega_1,\omega_2)E'_j(\omega_1)E'_k(\omega_2) + \\ & \gamma_{ijkl}(-\omega;\omega_1,\omega_2,\omega_3)E'_j(\omega_1)E'_k(\omega_2)E'_l(\omega_3) + \cdots \quad , \end{aligned} \tag{2-13}$$

where α is the linear polarizability, β is the hyperpolarizability and γ is the second hyperpolarizability. The dye molecules are of the form of a donor(D)-acceptor(A) molecule (Figure 2-3). The dye molecule used in this work is DR1. These hyperpolarizable molecules are long molecules which have a strongly polarizable conjugated π-electron system. The resulting DπA molecules lead to large hyperpolarizabilities.

The bulk nonlinear susceptibility is related to the molecular polarizability by,

$$\chi^{(2)}_{IKJ}(-\omega;\omega_1,\omega_2) = Nf(\omega)f(\omega_1)f(\omega_2)\beta_{ijk}(-\omega;\omega_1,\omega_2)\left\langle O_{Ii}O_{Jj}O_{Kk}\right\rangle \quad , \tag{2-14}$$

where N is the number density of hyperpolarizable molecules, $f(\omega_i)$ are the local field correction factors, β is the molecular hyperpolarizibility and $\left\langle O_{Ii}O_{Jj}O_{Kk}\right\rangle$ is the polar order or orientational ensemble average. The polar order relates the alignment of the molecules to the bulk reference frame. For a large bulk nonlinear susceptibility, there

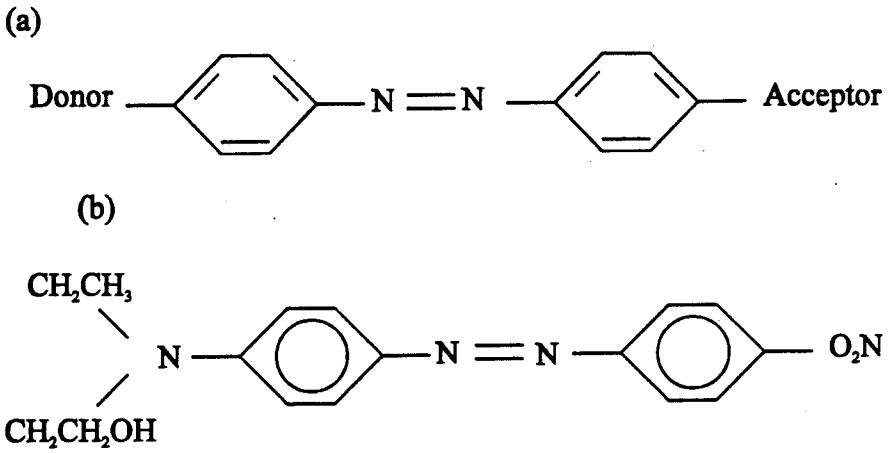

Figure 2-3 The basic configuration of a (a) a general π-conjugated azo-dye structure with a Donor, acceptor and π bridge, and (b) DR1 (used in this work).

must be a high concentration of dye molecules in the polymer. In guest host systems, the concentration is often limited because of solubility problems and precipitation of the dye molecules. Side-chain and cross-link systems can support higher concentrations. The local field factors are determined by the type of polymeric system. Larger molecular hyperpolarizibilities can be obtained for longer π-electron systems and different acceptor/donor groups. The only parameter that is readily available to the device designer is the polar order of the molecules. The polar order is obtained by poling the polymer. During poling, the temperature of the polymer is raised to a temperature near the glass transition temperature (T_g) of the polymer. The glass transition temperature is the temperature at which the chain molecules have enough energy to rotate about each other. Once the material has reached the glass transition temperature, a strong electric field (> 50 V/μm) is applied across the polymer. The material is kept in this state for 10 to 30 minutes and then it is cooled to room temperature with the poling field still applied. This "freezes" in the

alignment of the molecules. There are many methods to describe the polar order caused by poling, but the most common are to use the measures of,

$$\chi_{33}^{(2)} = NF\beta_{33}\left\langle \cos^3(\theta)\right\rangle \quad \text{and}$$
$$\chi_{13}^{(2)} = NF\beta_{13}\left\langle \frac{1}{2}\cos(\theta)\sin^2(\theta)\right\rangle \quad , \tag{2-15}$$

where $F = f(\omega)f(\omega_1)f(\omega_2)$ and θ is the angle between the permanent dipole moment and the electric poling field. Using Langevin functions to describe the polar order caused by poling results in[41],

$$\frac{\chi_{13}}{\chi_{33}} \approx \frac{1}{3}. \tag{2-16}$$

For poled polymers the poling field is always assumed to be along the z-direction, and is defined as the polar axis. The alignment of the molecules is along the polar axis, resulting in the electro-optic tensor,

$$\begin{bmatrix} 0 & 0 & r_{13} \\ 0 & 0 & r_{23} \\ 0 & 0 & r_{33} \\ 0 & r_{42} & 0 \\ r_{51} & 0 & 0 \\ 0 & 0 & 0 \end{bmatrix} . \tag{2-17}$$

By the symmetry of the material, $r_{13} = r_{23}$ and $r_{42} = r_{51}$. For a dispersionless material, $r_{13} = r_{23} = r_{42} = r_{51}$, due to Kleinman symmetry [42]. The electro-optic tensor becomes,

$$\begin{bmatrix} 0 & 0 & r_{13} \\ 0 & 0 & r_{13} \\ 0 & 0 & r_{33} \\ 0 & r_{13} & 0 \\ r_{13} & 0 & 0 \\ 0 & 0 & 0 \end{bmatrix} \tag{2-18}$$

The electro-optic coefficient r_{33} is the component parallel to the polar axis, and the r_{13} component is perpendicular to the polar axis. For an electric field applied along the z-direction (poling direction) the resulting index ellipsoid is,

$$\left(\frac{1}{n_x^2} + r_{13}E_z\right)x^2 + \left(\frac{1}{n_y^2} + r_{13}E_z\right)y^2 + \left(\frac{1}{n_z^2} + r_{33}E_z\right)z^2 + 2yzr_{13}E_z + 2xzr_{13}E_z = 1 \tag{2-19}$$

If the light propagating through this material is propagating in the x-direction, then the index of refraction change corresponds to r_{33} along the z-axis, and r_{13} along the y-axis,

$$n_z = n_e + \frac{n_e^3 r_{33} E_z}{2} \quad \text{and} \quad n_z = n_e + \frac{n_e^3 r_{33} E_z}{2} . \tag{2-20}$$

Because of the direct relationship between χ and r, r_{33} is also approximately 3 times greater than r_{13}. By using the same electrodes for poling as for modulation, the larger electro-optic coefficient contributes to the operation of the modulator or switch.

2.4 Properties of the Polymers

Polymers have had extensive use in the electronics industry, both as photolithographic materials and as interlevel dielectrics for VLSI. Because VLSI is a multi-layered technology, the requirements of the interlevel dielectrics are very

similar to those of the polymers for electro-optic applications. Some of the desired properties of interlevel dielectrics for VLSI are reproduced in the Table 2-1 [43].

Table 2-1 Properties of interlevel dielectrics for VLSI

1.	Low dielectric constant for frequencies up to ~20 MHz, in order to keep capacitance between metal lines low.
2.	High breakdown field strength (>5 MV/cm).
3.	Low leakage, even under electric fields close to the breakdown field strength. Bulk resistivity should exceed 10^{15} Ω-cm.
4.	Low surface conductance. Surface resistivity should be > 10^{15}.
5.	No moisture absorption or permeability to moisture should occur.
6.	The films should exhibit low stress, and the preferred stress is compressive (~$5x10^{8}$ dynes/cm^{2}), since dielectric films under tensile stress exhibit more of a tendency to crack.
7.	Good adhesion to aluminum, and of aluminum to the dielectric. (Good adhesion is also needed to the other conductors used in VLSI, such as doped polysilicon and silicides). In cases of poor adhesion (such as with gold or CVD W), a glue layer (such as Ti or Ti:W) may need to be applied between the conductor and the dielectric.
8.	Good adhesion to dielectric layers above or below. Such dielectric layers could be thermal oxides, doped-CVD oxides, nitrides, oxynitrides, polyimides, or spin-on glass.
9.	Stable up to temperatures of 500 °C.
10.	Easily etched (by wet or dry processing).
11.	Permeable to hydrogen. This is important for IC processing, in which an anneal in a hydrogen containing ambient must be used to reduce the concentration of interface states between Si and the gate oxides of MOS devices.
12.	No incorporated electrical charge or dipoles. Some polyimides in particular contain polar molecules that can orient themselves in an electric field and give rise to an electric field even when the externally applied field is removed.
13.	Contains no metallic impurities.
14.	Step coverage that does not produce reentrant angles.
15.	Good thickness uniformity across the wafer, and from wafer to wafer.
16.	In the case of doped oxides, good dopant uniformity across the wafer, and from wafer to wafer.
17.	Low defect density (pinholes and particles).
18.	Contains no residual constituents that outgas during later processing to the degree that they degrade the properties of the other layers of the interconnect system (e.g. outgassing from some polyimide films, SOG films or low-temperature TEOS films).

Most of the requirements listed in Table 2-1 are necessary because the structure is very small and compact, leading to very small line spacing, and because the structures are extended to multiple layers. One notable exception to the similarities is item #12 of Table 2-1. Dipoles are necessary in nonlinear optical polymers in order for the electro-optic properties of the poled polymer to exist. For optical applications, optical properties of the polymer, such as optical loss and optical index of refraction, are also important. For electro-optic devices, materials with large electro-optic coefficients and small dielectric constants are desired. The nonlinear materials must also be able to withstand electronics processing temperatures up to 500 °C and have a long lifetime. The lifetime of a guest host system (τ) is related to the glass transition temperature and the operating temperature (T) by the empirical relationship [41],

$$\log \tau \propto \frac{1}{T_g + 50 - T} \left(\frac{1}{K}\right) . \qquad (2\text{-}21)$$

By finding materials with higher glass transition temperatures, the lifetime of the polymers can be increased significantly. Materials with high glass transition temperatures are also desired because a high glass transition temperature generally corresponds to materials with low coefficients of thermal expansion, low moisture absorption and high chemical resistance. The optical loss, index of refraction, electro-optic coefficient and lifetimes of the polymeric materials are functions of the composition of the material and each new material must be characterized.

The polymer used in the work described in this thesis is a doped polymer system call PMMA/DR1 (Disperse Red 1 Poly - Methyl Methacrylate) supplied to the

University of Colorado by IBM Almaden Research center. Table 2-2 shows the information available about this polymer in the spec sheet supplied by IBM. The concentration of dye is given in mer% which is the percentage of monomer units that contain a chromophore. From Table 2-2, it can be seen that the dielectric constant of the material is only given at two discrete frequencies, that are well below the desired frequency of operation of an electro-optic device. The electro-optic coefficient is also listed, but not as a function of the poling configuration or poling parameters (poling voltage, time and temperature).

Table 2-2 Specification of the doped polymer system supplied by IBM Almaden Research Center

PMMA/DR1		
Optical index of refraction	n	1.560 +/- 0.002 @ 0.83 mm 1.547 +/- 0.002 @ 1.06 mm 1.545 +/- 0.002 @ 1.32 mm
Dielectric constant	ε	3.447 @ 100 Hz and 25 °C 3.153 @ 10 kHz and 25 °C
Electro-optic coefficient/poling field	r_{33}	0.050 $\frac{pm/V}{V/\mu m}$ @ 1.32 μm
Dye Content		10 mer %*
Glass transition temperature	T_g	131 °C

The goal of this work is to develop techniques that can be used to completely characterize the polymer materials as they would be used in high speed electro-optic applications. Therefore, the properties are determined for optical waveguides formed in thin films of the polymer, as opposed to properties of the bulk material and are characterized over the frequency range of operation (<40 GHz). The effect of the various fabrication steps on the properties is also of interest. As new materials are

being developed, standard techniques that can be used characterize them are necessary. The four main properties of the polymer that must be characterized in terms of the fabrication parameters and device configuration are:

1. Optical index of refraction of the material
2. Optical loss of a waveguide channel
3. Dielectric constant of the polymer at frequencies up to 40 GHz
4. Electro-optic coefficient of a poled polymer.

Once the material has been completely characterized, the device performance can be optimized by the device design, resulting in high speed electro-optic devices with low switching voltages that are fiber compatible.

The index of refraction of the thin film polymeric can be measured using a technique of prism coupling as shown in Figure 2-4.

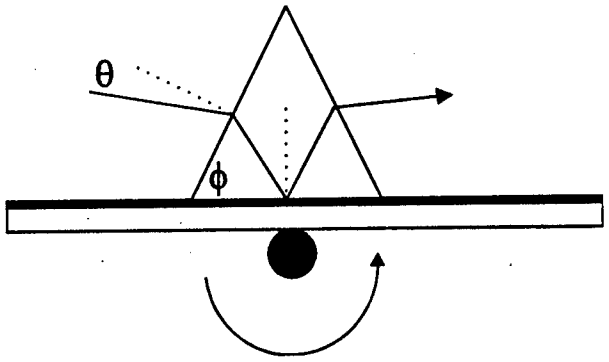

Figure 2-4 Prism coupling technique for determining the effective index of the film.

By rotating the sample, the light is coupled into the waveguide at different angles exciting the different modes supported by the waveguide. The effective index of the waveguide is related to the angle at which the mode is excited by,

$$n_{eff} = \frac{\beta}{k_o} = n_p \sin\left(\phi + \sin^{-1}\left(\frac{\sin(\theta)}{n_p}\right)\right) \qquad (2\text{-}22)$$

where ϕ is the prism corner angle, n_p is the prism index of refraction, θ is the input m-line coupling angle and $k_o = 2\pi/\lambda$. This technique is useful for determining the necessary fabrication parameters and waveguide geometry for single mode channels.

There are several techniques for determining the loss in an optical channel. In all cases, the light must be coupled into the waveguide, which is an additional source of loss. The light can be coupled in either by butt coupling a fiber up to the waveguide or by prism coupling light in the waveguide. The most direct way to measure the loss is to measure the optical power through a channel, and repeat the measurement as the channel is shortened (cutback). The light can also be coupled out of the waveguide using prisms at different distances along the length of the sample. The loss can also be determined by measuring the light scattered from the channel along the length of the device. In most measurement techniques, it is difficult to separate the coupling loss from the loss in the channel. This problem can be eliminated by using a mode matching technique [44], [45], shown in Figure 2-5. Light is coupled into the optical channel. A portion of the light at the output of the channel is then reflected back into the channel. This reflected light becomes the input light to the optical channel. It is perfectly matched to the mode of the waveguide because it was formed by the waveguide. The key to this technique is the ability to separate loss due to modal mismatch when coupling in the light from loss in the channel.

Chapter 4 will describe a measurement technique for determining the dielectric constant of a thin film of the polymer from 0.5 GHz to 40 GHz using coplanar waveguide TRL standards and results from Chapter 3. Chapter 5 will describe a

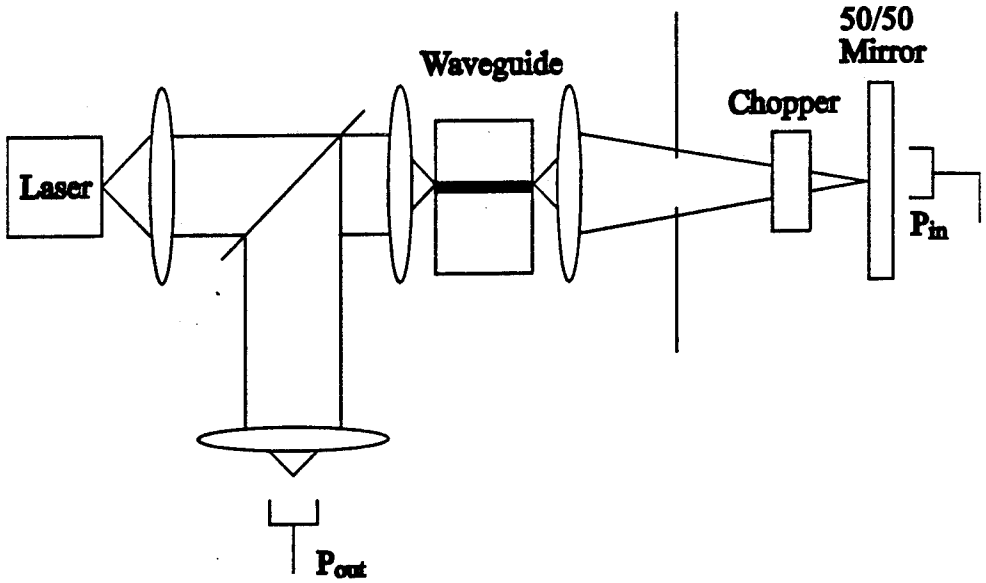

Figure 2-5 Measurement setup for determining the waveguide loss by mode-matched input coupling.

measurement technique for determining the electro-optic coefficient of a transversely poled channel under different poling conditions. This setup can be easily modified to include the microwave-optical frequency response of a poled sample.

2.5 Fabrication

The basic configuration of the polymeric structure used for the work described in this thesis is shown in Figure 2-6. A single polymeric device fabricated in this configuration consists of four layers on top of a rigid substrate: the coplanar waveguide electrodes, the bottom buffer layer, the NLO polymer layer and the top buffer layer. Optical channels are formed in the polymer layer by UV bleaching the areas outside the optical guides. The advantage of using this configuration to fabricate polymeric electro-optic devices is that each layer of the device is compatible

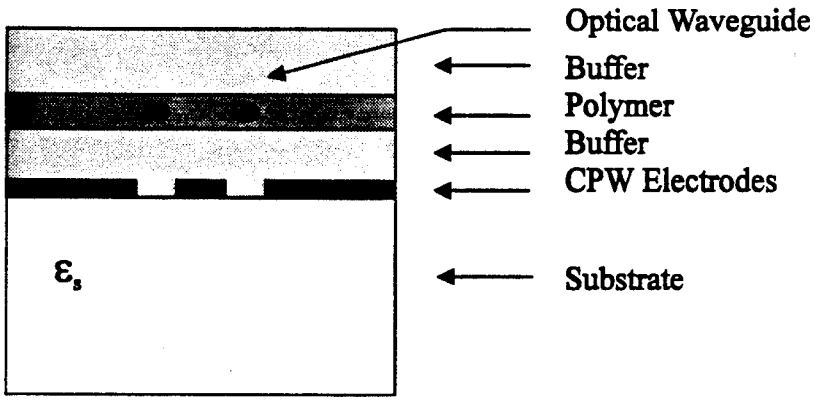

Figure 2-6 Multi-layered structure consisting of coplanar waveguide electrodes and UV bleached waveguides.

with planar processing technology. This allows the structure to be extended vertically to include multiple multi-layered devices. The device shown in Figure 2-6 is fabricated using a metal evaporation system, a spinner, a UV source, a wafer saw and an oven, all of which are found in a basic clean room. A brief description of the fabrication procedure used for this structure will be presented below, with most of the specific material details included in Appendix A.

The only requirements of the substrates used in this configuration is that they be non-conductive, so that the electrodes can be placed directly on the surface of the substrate, and that they be mechanically rigid enough to support the additional layers placed on top of the metal. For good adhesion between the substrate, metal, buffers and polymers, the expansion coefficient of the materials should be similar [46]. Fused quartz wafers (2" in diameter and 0.025" thick) were used as the substrate for the device described in this thesis. Some preliminary work was also done using ceramic wafers [47] and fiber glass substrates. Quartz is an appropriate substrate for

these devices because quartz is non-conductive, has a smooth surface, and is well characterized, mechanically, optically and electrically.

For high speed devices, the electrodes are designed to be traveling wave electrodes rather than bulk electrodes. The three basic types of traveling wave electrodes, coplanar waveguide (CPW), coplanar strip (CPS) and microstrip, are shown in Figure 2-7.

Although there has been a great deal of work done using microstrip electrodes for polymeric devices, coplanar strip and coplanar waveguide electrodes are preferred for multi-layered structures. The impedance of a microstrip electrode depends on the substrate thickness, substrate dielectric and width of the center conductor (S). For a given substrate, the width of the center conductor is determined by the desired electrode impedance.

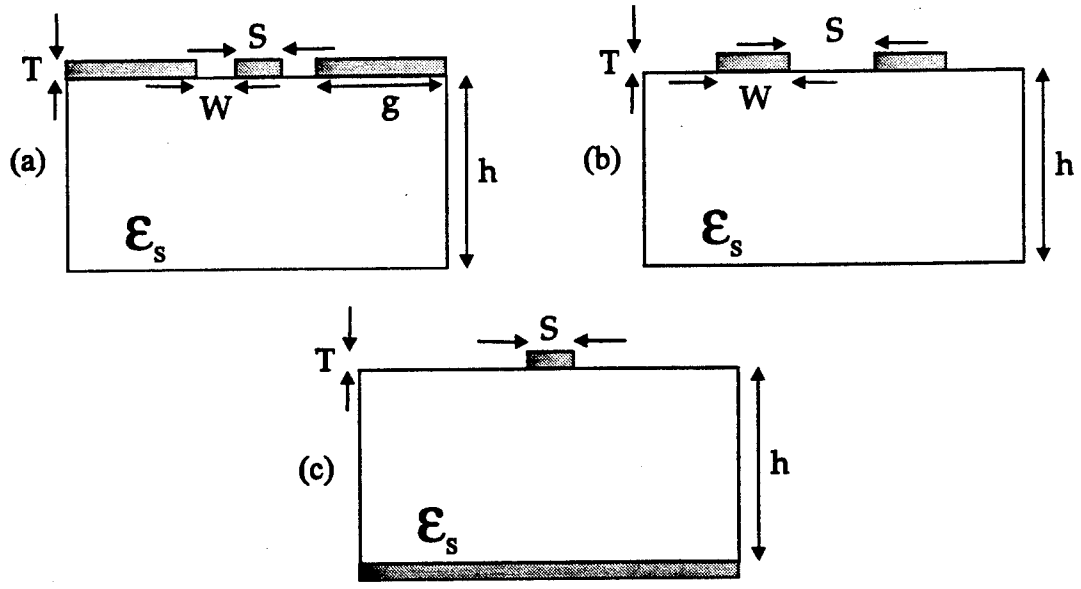

Figure 2-7 Traveling wave electrode configuration for (a.) coplanar waveguide (CPW) , (b.) coplanar strip (CPS) and (c.) microstrip.

For coplanar strip and coplanar waveguide electrodes, the structure can be designed to have the desired impedance by varying both the center conductor and gaps widths for a certain substrate dielectric. The impedance is only slightly influenced by the thickness of the layers. Coplanar electrodes can be stacked vertically without significantly altering the impedance of the electrodes at each layer, and the conductor widths and gaps can be optimized for the device performance without changing the impedance of the electrodes.

The metal electrodes are fabricated by evaporation, electro-plating or sputtering. The metal thickness is usually limited to thicknesses less than 0.5 μm by evaporation, but techniques such as electro-plating and sputtering can be used for thicker metal electrodes. For devices operating at frequencies in the GHz range, metal thicknesses of 2 to 3 μm are required. Standard photolithographic techniques are used to form the electrode structure. The procedure includes coating the metal with a positive photoresist, exposing the photoresist to a UV source with a dark field mask, developing the photoresist and then etching away the metal.

After the electrodes have been fabricated, a buffer layer is spun on top of the electrodes. The bottom buffer layer provides vertical optical guiding in the polymer and isolates the tails of the optical field from the electrodes. The buffer material must have a low solvent content in its final state, have low optical loss and have an index of refraction slightly lower than the polymer. The buffer can either be an undoped-polymer or an optical quality acrylate. The buffer used in these experiments is a UV cured acrylate supplied by IBM. The index of refraction of the buffer is 1.51 and

when spun at 3000 rpm for 30 seconds, provides a 5 μm thick layer. The buffer must be able to fill in the gaps of the metal electrodes and planarize the top surface. Measurements of a 5 μm buffer layer spun on top of aluminum electrodes 0.5 μm thick were made on a thickness monitor (Dektak) and indicate that the surface thickness varies less than 0.08 μm above gaps in the metal.

After the buffer has been thoroughly cured and the solvents removed, the polymer is spun on top of the buffer. A spin speed of 3000 rpm for 60 seconds results in a polymer thickness of 2.2 μm. The spin curve for the polymer used in this work is shown in the Appendix A. The thickness of the polymer is controllable to within 0.1 μm. The solvents must also be removed from polymer layer by baking.

The next step is to form optical channels in the polymer which provide horizontal guiding. The technique used for forming optical channels in this work is UV bleaching [48]. The polymer layer is masked off exposing the areas outside of the channels . The polymer is then exposed to a UV source (see Appendix A). This process is not thoroughly understood, but the result of bleaching is to lower index of refraction. This is an irreversible process. The index difference caused by bleaching can be well controlled by varying the UV exposure time. For the polymer used in this work, an index difference (n_{TE}) of 0.01 resulted from UV bleaching for 48 hours. Several factors can decrease the bleaching time, including the atmosphere surrounding the sample during bleaching and the temperature of the sample during bleaching. A shrinkage of approximately 5% has been observed for bleached polymers.

Two other techniques used for channel formation are laser ablation [49],[50] and reactive ion etching (RIE) [51] (see Appendix A). In both of these techniques, the material outside the channels is physically removed, leaving rib waveguides. The disadvantage of these techniques is that the surface is no longer planar and cannot be extended vertically without an additional planarization step.

After the optical channels have been formed, the top buffer layer is then spun on top of the polymer layer. The top buffer layer provides the vertical guiding of the optical mode. Although the electrodes are buried below two buffer layers and the polymer layer, the buffer must also have a high dielectric breakdown strength so that a large poling voltage can be applied across the electrodes without breaking down the material.

The next step is to prepare the endface of the sample so that light can be coupled into and out of the optical waveguide. The two techniques of laser ablation and RIE used to form optical channels can also be used to prepare the endface, but are not used in this work. Endfaces with a surface roughness of less than 0.1 μm have been achieved using a wafer saw (Figure 2-8). The sample is mounted to a cutting substrate using either tape or wax. By varying the forward cut speed, spindle speed and type of blade used, the surface quality can be optimized for a variety of materials and configurations (Appendix A).

The final step in fabricating an electro-optic device is to pole the material. As mentioned earlier, poling aligns the dye molecules in the polymer, causing the material to have an electro-optic coefficient related to the poling field strength and

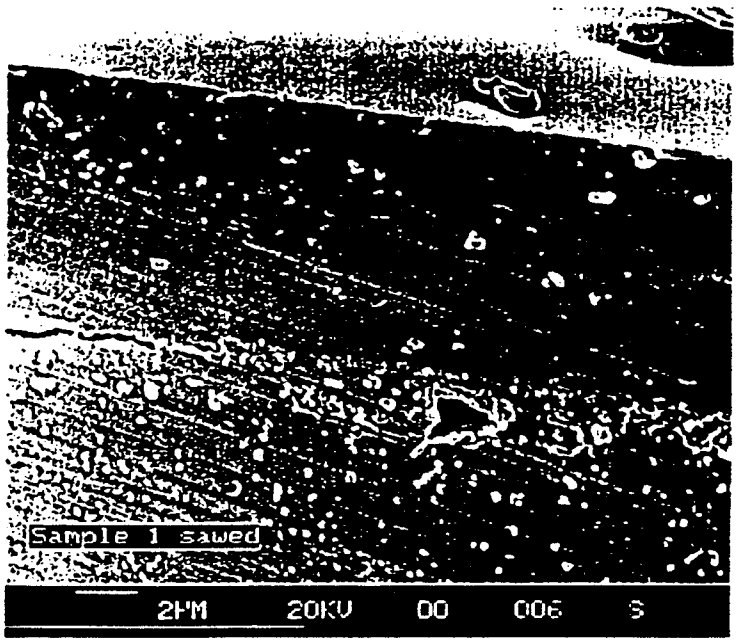

Figure 2-8 Endface of structure prepared by wafer saw.

device geometry. Chapter 5 will describe a technique developed to pole an optical waveguide and monitor the poling process as a function of the poling temperature, poling field strength and poling time.

2.6 Design Considerations

As was previously mentioned, in order to design a high speed device that is fabricated with NLO polymers, the index of refraction, the optical loss, the electro-optic coefficient and the dielectric constant of the material must be determined. Once the polymer and buffer materials are characterized, the actual device can be designed

and its performance optimized. The fabrication parameters of a device effect the optical performance, the electrical performance and the electro-optic performance of the device.

The optical performance of a device can be altered by varying the thicknesses of the buffer layers and polymer layer, the width of the bleached channel, the bleaching parameters (time, temperature, atmosphere, etc.) and length of the optical channel. The buffer layer should be thick enough so that the tails of the optical field don't interact with the metal, causing high optical loss. The required buffer thickness depends on the index difference between the polymer layer and the buffer layer. The thickness of the bottom buffer (t_{BB}) is determined by the allowable number of decay constants (N) of the optical field, the index of the guide and index difference between the polymer and buffer,

$$t_{BB} \propto \frac{\lambda N}{\pi\sqrt{2n\Delta n}} \quad . \tag{2-23}$$

If the allowable N is 3, the thickness of the buffer must be at least 3.6 μm for a waveguide formed in the polymer and buffer used in this work.

For a single mode channel waveguide to be fabricated in the polymer, the waveguide must be designed to be single mode for both the vertical and horizontal dimensions. The confinement in the vertical direction puts constraints on the thickness of the polymer for a given index difference between the unbleached polymer and the buffer at the operating wavelength. Similar requirements on the index difference between the unbleached polymer and the bleached polymer for a given waveguide width are also present for the horizontal confinement. The

conditions for vertical and horizontal confinement can be written independently as,

$$
\begin{aligned}
V &= \frac{\pi\ W}{\lambda}\sqrt{2n_p\Delta n_h} = \pi \\
\Delta n_h &= n_p(\text{unbleached}) - n_p(\text{bleached}) \\
V &= \frac{\pi\ D}{\lambda}\sqrt{2n_p\Delta n_v} = \pi \\
\Delta n_v &= n_p(\text{unbleached}) - n(\text{buffer})
\end{aligned}
\qquad (2\text{-}24)
$$

where W_o is the channel width and D is the thickness of the polymer layer. For an actual channel waveguide, the effective index method must be used to determine the mode parameters of the waveguide [52]. The effective index method was used to calculate the effective index of the structure shown in Figure 2-9, where t_{TB} and t_{BB} are the thickness of the top buffer and bottom buffer, respectively.

Using the effective indices of each region, a single mode channel requires the width (w_o) to be 4 μm for the given index profile. A step index distribution was assumed for this calculation. The actual index distribution is a function of the bleach time and polymer thickness. The bleaching is not uniform throughout the polymer, resulting in a smaller index change deeper into the polymer. A program developed at the Guided Wave Optics Laboratory, called Chan-Beta, can be used to calculate the optical field distribution for an arbitrary index profile.

The device must also be designed to be compatible with optical fibers. Because the geometries are so different for an optical fiber and a waveguide channel, the modes will be different and can result in large coupling losses if the match is not optimized. The different index profiles result in different numerical apertures which can also cause a coupling loss. The conditions for single mode confinement in an

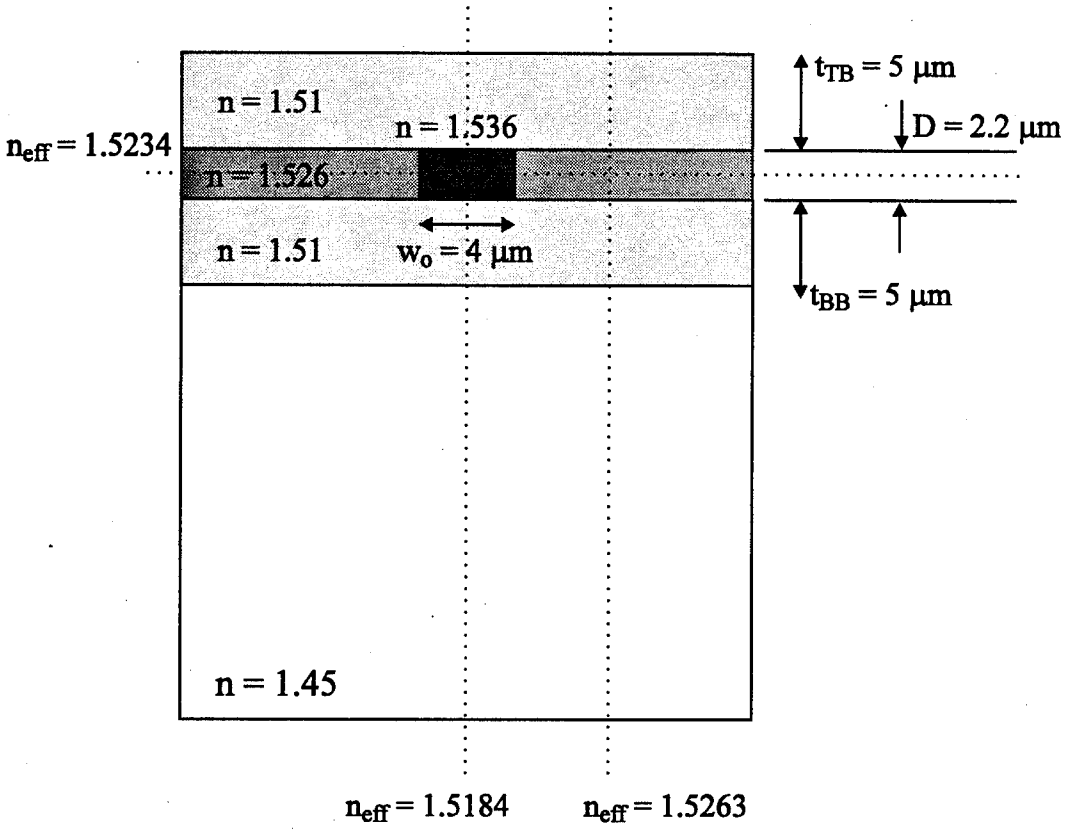

Figure 2-9 Structure used to calculate the effective index of the channel.

optical fiber (with core diameter of 2a) and a slab waveguide (of thickness D) and the corresponding numerical apertures are give in Table 2-3,

Table 2-3 Conditions for single mode waveguides in optical fibers and slab waveguides and corresponding numerical apertures.

Optical Fiber	Slab Waveguide
$v = \frac{2\pi a}{\lambda}\sqrt{2n_{core}\Delta n}$	$v = \frac{\pi D}{\lambda}\sqrt{2n_p\Delta n}$
$v = 2.14$ for single mode	$v = \pi$ for single mode
$NA_f = \sqrt{2n_{core}\Delta n} = 0.12$	$NA_p = \sqrt{2n_p\Delta n}$
for $\lambda = 1.3\mu m$, $2a = 7.5\mu m$	

Because of the fabrication flexibility of polymeric devices, the layer thicknesses and index differences can be varied. Figure 2-10 shows the required index difference for a given polymer index of refraction to match either the numerical apertures or the actual core diameters of a single mode fiber and a single mode slab waveguide.

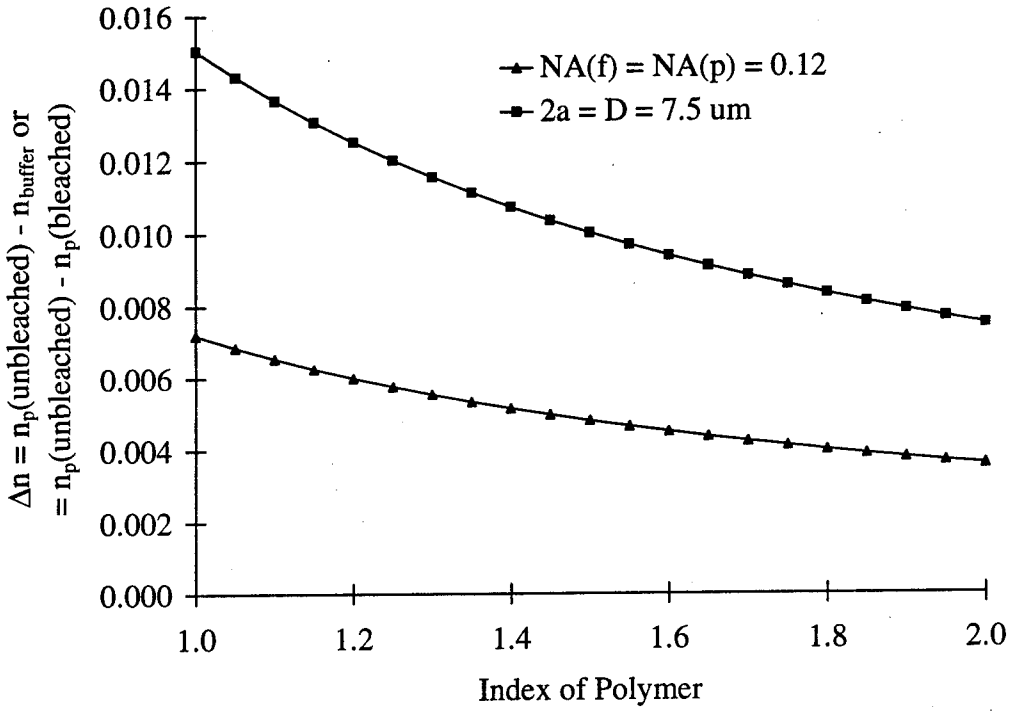

Figure 2-10 Index difference required to either match numerical apertures or the actual waveguide dimensions.

Both the difference in numerical apertures and core diameters lead to a coupling loss,

$$\text{LossDifference(dB)} = 20\log\left(\frac{2t}{2a}\right) + 20\log\left(\frac{NA_p}{NA_f}\right) . \qquad (2\text{-}25)$$

If the numerical aperture of the fiber is 0.12, the diameter of the fiber is 7.5 μm, and the index of the polymer is 1.5, the thickness of the polymer and the index difference can be varied to limit the coupling loss to 1 dB, where,

$$\Delta n = \frac{NA_f}{2n_p} 10^{\left[\frac{1-20\log\left(\frac{D}{2a}\right)}{20}\right]} \qquad (2\text{-}26)$$

and shown in Figure 2-11.

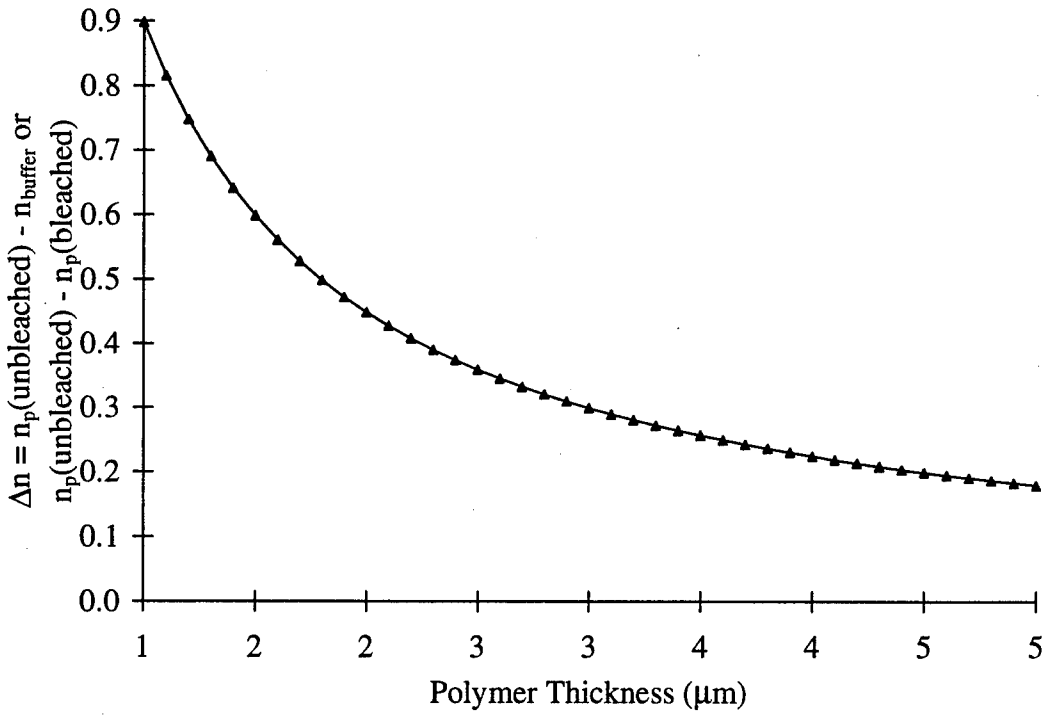

Figure 2-11 Index difference and polymer thickness required for a coupling loss of 1 dB.

The electrical performance of the device is a function of the dimensions of the waveguide (G, W, S, T), the length of the electrodes (L) and the dielectric materials that surround the electrodes. The field distribution impedance, capacitance, loss and effective dielectric constant can all be altered by varying any one of these parameters. Chapter 3 will show how these factors effect the device performance, especially the effect caused by thick electrodes and mutliple dielectric layers.

The nonlinearity of the material must be produced during the poling process. Since the electro-optic property is caused by the alignment of the molecules with the electric poling field, the distribution and magnitude of this electric field in the waveguide region is important. The dimensions of the waveguide determine the electric field distribution. There is a tradeoff between field strength in the waveguide region and the optical loss due to the thickness of the bottom buffer layer. A thinner buffer layer results in a large electric field for poling and switching, but a larger optical loss due to the tails of the optical fields being influenced by the electrodes.

The optimum location of the optical guides relative to the electrode center conductor and gaps, also results in a tradeoff between the orientation for maximum electro-optic effect (r_{33}) and the electric field distribution for poling and switching. If the optical guides are placed above the gaps in the metal electrodes, the width of the gap determines how quickly the strength of the field drops off in the vertical direction, but if the gaps are too wide the switching voltage will be too big. The overlap integral (Γ) and is a measure of the overlap of the optical field and the microwave field,

$$\Gamma = \left(\frac{W}{V}\right)\frac{\iint |E_o|^2 E_m dxdy}{\iint |E_o|^2 dxdy} \qquad (2\text{-}27)$$

and can be optimized in the device design.

Two of the main design criterion for these electro-optic devices, is that they have a low switching voltage and large bandwidths. The voltage-length product of an electro-optic device is given by,

$$V \cdot L = \frac{\lambda W}{n^3 r \Gamma} \quad . \tag{2-28}$$

From Equation (2-25), it is evident that the switching voltage for a given device length can be minimized by varying the geometry of the structure (W and Γ) or by using a material with a higher index of refraction or higher electro-optic coefficient. By minimizing the length, the optical loss in the waveguide can also be minimized. For lumped electrodes, the bandwidth length product is given by,

$$\Delta f \cdot L = \frac{1}{\pi RC} \quad . \tag{2-29}$$

The capacitance and bandwidth-length product for a coplanar waveguide coated with a thin dielectric layer is shown in Figure 2-12.

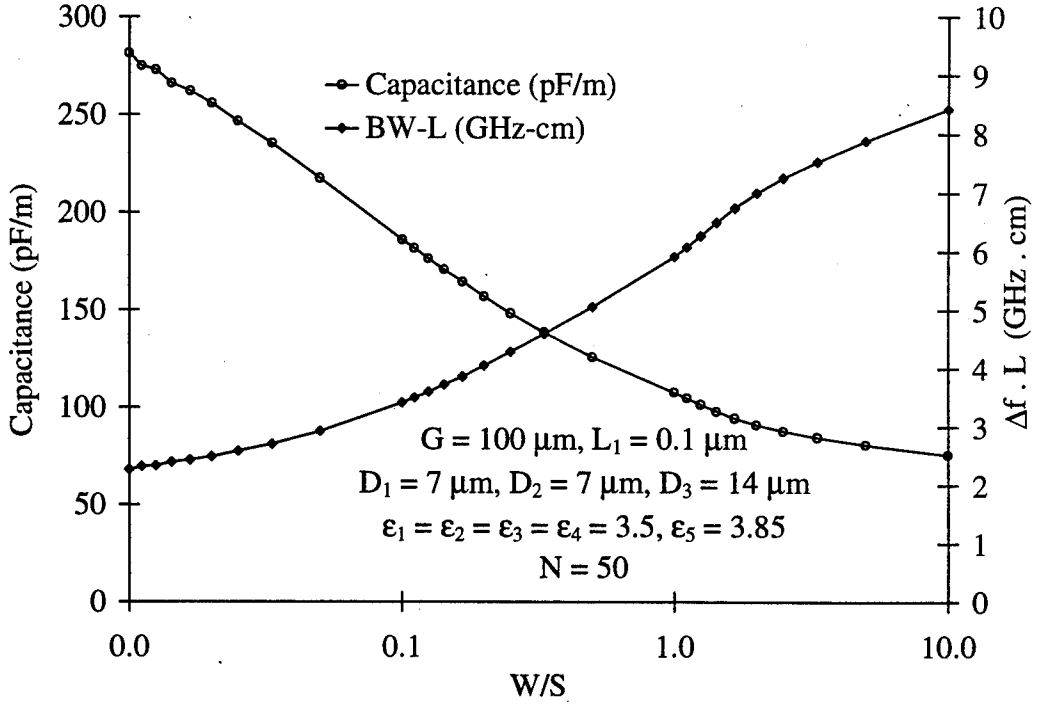

Figure 2-12 Capacitance and bandwidth-length product for a coplanar waveguide electrode on a quartz substrate.

By reducing the capacitance of the structure, the bandwidth of the device can be increased. For traveling wave electrodes, the bandwidth length product is given by,

$$\Delta f \cdot L = \frac{2c}{\pi} \frac{1}{\left(\sqrt{\varepsilon_{eff}} - n\right)} \tag{2-30}$$

The bandwidth is increased by matching the velocities of the electrical signal and the optical signal. For a polymer having a dielectric constant of 3.153 and an optical index of 1.545, the bandwidth length product is 82.8 GHz-cm. Because the effective index can be varied by altering the electrode geometry and the index of refraction can be varied by controlling the bleaching time, the bandwidth-length product can be optimized.

2.7 Conclusion

Nonlinear polymers are ideal materials for fabricating fiber compatible, high speed electro-optic switches. They have the potential of having very large electro-optic coefficients and are ideal for building multi-layered structures. Once the material has been completely characterized for the fabrication parameters and device geometry, the device performance can be optimized. Polymers offer the flexibility of building novel electro-optic devices. This same flexibility leads to many tradeoffs in the device design.

Chapter 3

MODELING MULTI-LAYERED STRUCTURES OF ORGANIC POLYMERS AND COPLANAR WAVEGUIDE ELECTRODES

3.1 Introduction

In the Chapter 2, the parameters that are available in the fabrication of electro-optic devices made from polymeric materials were presented. By determining the electric field distribution within the multi-layered structure, the electro-optic device performance can be optimized. Two important design considerations are the bandwidth of the device, which is related to the capacitance and effective dielectric constant of the structure, and the impedance of the electrodes, which should be matched to the source and load impedances. The capacitance and impedance of the structure, are functions of the device geometry and dielectric constants of the materials and can be determined from the quasi-static electric field distribution in the structure. In order to observe the loss and dispersion of the electrode structure, the finite conductivity of the metal and the dielectric loss must be included.

This chapter first describes the motivation behind developing a model to determine the electric field distribution for a structure of thick coplanar waveguide electrodes surrounded by multiple anisotropic dielectric materials. The next section describes the two different configurations that were considered and the algorithm that

was used to determine the electric field distribution. The effect of the thick metal electrodes and a dielectric layer above the electrodes on the capacitance, effective dielectric and impedance of the structure will then be presented. By computing the overlap integral, the best positioning of the optical guides relative to the electrode gaps can be determined. The final section will describe how the model can be extended to include conductor loss, dielectric loss and waveguide discontinuities.

3.2 Motivation

Electro-optic devices made from inorganic crystals as well as from organic polymers are multi-layered structures that depend on the overlap of the optical fields in the waveguide channel and the microwaves field generated by the electrodes. Extensive work has been done by previous students at the Guided Wave Optics Laboratory in determining the optical fields of integrated optical devices, specifically in optical waveguides formed by proton exchange and titanium indiffusion in $LiNbO_3$ and $LiTaO_3$ [53], [54]. Techniques have been developed to accurately predict the optical fields and propagation constants from the fabrication parameters. Similar work is being done on integrated optical devices made from organic polymers to predict the optical fields produced in an optical channel formed by bleaching. By tailoring the bleach time, anneal time, anneal temperature and poling conditions, optical channels with the desired optical index distribution and anisotropy can be fabricated.

The electrical fabrication parameters, such as metal thickness, dielectric

thickness, and electrode widths and gaps, will effected the electric field distribution generated by the electrodes. From the electric field distribution, the equivalent circuit parameters of the transmission line can be computed. The field distributions resulting from the optical and electrical modeling tools can be used together to form a CAD tool for electro-optic devices that can be used predict device performance from fabrication and design parameters.

The configuration used for this work in polymeric devices, consists of a substrate, coplanar waveguide electrodes and three dielectric layers. Because the polymer layers are typically 2 to 5 μm thick and the metal thickness ranges from 0.5 to 2 μm, the modeling of the electric field must include the effect of the thick metal electrodes. If the metal was assumed to be infinitely thin, the structure would be symmetric at the metal-to-substrate interface and the electric field distribution would be identical on both sides of the metal. Since the metal is of finite thickness, the structure is no longer symmetric at the metal-to-substrate interface, and the electric field is altered by the thickness of the metal.

One of the biggest advantages of using polymer optical waveguides and coplanar waveguide electrodes is that devices can be extended vertically using multiple layers. (See Appendix B for a general description of the impedance of CPW electrodes.) The model for the electric field distribution must include the effect of multiple dielectric layers. In devices made from inorganic crystals, such as $LiNbO_3$, a buffer layer is placed between the substrate and the metal electrodes to minimize the optical loss that occurs if the tails of the optical fields extend to the metal. For

devices made from organic polymers, a buffer layer is placed above and below the polymer to provide the vertical optical guiding, as well as to minimize the optical field-to-metal interaction. The model must include anisotropic dielectric materials because the inorganic crystals are anisotropic and the polymers become anisotropic after poling.

There has been extensive work on modeling the electrode structures used in electro-optic devices, but the analysis is usually directed either toward the effect of thick electrodes or the effect of multiple layers. For structures with infinitely thin electrodes on an anisotropic dielectric material, conformal mapping can be used to find an analytical solution to the electric field distribution [55], [56], [57], [58], [59]. Most models of coplanar waveguide structures with finite metalization are based on the moment matching method or variations of this, including the projection method [60], the method of lines [61] and the point matching method [62]. One approach used to determine the electric field distribution in a multiple dielectric structure with infinitely thin electrodes is to approximate the charge distribution on the electrodes and then integrate the product of the charge distribution and the Green's function to determine the electric field distribution [63]. The spectral-domain approach can be used to model a multiple dielectric structure with electrodes of finite thickness [64], [65], [66], [67]. The model described in this chapter takes both electrode thickness and multiple anisotropic dielectric layers into account by using a Fourier series expansion of the potential throughout the structure and then solving the Laplace equation.

The model presented here is based on the approach developed by Hang Jin, *et al.* [68], [69], which is used to model a structure with an isotropic buffer layer placed between thick coplanar strip (CPS) electrodes and an anisotropic substrate. This model has been modified to include several anisotropic layers placed on top of coplanar waveguide electrodes as well as several anisotropic layers below the electrodes. This configuration is very general and can be applied to many different configurations. The model can be used for polymeric devices built by coating CPW electrodes with polymers as well as for devices made from inorganic crystals where a buffer layer placed between the electrodes and the substrate. The model can also be used to describe coplanar strip electrodes instead of coplanar waveguide electrodes by varying the electrode widths and gaps.

3.3 Development of Model

There are many configurations proposed for polymeric devices, depending on whether the electrodes are microstrip, coplanar strip, coplanar waveguide or asymmetric coplanar electrodes. Two different configurations using symmetric coplanar waveguide electrodes have been considered in this analysis. The first configuration (CPW_D4), shown in Figure 3-1, consists of thick coplanar waveguide electrodes with two anisotropic dielectric layers below the electrodes and two anisotropic dielectric layers above the electrodes. This structure would most commonly be used for electro-optic devices made from inorganic crystals, where a buffer layer is placed between the electrodes and the substrate.

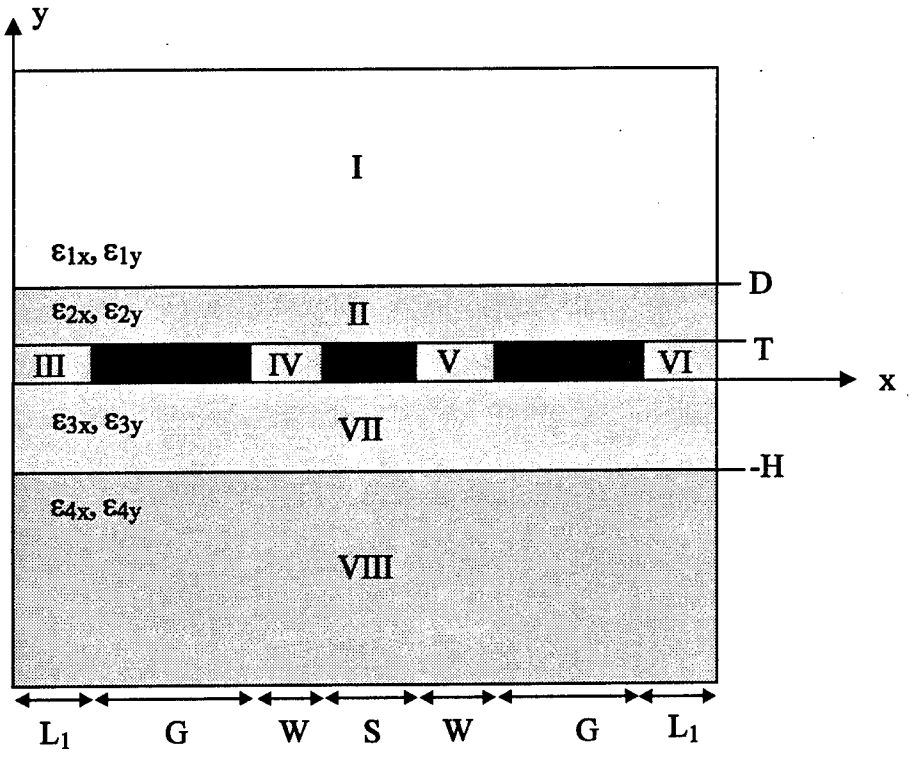

Figure 3-1 Configuration (CPW_D4) with two dielectric layers above and two dielectric layers below the thick coplanar waveguide electrodes.

The second configuration (CPW_D5), shown in Figure 3-2, consists of one dielectric layer below and four dielectric layers above the coplanar waveguide electrodes. This structure is used in the electro-optic devices made from polymeric materials, where the buffer/polymer/buffer layers are placed above the electrodes. This model could be easily extended to include additional electrode and dielectric layers.

For the structure shown in Figure 3-2, the thickness of the electrodes is T, the width of the center conductor is S, the width of the gaps is W and the width of the ground electrodes is G. The distance between the outer edge of the ground electrode and the electric walls at x = -(L/2) and x = (L/2) is L_1. This spacing was included so that voltages on the electrodes could be independent, with V_1 the voltage on left

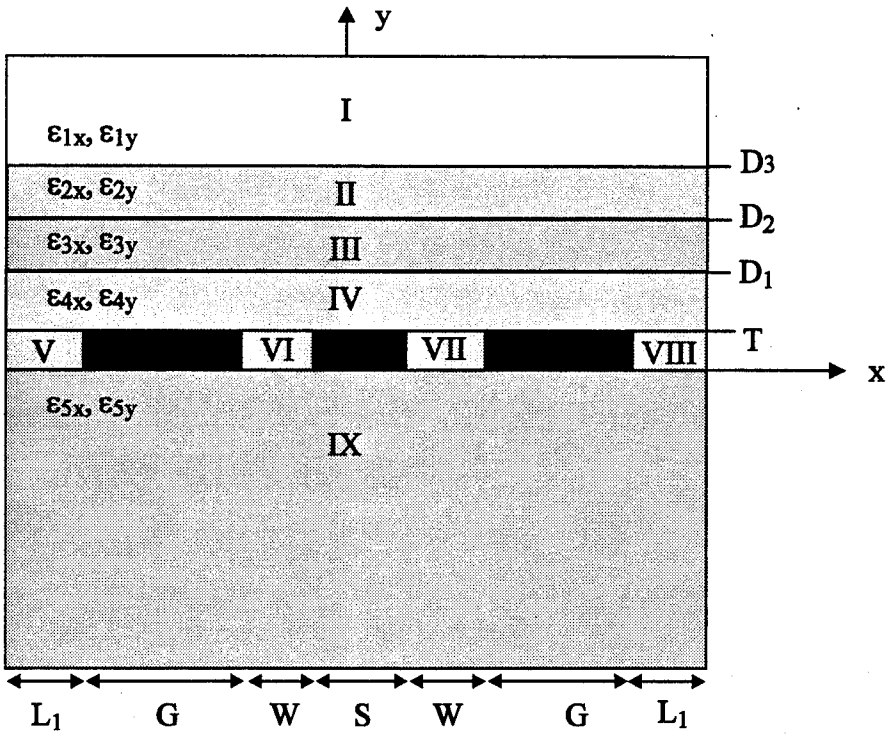

Figure 3-2 Configuration (CPW_D5) with 4 dielectric layers above the thick coplanar waveguide electrodes.

electrode, V_2 the voltage on center electrode and V_3 the voltage on right electrode. All of the dielectric layers are considered to be anisotropic for complete generality. The bottom substrate and top dielectric layer are assumed to be infinitely extending in y. The y-axis is defined at the center of the structure to take advantage of the symmetry of the structure.

The algorithm used to solve for the electric field distribution in the structure was very similar for both configurations. The algorithm will be presented for the configuration in Figure 3-2 because it is more general and has been optimized to take advantage of the symmetry of the electrodes and gaps.

The model used to calculate the field distribution is based on a quasi-static

approach to solving the Laplace equation for the potential in each region of the structure in Figure 3-2,

$$\nabla(\bar{\bar{\varepsilon}} \cdot \nabla\phi_i) = 0 \quad . \tag{3-1}$$

The quasi-static approach is appropriate because at microwave frequencies, the wavelength of the signal is much larger than the transverse dimensions of the waveguide. The solution for the electric field distribution is then a two dimensional electro-static problem. Each dielectric region is assumed to be anisotropic with the principal dielectric axes lined up along the x and y directions,

$$\bar{\bar{\varepsilon}} = \varepsilon_{ix}\hat{x} + \varepsilon_{iy}\hat{y} \quad . \tag{3-2}$$

By dividing the structure into nine regions, with i being the label for each region in Figure 3-2, Equation (3-1) can be written as,

$$\varepsilon_{ix}\frac{\partial^2\phi_i}{\partial x^2} + \varepsilon_{iy}\frac{\partial^2\phi_i}{\partial y^2} = 0. \tag{3-3}$$

Once the potential has been determined throughout the structure, the static electric field distribution can be determined by,

$$\bar{E}(x,y) = -\nabla\phi(x,y). \tag{3-4}$$

It is assumed that there are two parallel-grounded and perfect-conducting electrodes at x = -(L/2) and x = (L/2). This allows the potential to be expanded as an odd periodic function with period 2L and expanded in terms of a Fourier sine series over x = -(L/2) to x = (L/2). The expansion of the potential in the nine regions results

in the following nine equations with 16 unknown Fourier coefficients{a_n, b_n, c_n, d_n, e_n, f_n, g_n, h_n, j_n, l_n, k_n, m_n, n_n, p_n, q_n, s_n),

$$\phi_1(x,y)=\sum_{n=1}^{N} a_n e^{\frac{-k_1 n\pi(y-D)}{L}} \sin\left(\frac{n\pi x}{L}\right) \tag{3-5}$$

$$\phi_2(x,y)=\sum_{n=1}^{N}\left[b_n e^{\frac{-n\pi k_2 y}{L}}+c_n e^{\frac{-n\pi k_2 y}{L}}\right]\sin\left[\frac{n\pi}{L}\left(x+\frac{L}{2}\right)\right] \tag{3-6}$$

$$\phi_3(x,y)=\sum_{n=1}^{N}\left[d_n e^{\frac{-n\pi k_3 y}{L}}+e_n e^{\frac{-n\pi k_3 y}{L}}\right]\sin\left[\frac{n\pi}{L}\left(x+\frac{L}{2}\right)\right] \tag{3-7}$$

$$\phi_4(x,y)=\sum_{n=1}^{N}\left[f_n e^{\frac{-n\pi k_4 y}{L}}+g_n e^{\frac{-n\pi k_4 y}{L}}\right]\sin\left[\frac{n\pi}{L}\left(x+\frac{L}{2}\right)\right] \tag{3-8}$$

$$\phi_5(x,y)=\frac{V_1}{L_1}\left(x+\frac{L}{2}\right)+\sum_{n=1}^{N}\left[h_n e^{\frac{-k_4 n\pi(T-y)}{L_1}}+j_n e^{\frac{-k_4 n\pi y}{L_1}}\right]\sin\left[\frac{n\pi}{L_1}\left(x+\frac{L}{2}\right)\right] \tag{3-9}$$

$$\phi_6(x,y)=V_1+\frac{(V_2-V_1)}{W}\left(x+\frac{S}{2}+W\right)+\sum_{n=1}^{N}\left[k_n e^{\frac{-k_4 n\pi(T-y)}{W}}+l_n e^{\frac{-k_4 n\pi y}{W}}\right]\sin\left(\frac{n\pi\left(x+\frac{S}{2}+W\right)}{W}\right) \tag{3-10}$$

$$\phi_7(x,y)=V_3+\frac{(V_3-V_2)}{W}\left(x-\frac{S}{2}-W\right)+\sum_{n=1}^{N}\left[m_n e^{\frac{-k_4 n\pi(T-y)}{W}}+n_n e^{\frac{-k_4 n\pi y}{W}}\right]\sin\left(\frac{n\pi\left(x-\frac{S}{2}-W\right)}{W}\right) \tag{3-11}$$

$$\phi_8(x,y)=\frac{-V_3}{L_1}\left(x-\frac{L}{2}\right)+\sum_{n=1}^{N}\left[p_n e^{\frac{-k_4 n\pi(T-y)}{L_1}}+q_n e^{\frac{-k_4 n\pi y}{L_1}}\right]\sin\left[\frac{n\pi}{L_1}\left(x-\frac{L}{2}\right)\right] \quad (3\text{-}12)$$

$$\phi_9(x,y)=\sum_{n=1}^{N} s_n e^{\frac{-n\pi k_5 y}{L}}\sin\left[\frac{n\pi}{L}\left(x+\frac{L}{2}\right)\right] \quad (3\text{-}13)$$

where,

$$k_i=\sqrt{\frac{\varepsilon_{ix}}{\varepsilon_{iy}}}. \quad (3\text{-}14)$$

These nine equations are valid over the regions shown in Figure 3-2 and satisfy the boundary conditions in the x-direction and the Laplace equation.

In order to determine the total potential distribution, the 16 coefficients need to be determined. The approach is to solve for the coefficients of regions II-VIII in terms of a_n and s_n by matching the boundary conditions at the interfaces in the y-direction. The first step is to solve the boundary conditions at y = D_3, D_2 and D_1 where,

$$\begin{aligned}
&\phi_1(x,D_3)=\phi_2(x,D_3) && \varepsilon_{1y}\frac{\partial\phi_1}{\partial y(x,D_3)}=\varepsilon_{2y}\frac{\partial\phi_2}{\partial y(x,D_3)}\\
&\phi_2(x,D_2)=\phi_3(x,D_2) && \varepsilon_{2y}\frac{\partial\phi_2}{\partial y(x,D_2)}=\varepsilon_{3y}\frac{\partial\phi_3}{\partial y(x,D_2)}\\
&\phi_3(x,D_1)=\phi_4(x,D_1) && \varepsilon_{3y}\frac{\partial\phi_3}{\partial y(x,D_1)}=\varepsilon_{4y}\frac{\partial\phi_4}{\partial y(x,D_1)}
\end{aligned} \quad (3\text{-}15)$$

and solve for the coefficients b_n, c_n, d_n, e_n, f_n, and g_n in terms of a_n.

The boundary conditions are also matched at y = 0 and y = T ,

$$\begin{aligned}
\frac{\partial\phi_4(x,T)}{\partial y} &= \frac{\partial\phi_5(x,T)}{\partial y} & \varepsilon_{4y}\frac{\partial\phi_4(x,0)}{\partial y} &= \varepsilon_{5y}\frac{\partial\phi_5(x,0)}{\partial y} \\
\frac{\partial\phi_4(x,T)}{\partial y} &= \frac{\partial\phi_6(x,T)}{\partial y} & \varepsilon_{4y}\frac{\partial\phi_4(x,0)}{\partial y} &= \varepsilon_{5y}\frac{\partial\phi_6(x,0)}{\partial y} \\
\frac{\partial\phi_4(x,T)}{\partial y} &= \frac{\partial\phi_7(x,T)}{\partial y} & \varepsilon_{4y}\frac{\partial\phi_4(x,0)}{\partial y} &= \varepsilon_{5y}\frac{\partial\phi_7(x,0)}{\partial y} \\
\frac{\partial\phi_4(x,T)}{\partial y} &= \frac{\partial\phi_8(x,T)}{\partial y} & \varepsilon_{4y}\frac{\partial\phi_4(x,0)}{\partial y} &= \varepsilon_{5y}\frac{\partial\phi_8(x,0)}{\partial y}
\end{aligned} \tag{3-16}$$

to get the coefficients h_n, j_n, l_n, k_n, m_n, n_n, p_n, and q_n, in terms of a_n, and s_n.

The last two boundary conditions require,

$$\phi_4(x,T) = \phi_5(x,T) + V_1 + \phi_6(x,T) + V_2 + \phi_7(x,T) + V_3 + \phi_8(x,T) \tag{3-17}$$

and

$$\phi_4(x,0) = \phi_5(x,0) + V_1 + \phi_6(x,0) + V_2 + \phi_7(x,0) + V_3 + \phi_8(x,0). \tag{3-18}$$

By plugging in the equations for the potential and the results from Equations (3-15) and (3-16), into Equations (3-17) and (3-18) and evaluating over the proper regions, a linear system of equations for a_n and s_n can be determined and written as,

$$\begin{aligned}
[A] &= [C1] + [MA1][A] + [MS1][S] \\
[S] &= [C2] + [MA2][A] + [MS2][S].
\end{aligned} \tag{3-19}$$

The summations for the potential are truncated at a finite index of N, so that [A], [S], [C1], and [C2] are vectors of length N, and [MA1[, [MS1], [MA2], and [MS2] are matrices of dimensions NXN. Equation (3-19) can be rewritten as,

$$\begin{bmatrix} [I]-[MA1] & [MS1] \\ [MA2] & [I]-[MS2] \end{bmatrix} \begin{bmatrix} [A] \\ [S] \end{bmatrix} = \begin{bmatrix} [C1] \\ [C2] \end{bmatrix} \tag{3-20}$$

or

$$[M] \begin{bmatrix} [A] \\ [S] \end{bmatrix} = [C] \tag{3-21}$$

where,

$$[A] = \begin{bmatrix} a_1 \\ a_2 \\ a_3 \\ \cdot \\ \cdot \\ \cdot \\ a_n \end{bmatrix} \text{ and } [S] = \begin{bmatrix} s_1 \\ s_2 \\ s_3 \\ \cdot \\ \cdot \\ \cdot \\ s_n \end{bmatrix} \tag{3-22}$$

and

$$[M]_{2Nx2N}.$$

It is now possible to solve for the vectors [A] and [S] by inverting the matrix [M]. Once the vectors [A] and [S] have been determined, the rest of the coefficients can be obtained from the relations resulting from Equations (3-15) and (3-16). By plugging the coefficients back into each potential equation, the potential in each region can be determined. The final step is to take the gradient of the potential distribution to determine the electric field distribution.

$$\overline{E} = -\nabla\phi(x,y) = \left[E_x(x,y), E_y(x,y)\right] \tag{3-23}$$

The algorithm just described is easy to implement and solve on a computer and provides a good tool for examining the electric field of various structures.

3.4 Results

The electric field distribution for the structure in Figure 3-2 was determined using a software package called MAPLE on an IBM Risc station. MAPLE is a mathematical manipulation language developed at the University of Waterloo. In this section, results obtained from this model will be compared to results obtained by the conformal mapping solution of structures with infinitely thin electrodes. From the electric field distribution determined using this model, the capacitance, effective dielectric and impedance for a given electrode structure can be determined. Because the dimensions and dielectric constants of the structure can be easily varied, the dependence of the waveguide parameters on electrode thickness, dielectric thickness and material dielectric constants can be determined.

3.4a Electric field

By using conformal mapping, an analytical solution for the x and y components of the electric field for infinitely thin electrodes on an anisotropic substrate. The resulting electric field components for a center conductor width of S, gap widths of W and infinitely extending ground planes are given by,

$$E_x = -\frac{V}{K(k')}\,\mathrm{Im}\left(\frac{dw}{dz}\right)$$
$$E_y = -\sqrt{\frac{\varepsilon_x}{\varepsilon_y}}\,\frac{V}{K(k')}\,\mathrm{Re}\left(\frac{dw}{dz}\right) \qquad (3\text{-}24)$$

where K(k) is the complete elliptical integral of the first kind and,

$$k = \frac{S}{S+2W}$$

$$k' = \sqrt{1-k^2}$$

$$h = \frac{S}{2}$$

$$z = x + iy$$

$$\frac{dw}{dz} = \frac{h}{\sqrt{\left(h^2 - k^2 z^2\right)\left(h^2 - z^2\right)}}.$$

The electric field components were calculated using Equation (3-24) with S = 10 μm, W = 10 μm, V = 1 Volt and $\varepsilon_x = \varepsilon_y = 3.85$. The components were also calculated for the same electrode dimensions with G = 10 μm, $L_1 = 0$, T = 0.01 μm, V = 1 Volt and N = 50 using the Fourier series analysis just described. Figure 3-3(a) and Figure 3-3(b) show the x and y components of the electric field 1 μm above the electrodes. As shown in Figure 3-3, the x component of the electric field is strongest in the gaps, and the y-component of the electric field is strongest at the edge of the electrodes. The singularities at the edge of the metal cause the field to be extremely large and most techniques must use be stabilized at these points.

Figure 3-4 shows the dependence of the x component of the electric field on the thickness of the electrodes. The metal thickness has a larger effect on the fields above the electrodes than on the fields below the electrodes. Figure 3-5 shows the vector field plot for the electric field, with the thickness of the lines corresponding to the field strength and the arrows indication the direction of the field lines. The field is strongest in the gaps.

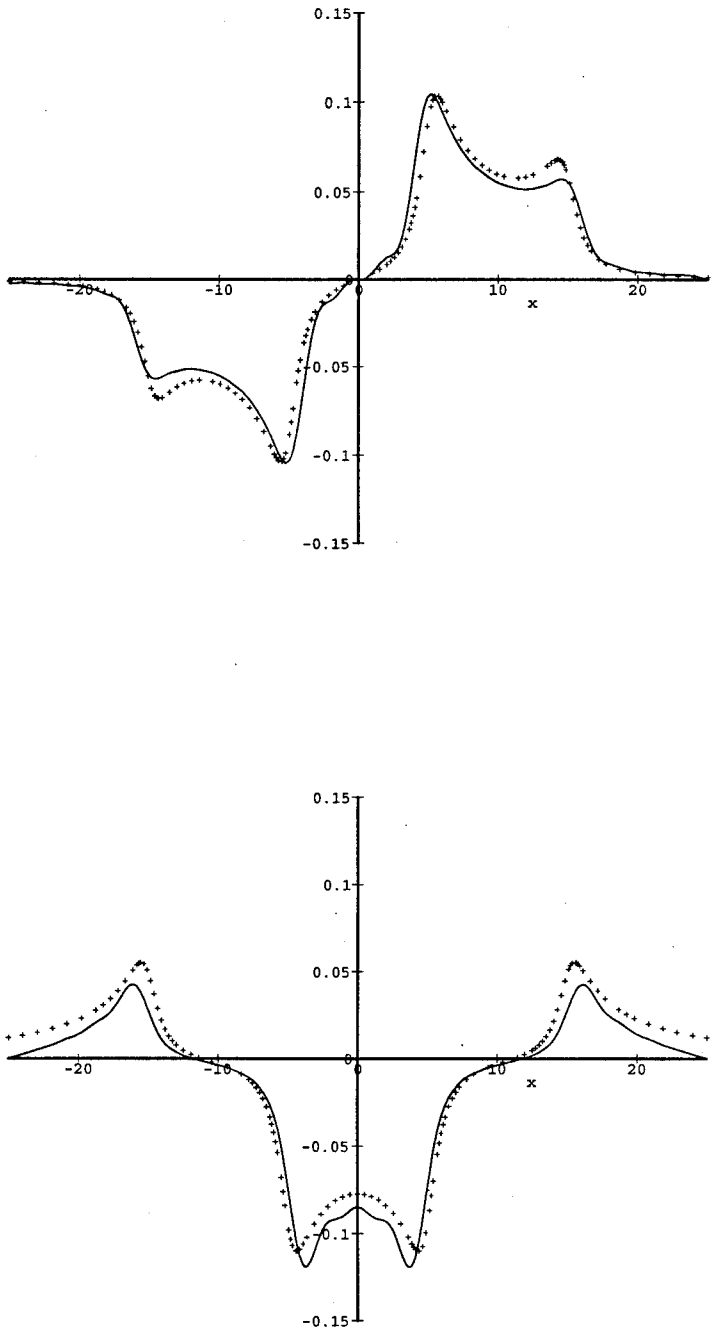

Figure 3-3 The components of electric field for S = 10 μm and W = 10 μm using conformal mapping (dotted line) and Fourier series solution with G = 10, L_1 = 0, T = 0.01 μm, V = 1 Volt and N = 50 for (a.) x-component and (b.) y-component.

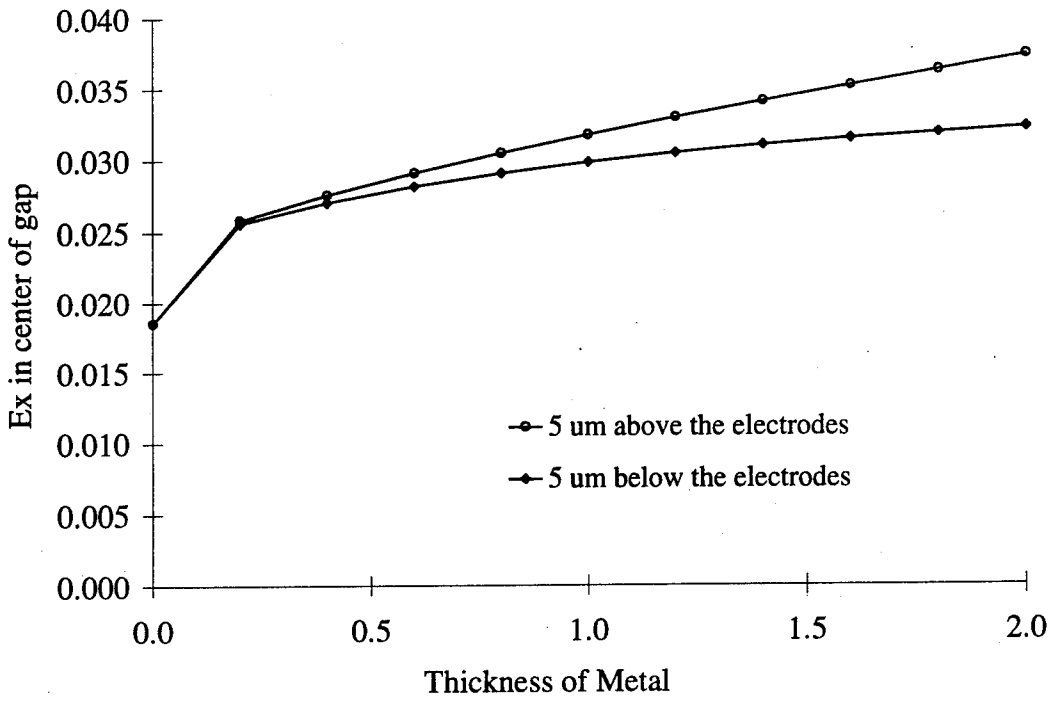

Figure 3-4 The electric field above and below a 50 μm gap in the electrodes for metal thicknesses ranging from 0.1 to 2 μm.

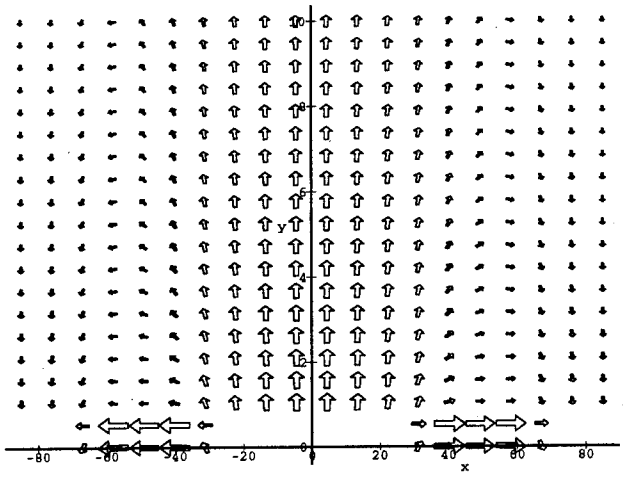

Figure 3-5 The vector field plot for a structure with CPW electrodes (S = 50 μm , W = 50 μm) on quartz , coated with 15 μm of a dielectric material (ε_p = 3.5).

The electric field obtained using this Fourier series expansion is dependent both on the dimensions of the structure and the number of terms in the expansion. For geometries with T/W and T/G less than 0.1, the field distribution is accurate for a finite truncation index. The electric field distribution will appear oscillatory for an insufficient truncation index or for aspect ratios greater than 0.1.

3.4b Capacitance

For a complete quasi-TEM model of coplanar structures, the equivalent circuit parameters per unit length (R, L, G and C) of the transmission line can be determined. If the conductors are considered to be ideal (very high conductivity), and the dielectric materials are considered to be lossless, then the capacitance and inductance of the transmission line are the only relevant circuit elements. The impedance, phase velocity and propagation constants, assuming non-magnetic dielectric materials, of a transmission line are given by,

$$Z = \sqrt{\frac{L}{C}} \qquad V_{ph} = \frac{1}{\sqrt{LC}} \qquad \beta = \omega\sqrt{LC}, \quad \text{where, } LC = \mu_o\varepsilon. \tag{3-25}$$

If all the dielectric materials are replaced with air (the electrodes are floating in air), then the waveguide parameters become,

$$Z_o = \sqrt{\frac{L}{C_o}} \qquad V_{ph} = \frac{1}{\sqrt{LC_o}} \qquad \beta = \omega\sqrt{LC_o}, \quad \text{where, } LC_o = \mu_o\varepsilon_o. \tag{3-26}$$

A useful quantity in describing transmission lines, is the effective dielectric constant (ε_{eff}) of the structure and is defined as the ratio of the capacitance of the structure (C)

to the capacitance of the structure with all the dielectrics replaced with air (C_o),

$$\varepsilon_{eff} = \frac{C}{C_o}. \tag{3-27}$$

The transmission line parameters can then be rewritten in terms of the effective dielectric constant and the speed of light in vacuum (c) as,

$$Z_o = \frac{1}{c\sqrt{C_o C}} \qquad V_{ph} = \frac{c}{\sqrt{\varepsilon_{eff}}} \qquad \beta = \frac{\omega}{c}\sqrt{\varepsilon_{eff}}, \quad \text{where,} \quad c = \frac{1}{\sqrt{\mu_o \varepsilon_o}}. \tag{3-28}$$

By determining C and Co, the transmission line can be completely characterized. The effect of the electrode thickness and multiple dielectrics on the line parameters of the CPW electrode can be determined from the capacitance of the structure.

The capacitance of a coplanar waveguide structure with infinitely thin electrodes on a substrate with dielectric constant ε_r can be calculated as,

$$C = 2(1+\varepsilon_r)\varepsilon_o \frac{K(k)}{K(k')}, \tag{3-29}$$

using the same definitions as in Equation (3-24). The capacitance of a coplanar waveguide structure can also be determined from the electric field distribution. The capacitance is related to the charge on the center electrode is given by,

$$C = \frac{|Q|}{|V_2 - V_1 - V_3|}. \tag{3-30}$$

The charge on the center conductor can be found by integrating the electric displacement vector,

$$\overline{D} = \varepsilon_o \overline{\overline{\varepsilon}} \cdot \overline{E} \tag{3-31}$$

along a closed path enclosing the center electrode. Figure 3-6 shows the closed path that was used to compute the charge on the center electrode.

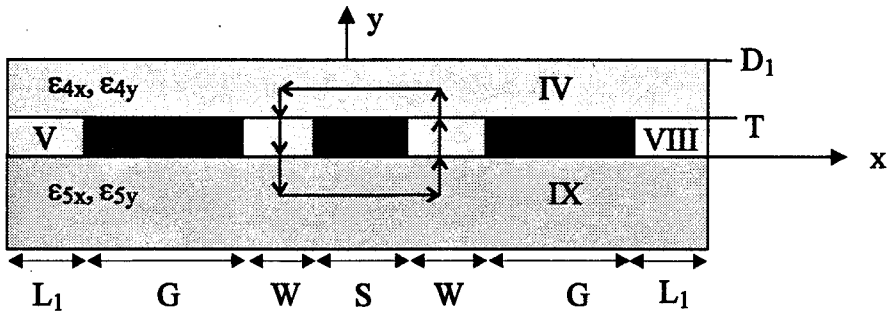

Figure 3-6 Path of integration for determining the charge on the center conductor.

By taking advantage of the symmetry of the electrodes in this configuration, the total charge Q on the center conductor can be computed by,

$$Q = |q_1| + |2q_2| + |2q_3| + |2q_4| + |q_5| \tag{3-32}$$

where,

$$q_1 = \int_{\frac{S+W}{2}}^{\frac{S+W}{2}} \varepsilon_{4y} E_{y4}\left(x, \frac{T+D_1}{2}\right) dx$$

$$q_2 = \int_{\frac{T+D_1}{2}}^{T} \varepsilon_{4x} E_{x4}\left(-\frac{S+W}{2}, y\right) dy$$

$$q_3 = \int_{T}^{0} \varepsilon_{4x} E_{x6}\left(-\frac{S+W}{2}, y\right) dy$$

$$q_4 = \int_{-\frac{T+D_1}{2}}^{0} \varepsilon_{5x} E_{x9}\left(-\frac{S+W}{2}, y\right) dy$$

$$q_5 = \int_{-\frac{S+W}{2}}^{\frac{S+W}{2}} \varepsilon_{5y} E_{y9}\left(x, \frac{-(T+D_1)}{2}\right) dx \qquad (3\text{-}33)$$

The structure used to determine the effect of a dielectric cap (ε_p) of thickness D_1 and the thickness of the metal (T) on the capacitance, effective dielectric constant and impedance is shown in Figure 3-7,

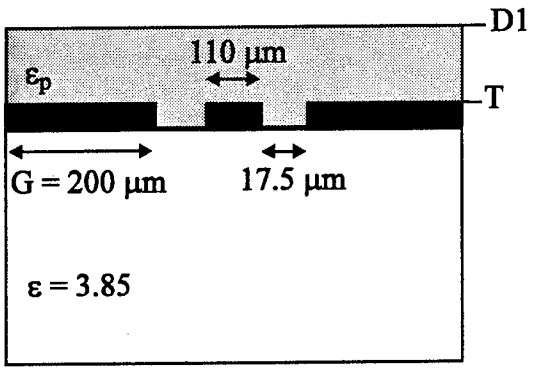

Figure 3-7 Structure used to determine the effect of a dielectric cap and thick metal electrodes on the capacitance, effective dielectric constant and impedance of the structure.

The electrode structure was designed to have a center conductor width of 100 μm and a gap width of 17.5 μm for 50 Ω lines on quartz (ε = 3.85). The actual electrodes after fabrication had a center conductor width of 110 μm and a gap width of 17.5 μm.

The required truncation index in the Fourier series was determined by finding the N at which the capacitance reached a steady value. This is dependent on the overall geometry of the structure, specifically the width to thickness ratio of the electrodes. The capacitance for the structure in Figure 3-7 was determined to be 91.5 pF/m with an N of 50 being sufficient as shown in Figure 3-8.

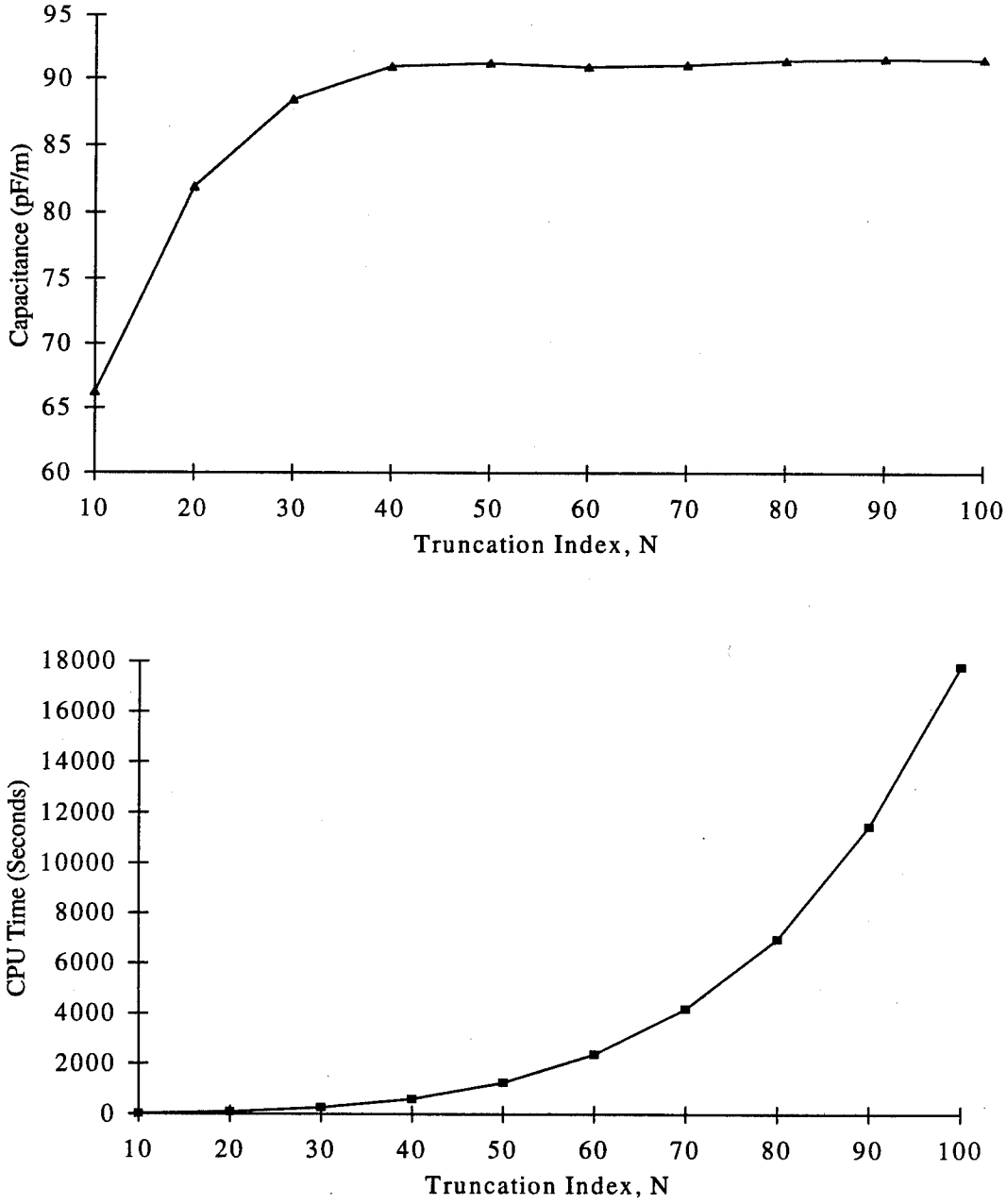

Figure 3-8 (a.) Capacitance vs. summation index and (b.) CPU time versus truncation index for structure with S=110 μm, W = 17.5 μm, G=200 μm L_1=100 μm, $\varepsilon_1 = \varepsilon_2 = \varepsilon_3 = \varepsilon_4 = 1$, $\varepsilon_5 = 3.85$.

Increasing the thickness of the electrodes can be thought of as adding and additional capacitance due to the parallel plate capacitance formed by the walls of the

electrodes. The addition of a dielectric cap over the electrodes will also increase the capacitance. The Fourier series model can be used to determine the sensitivity of the capacitance on the dielectric constant of the dielectric cap. The effect of metal thickness, thickness of the dielectric cap and the dielectric constant of the dielectric cap on the capacitance of the same structure is shown in Figure 3-9.

3.4c Effective dielectric constant

As was described earlier, the effective dielectric constant of a structure is a useful parameter that can be determined from the capacitance of the structure. The product of the bandwidth of an electro-optic modulator and the interaction length is given by,.

$$\Delta f \cdot L = \frac{2c}{\pi} \frac{1}{(n_m - n_o)} \tag{3-34}$$

where

$$n_m = \sqrt{\varepsilon_{eff}}.$$

and can be increased by matching the velocity of the light in the optical waveguide and the phase velocity of the electrical signal.

There is a larger velocity mismatch in $LiNbO_3$, where $\varepsilon_x = 43$ and $\varepsilon_y = 28$, than in polymers where ε ranges between 3 and 4. In both cases, the metal electrode thickness and the presence of an additional dielectric material can alter this mismatch As shown in Figure 3-10, the effect of the metal thickness and the dielectric constant of the dielectric cap can be used to tailed the effective dielectric constant.

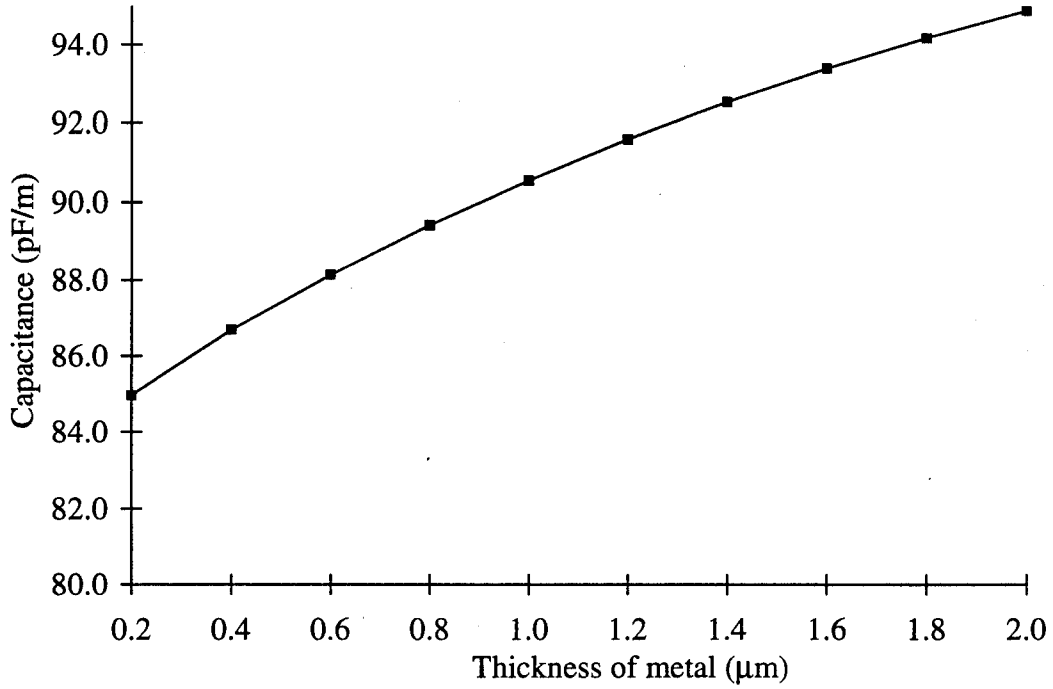

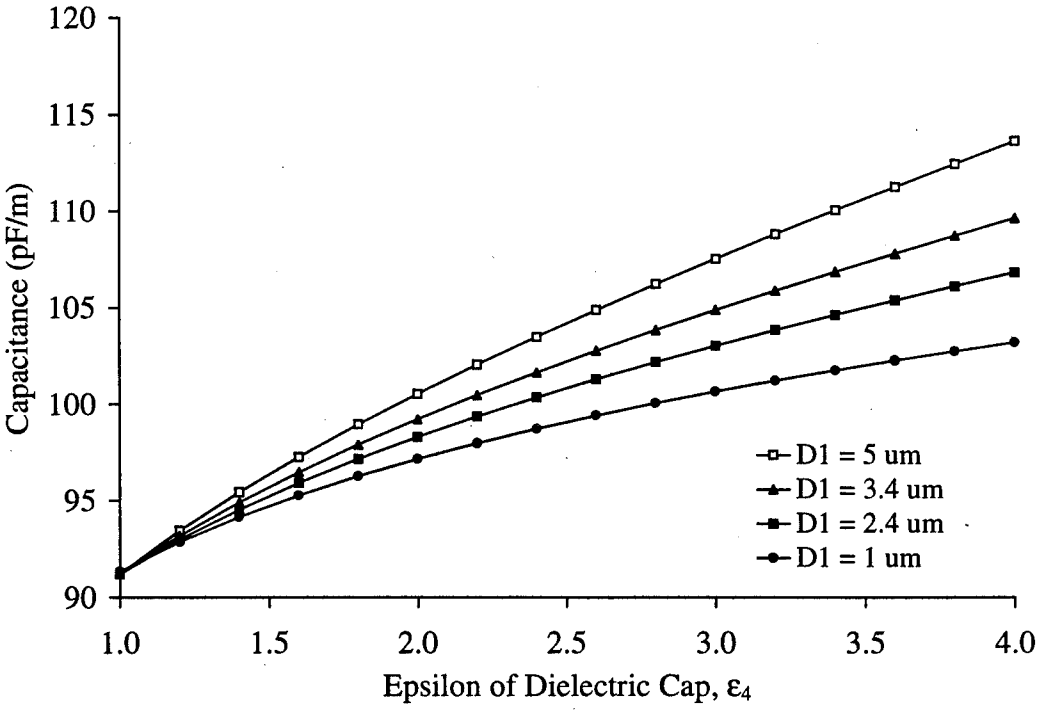

Figure 3-9 Capacitance vs. thickness of the electrode and dielectric constant and thickness of a dielectric cap for a structure with S=110 μm, W = 17.5 μm, G=200 μm L_1=100 μm, $\varepsilon_1 = \varepsilon_2 = \varepsilon_3 = \varepsilon_4 = 1$, $\varepsilon_5 = 3.85$.

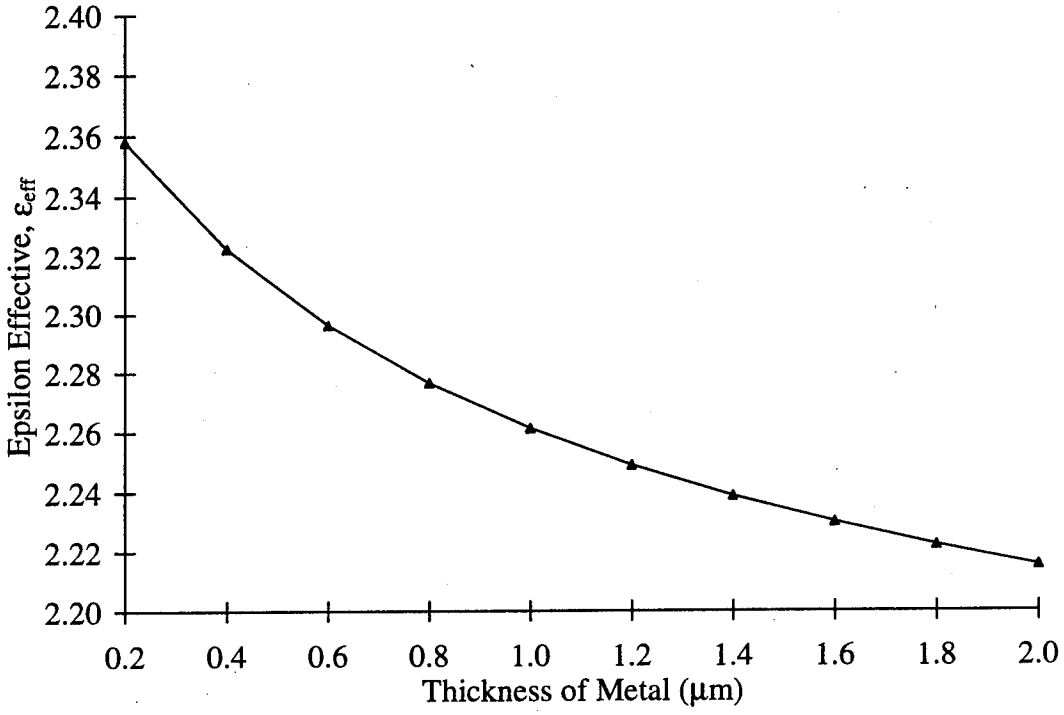

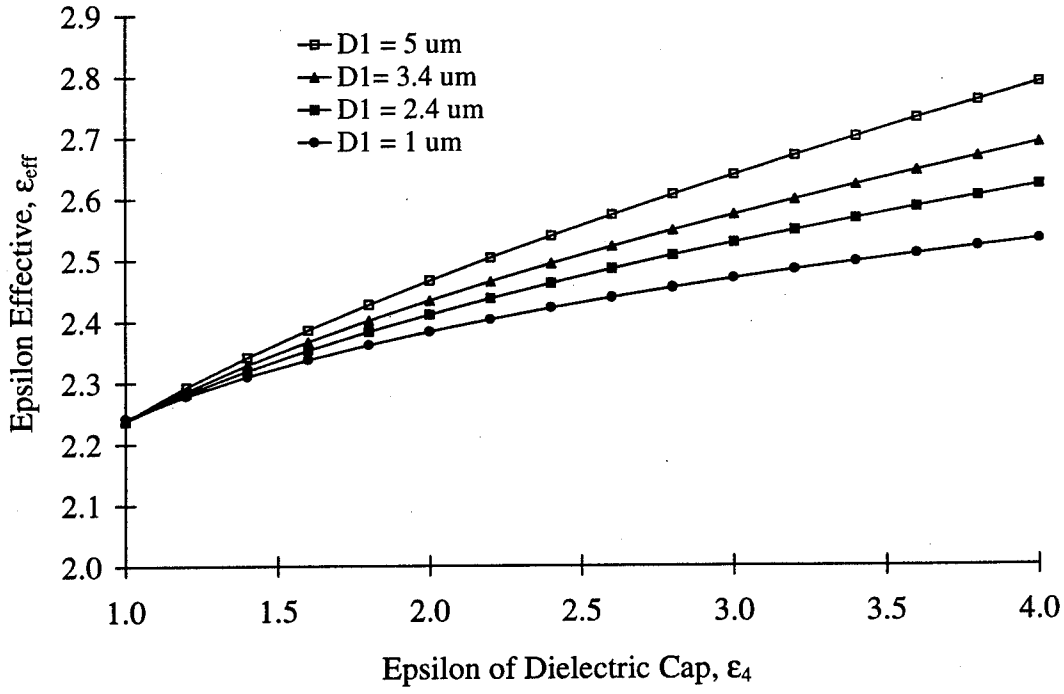

Figure 3-10 Epsilon effective vs. thickness of the electrode and dielectric constant and thickness of a dielectric cap for a structure with S=110 μm, W = 17.5 μm, G=200 μm L_1=100 μm, $\varepsilon_1 = \varepsilon_2 = \varepsilon_3 = \varepsilon_4 = 1$, $\varepsilon_5 = 3.85$.

3.4d Impedance

Because the impedance of the electrode structure can also be related to the capacitance and effective dielectric constant, the impedance also varies with metal thickness and the presence of a dielectric cap as shown in Figure 3-11.

3.5 Extensions to the Model

A complete model of a coplanar waveguide structure must include the finite conductivity of the metal and effect of waveguide discontinuities on the field distribution. In both the conformal map solution and the Fourier series analysis, the metals are assumed to be perfect conductors and the dielectrics are assumed to be lossless. For low frequencies, the line parameters can be easily determined using transmission line equations. When one or more of the dimensions of the transmission line are comparable to the skin depth, the resistance and inductance of the lines vary significantly with frequency, while the capacitance and conductance remain independent of frequency. Several authors have developed descriptions of the conductor loss due to skin depth effects [70], [71]. The situation is complicated because the current and fields propagate throughout the cross section of the conductor instead of near the surface of the conductor.

The electrodes used in microwave circuits are usually fabricated to be 2 to 3 μm in order to reduce the ohmic losses and increase the frequency response. For a good conductor, the ohmic loss (α) is inversely proportional to the skin depth (δ) which decreases as the square root of frequency,

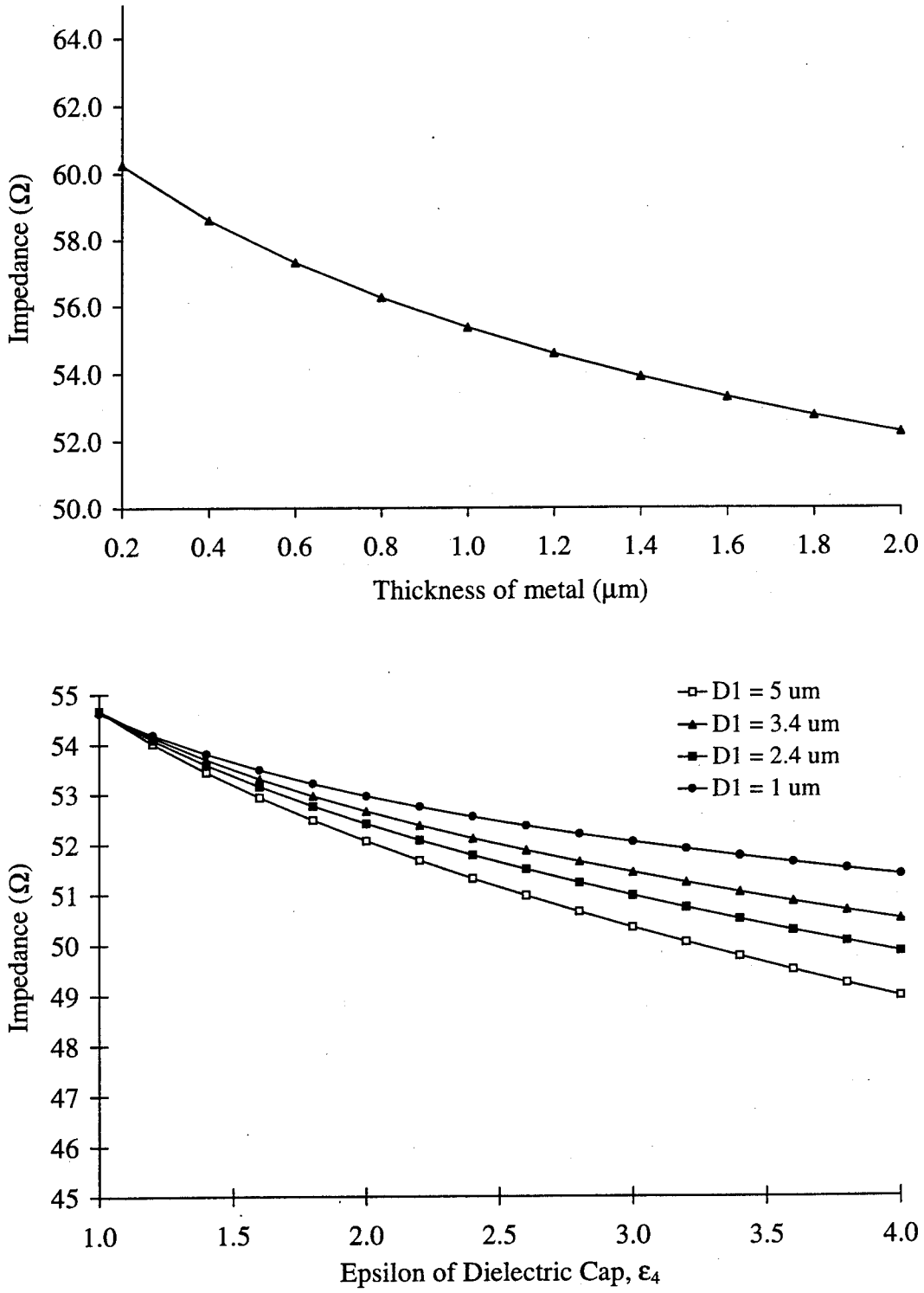

Figure 3-11 Impedance vs. thickness of the electrode and dielectric constant and thickness of a dielectric cap for a structure with S=110 μm, W = 17.5 μm, G=200 μm L_1=100 μm, $\varepsilon_1 = \varepsilon_2 = \varepsilon_3 = \varepsilon_4 = 1$, $\varepsilon_5 = 3.85$.

$$\delta = \frac{1}{\sqrt{\pi f \mu \sigma}} \propto \frac{1}{\alpha}. \tag{3-35}$$

Figure 3-12 shows the skin depth in microns for three commonly used metals having different conductivities (σ).

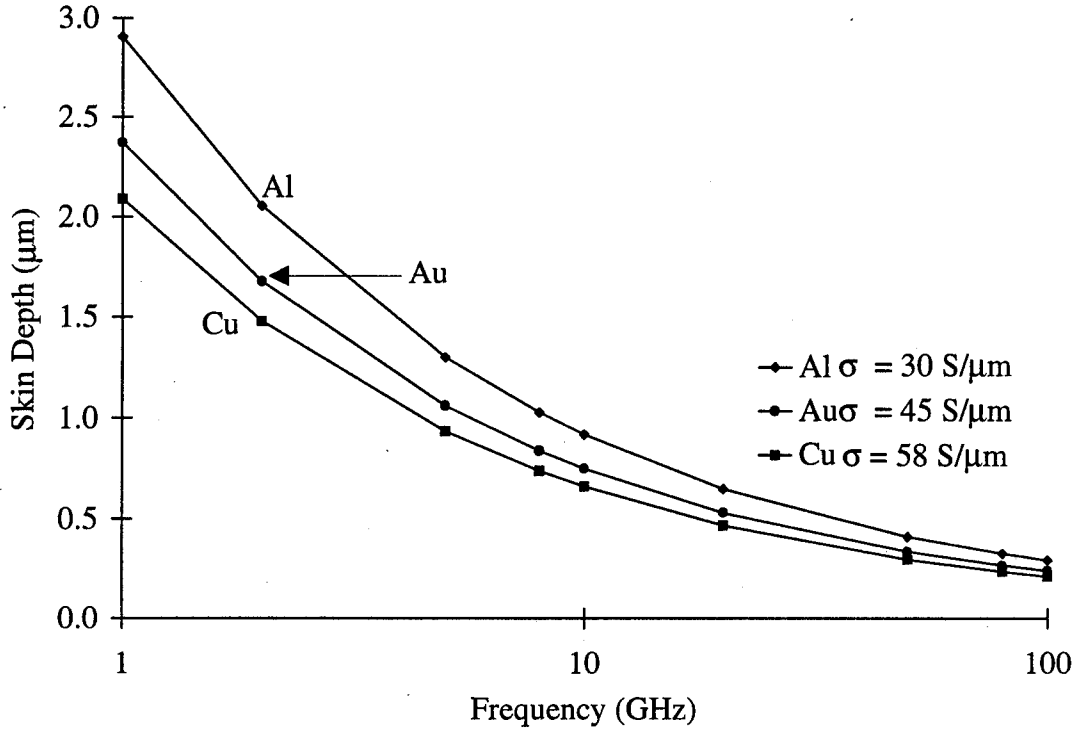

Figure 3-12 The skin depth in μm for aluminum (σ = 30 S/μm), gold (σ = 45 S/μm) and copper (σ = 58 S/μm).

The associated skin depth resistance per unit length for a given width (W) of channel increases as the square root of frequency and can be approximated by,

$$R_s = \frac{1}{\sigma \delta W} \tag{3-36}$$

Figure 3-13 shows the dc resistance of metal electrodes 10 μm wide and 2 μm thick

and the corresponding skin depth resistance for several metals.

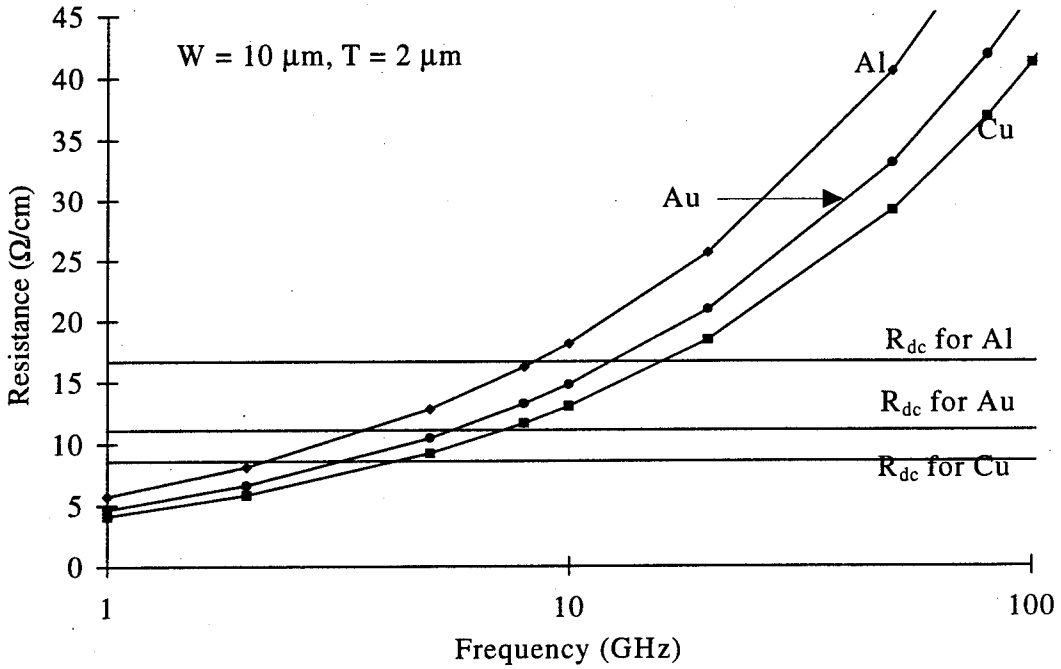

Figure 3-13 The DC resistance and effective skin depth resistance for a 10 um wide electrode of aluminum, gold and copper.

W. Heinrich has developed a quasi-TEM description of coplanar lines with non-ideal conductors of finite thickness and lossy dielectrics using closed form approximations [72]. Figure 3-14 shows that the resistance and inductance are functions of the metal thickness and conductivity. The resistance and inductance are not changed by the loss in the dielectric. For a perfect conductor the resistance will be zero and the inductance constant with frequency. Figure 3-15 shows that the capacitance is a function of the metal thickness, but is not changed by the conductivity of the metal or the loss in the dielectric. The conductivity, shown in Figure 3-15, is only dependent on the loss in the dielectric, not on the thickness or conductivity of the metal electrodes.

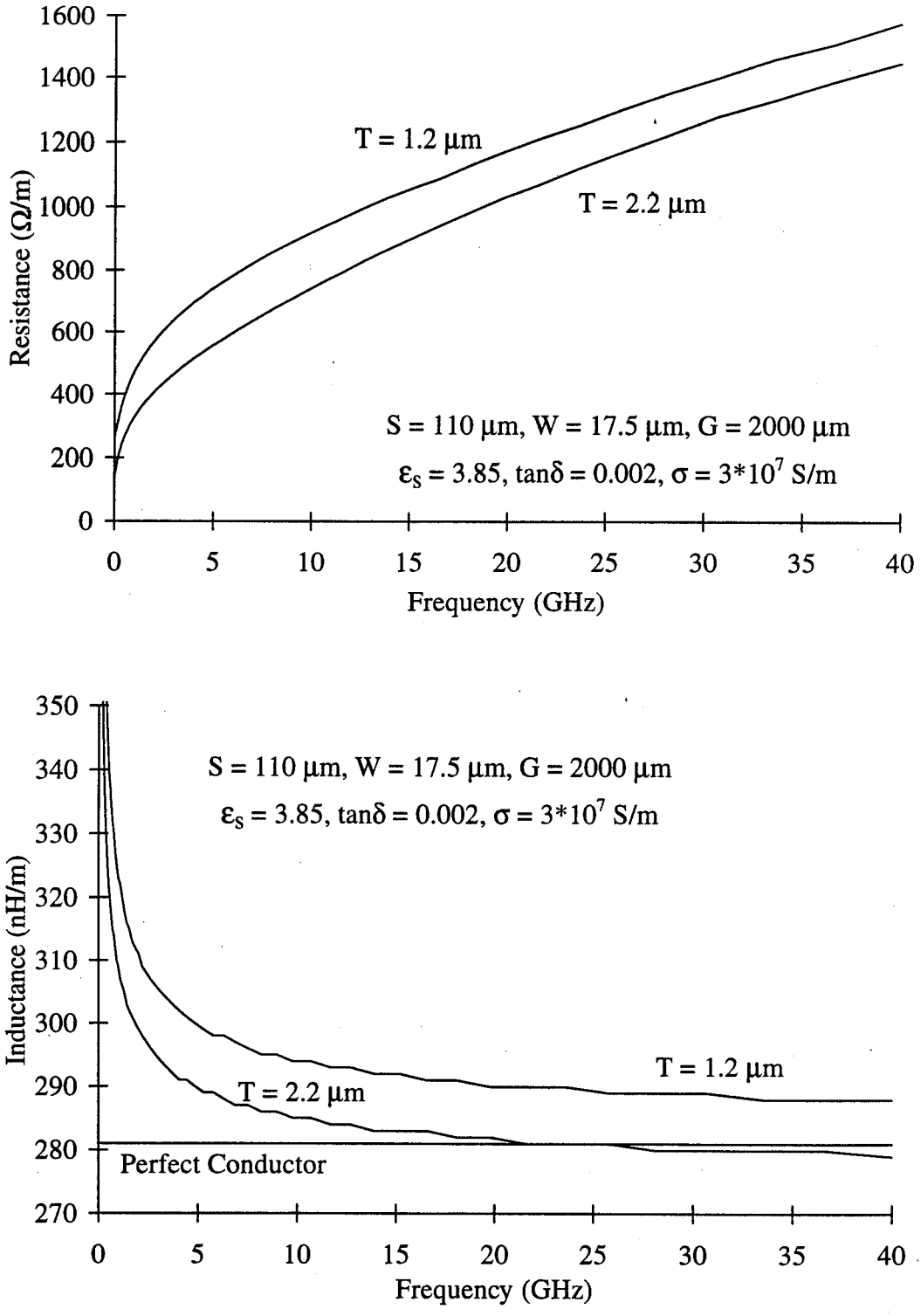

Figure 3-14 Resistance and inductance per unit length for a CPW structure on quartz ($\varepsilon_s = 3.85$).

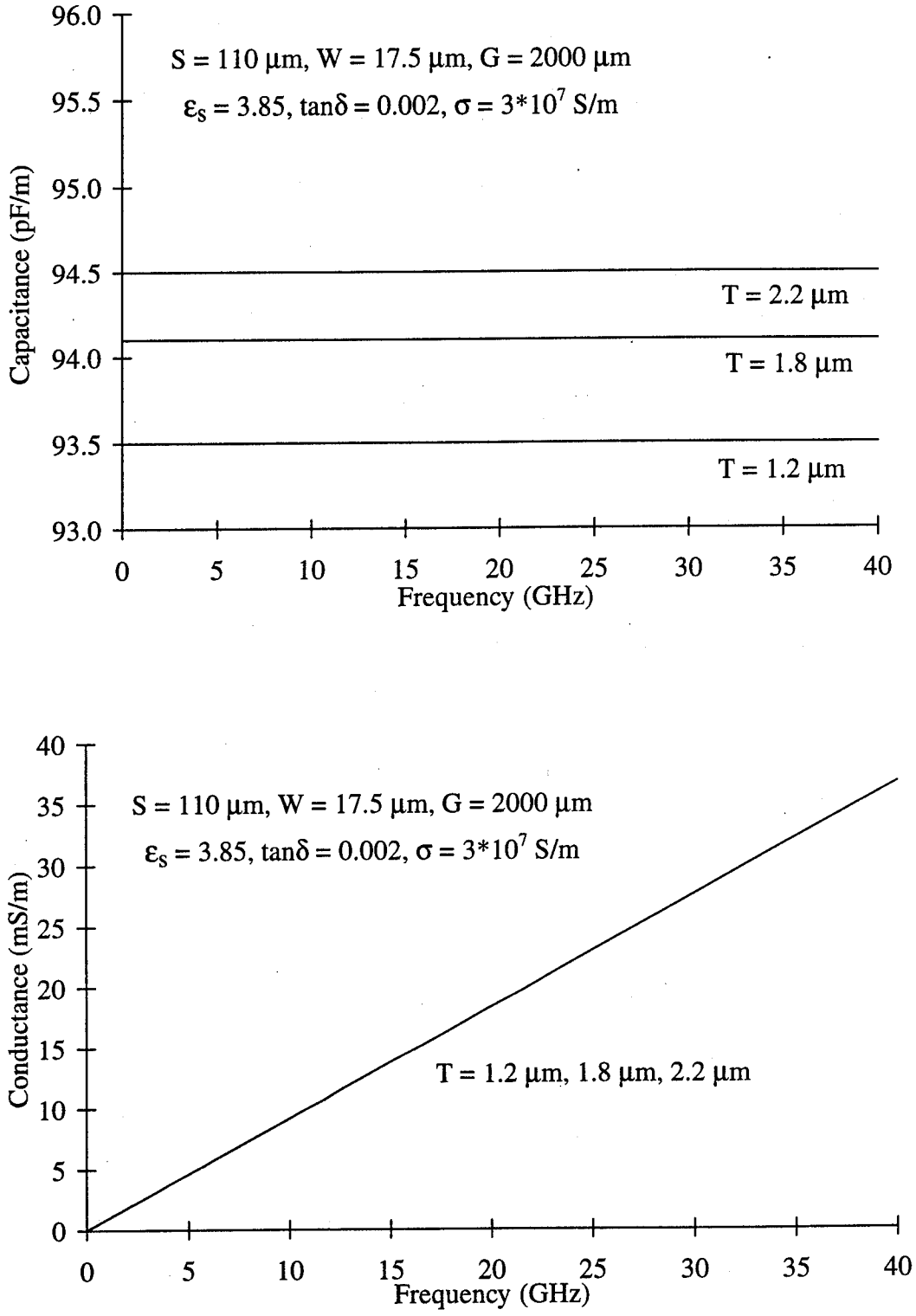

Figure 3-15 Capacitance and conductance per unit length for a CPW structure on quartz ($\varepsilon_s = 3.85$).

As shown in Figure 3-14 and Figure 3-15, the dispersion of a transmission line is due to the metal thickness and conductivity and only shows up in the resistance and inductance. The capacitance is only a function of the waveguide geometry and the dielectric materials. This information will be used in Chapter 4, in determining the dielectric constant of a thin polymer film.

A technique has been developed at the Guided Wave Optics Laboratory for modeling planar discontinuities in coplanar waveguides [73]. This technique is useful when modeling bends and tapers in CPW electrodes. It can also be extended to include active devices and three-dimensional discontinuities.

3.6 Conclusion

A valuable tool has been developed which can be used in many aspects of polymeric electro-optic device design. A model has been developed which will be valuable in the design of polymeric devices constructed with CPW electrodes. The solution is obtained by expanding the potential in each of the regions of the structure in terms of a Fourier series. The problem initialization is cumbersome, but the resulting computer program is extremely easy to use and very versatile. The resulting electric field distribution has been used in determining the dielectric constants of thin polymer films and determining the electro-optic coefficients of poled polymer waveguides as will be discussed in Chapters 4 and 5.

Chapter 4

MICROWAVE CHARACTERIZATION OF THIN FILM MATERIALS

4.1 Introduction

A technique for measuring the dielectric properties of thin film materials is presented. This technique has been used to measure the complex dielectric constant of thin films of nonlinear optical (NLO) polymers used in electro-optic applications over the frequency range of 0.5 GHz to 40 GHz. The technique is based on measurements of the transmission line parameters of coplanar TRL calibration standards coated with a thin dielectric film. Because thin film dielectrics are used in a wide variety of applications, including integrated optics and electronics, a technique for determining the dielectric constant of multi-layer dielectrics over the frequency range of DC to 100 GHz, with thicknesses ranging from 1 to 5 μm, can be very useful. Although this technique was developed to measure the dielectric constant of thin polymer films used in integrated optics, the technique is general and can be applied to any thin film dielectric material.

In microelectronic applications, thin film dielectrics are placed between the layers of multi-layered circuits. A low dielectric constant is desired to minimize interconnect capacitance, propagation delay and crosstalk between signal lines [74].

For electro-optic devices fabricated in inorganic crystals, thin dielectric materials are used as buffer layers placed between the optical guides and the metal electrodes. The devices described in this thesis are made entirely from thin film dielectric materials, making the dielectric characterization crucial to the device design.

As mentioned in Chapter 2, in the design of high speed integrated electro-optic devices, the dielectric constant of the materials at the modulating frequencies, as well as the optical index of refraction at the operating wavelength must be known. The efficiency of an electro-optic modulator is increased by matching the phase velocities of the optical and microwave signals [75]. The product of the bandwidth (Δf) and interaction length (L) of a switch or modulator with traveling wave electrodes is given by,

$$\Delta f \cdot L = \frac{2c}{\pi} \frac{1}{\left[n_m(f) - n_o(\lambda)\right]} \tag{4-1}$$

where,

c = velocity of light in vacum
$n_o(\lambda)$ = optical index of refraction
$n_m(f) = \sqrt{\varepsilon_{eff}}$ = index of refraction of modulation signal.

By matching the velocities of the optical and modulation signals, devices with high bandwidths or long interaction lengths can be realized with the accompanying low switching voltage [76].

As shown in Chapter 3, the effective dielectric constant of the structure is dependent on the thicknesses of the dielectric layers, the dielectric constants of the individual layers, and the thickness of the metal. The technique described in this

chapter can be used to determine the dielectric constants of the individual layers. The effective dielectric constant of the structure can then be matched to the optical index by varying the thicknesses of the dielectric layers and the thickness of the electrodes. The technique presented in this chapter was developed to determine the dielectric properties of nonlinear organic polymers, specifically the effect of multiple dielectric layers and the changes in the dielectric constant due to various fabrication steps.

The dielectric properties of materials are generally measured either on bulk materials over a wide frequency range or on thin layers of materials at a single frequency. For example, the dielectric properties of various bulk materials can be measured using the HP85070A Dielectric Probe Kit for frequencies ranging from 200 MHz to 20 GHz [77]. The dielectric constant of thin films is generally determined at a single frequency using resonance techniques [78], [79]. An extensive list of the dielectric properties of interconnect dielectrics in the kHz range has been compiled [80]. Mohapatra, *et al.*, measured the microwave loss of poled and unpoled nonlinear optical polymers by imbedding the polymers in coplanar waveguide structures [81]. The loss of the polymer material was determined by replacing the polymer with SiO_2, and comparing the loss measurements.

This chapter will describe a method for determining the dielectric properties of thin film materials over a broad frequency range. We will first give a brief description of the structures used for the measurements. The deembeding procedure used to compute the propagation constant of this structure will then be described.

From the measured propagation constants of a Reference Structure and a Test Structure, the distributed circuit elements of capacitance, resistance, inductance and conductance of the structures can be determined. Combining these results with the calculated capacitance of a CPW structure with thick electrodes, the dielectric constant of the thin film can be determined.

4.2 Test Device Configuration

This technique for determining the dielectric constant of a thin film is based on measuring the complex propagation constant of two coplanar waveguide structures (Figure 4-1). The Reference Structure, consists of six coplanar lines designed to have an impedance of 50 Ω for the dielectric constant of the substrate. These six lines comprise a calibration standard for transmission lines referred to as a TRL (THRU, LINE, REFLECT). A more detailed description of a TRL calibration will be presented in the next section.

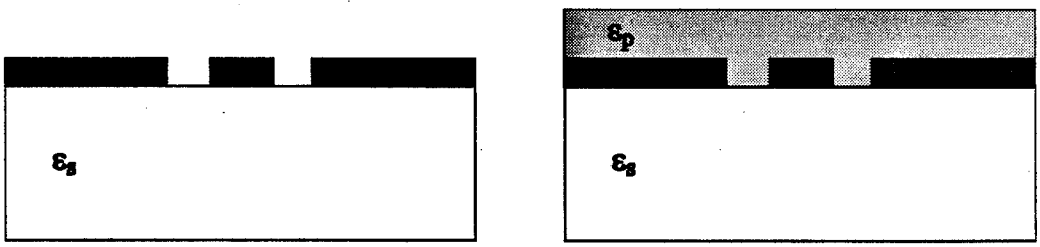

Figure 4-1 Reference and Test Structure

Once the propagation constant of the Reference Structure has been measured, the same structure is coated with the thin film dielectric. The structure with the

dielectric layer is referred to as the Test Structure. By using the same substrate and electrodes for the Reference Structure and the Test Structure, the line resistance and inductance per unit length are guaranteed to be identical. The dielectric material placed on top of the metalization only changes the capacitance and conductance per unit length. The dielectric constant of the thin layer can then be determined from the change in capacitance due to the added dielectric layers.

4.3 Extracting Waveguide Parameters From TRL Calibration

Network analyzers are commonly used to characterize a two-port network or component in terms of the S-parameters. The S-parameters contain the magnitude and phase response of a signal transmitted through and reflected from the sample, relative to the incident signal at each port [82].

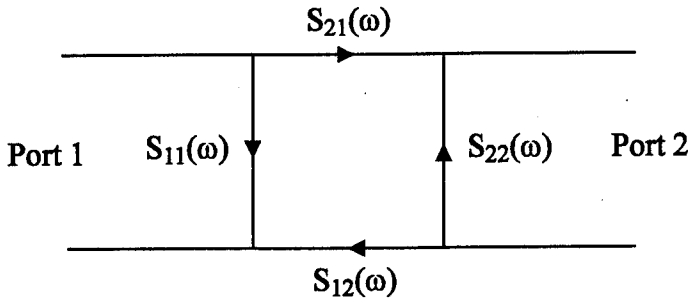

Figure 4-2 Definition of S-parameters in a two port network.

Dielectric measurements can be made by inserting the test sample into a fixture consisting of a coaxial or waveguide transmission line. Assuming the sample fixture is matched to the source and load impedances, the complex permittivity can be determined from the measured S-parameters. The refection coefficient is related to

the S-parameters by,

$$\Gamma(\omega) = K \pm \sqrt{K^2 - 1} \tag{4-2}$$

where,

$$K(\omega) = \frac{\left[S_{11}^2(\omega) - S_{21}^2(\omega)\right] + 1}{2S_{11}(\omega)}.$$

The complex dielectric constant can then be related to the reflection coefficient by,

$$\varepsilon_r(\omega) = \left(\frac{1-\Gamma(\omega)}{1+\Gamma(\omega)}\right)^2. \tag{4-3}$$

TRL calibration standards are used when making S-parameter measurements of a device on a network analyzer. These standards provide an easy way to remove the effects of the measurement system (probe contact, impedance mismatches, etc.) from a structure or device being measured [83], [84]. The TRL approach of calibration is unique in that it can be applied to non-coaxial devices and relies on transmission lines rather than discrete impedance standards such as opens and shorts. A TRL calibration requires a minimum of 10 measurements to calculate the 8 error constants that make up an error model for the system [85].

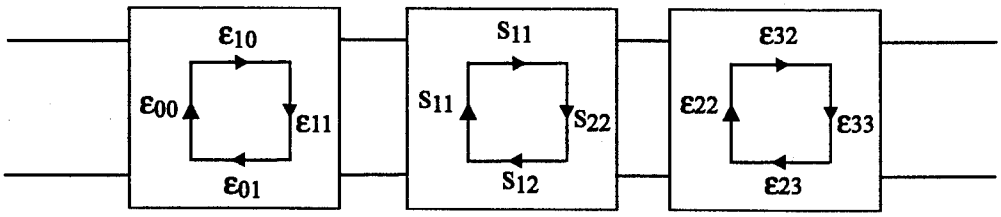

Figure 4-3 Eight of the errors terms in the TRL error model.

The basic TRL standard consists of three transmission lines including a THRU (T) connecting port 1 and port 2, a REFLECT (R_1,R_2) providing identical high reflections at each port and a LINE (L) of different length than the THRU. Because there are 10 measurements made in a TRL calibration, and 8 error coefficients, the complex reflection coefficient and the propagation constant of the line are determined along with the error coefficients. In the design of TRL standards, it is recommended that the insertion phase over the LINE be between 20^o and 60^o where ,

$$\Delta L(cm) = L_{LINE} - L_{THRU} = \frac{15}{\sqrt{\varepsilon_{eff}}[f_1(GHz) + f_2(GHz)]} \tag{4-4}$$

For large bandwidth measurements, it is often necessary to use several LINEs to meet this phase requirement. When several lines are used, the frequency range of each line is overlapped to provide a continuous calibration over the frequency range.

The TRL calibration is done on a probe station connected to a network analyzer. The probe station consists of a vacuum chuck used to hold the sample, 2 probes attached to micropositioners and a microscope. The probes used in this work were Tektronix, TMP 9615. These probes are designed to make contact with a coplanar waveguide structure and are connected to a coaxial line through a SMA connector. The S-parameters of each line are measured over the frequency range of interest and stored in the computer for future computation (Figure 4-4). The measurements can be made at higher frequencies, depending on the test set used.

Although a TRL calibration is designed to calibrate the measurement system and account for impedance mismatches, it also results in the complex propagation

constant of the line [86]. The complex propagation constants of the Reference Structure and the Test Structure can be accurately determined from the measured S-parameters using a multi-line TRL calibration technique developed by Marks and Williams at NIST [87]. The resulting complex propagation constants of the Reference Structure and Test Structure can then be used to find the equivalent circuit elements of the coplanar waveguide

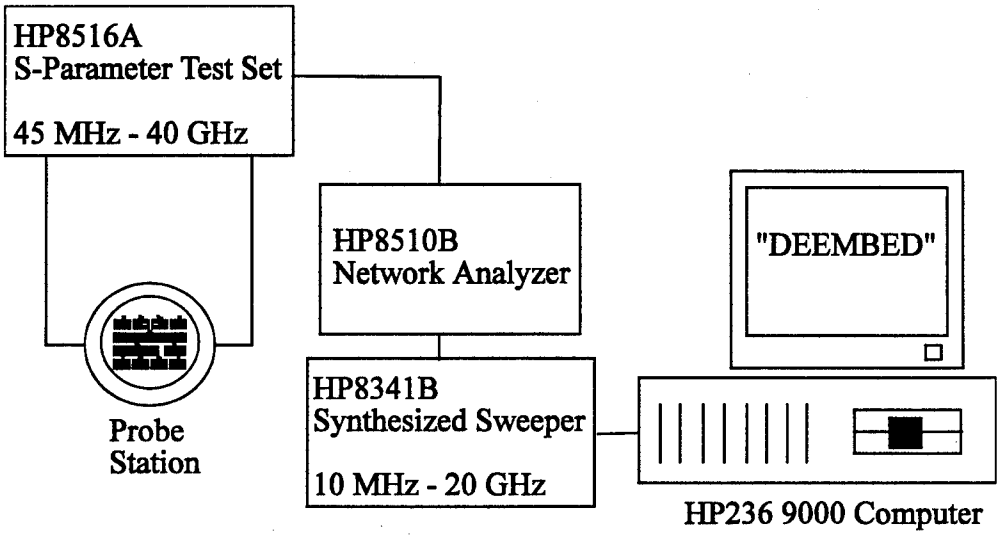

Figure 4-4 Measurement setup for determining the waveguide propagation constant.

transmission lines. The dielectric constant of the thin film can be extracted from the change in the capacitance of the Reference Structure and the Test Structure due to the top dielectric layer.

4.4 Extracting Dielectric Properties From The Waveguide Parameters

The process of extracting the dielectric properties of the thin film material from the propagation constants of the Reference Structure and the Test Structure

begins with determining the equivalent circuit parameters of the two waveguide structures. The propagation constant of a transmission line is given by,

$$\gamma(f) = \alpha(f) + j\beta(f) \tag{4-5}$$

where,

$\gamma(f)$ = propagation constant
$\alpha(f)$ = attenuation constant
$\beta(f)$ = phase constant.

A transmission line can be represented by a distributed resistance (R), inductance (L), capacitance (C) and conductance (G) per unit length (Figure 4-5). The value of each lumped element is frequency dependent.

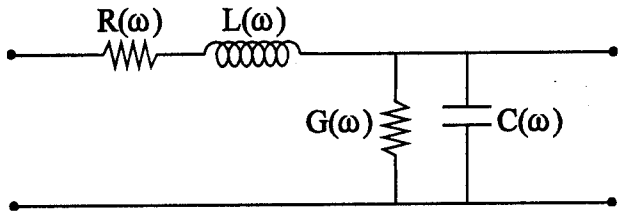

Figure 4-5 Equivalent lumped elements of a transmission line.

The propagation constant of the transmission line can be written in terms of the lumped circuit elements as,

$$\gamma\ (\omega) = \sqrt{[R(\omega) + j\omega L(\omega)][G(\omega) + j\omega C(\omega)]}. \tag{4-6}$$

The propagation constants of the Reference Structure and the Test Structure are determined from the TRL calibration. Let the propagation constant of the Reference Structure be given by,

$$\gamma_1(\omega) = \sqrt{[R_1(\omega) + j\omega L_1(\omega)][G_1(\omega) + j\omega C_1(\omega)]} \tag{4-7}$$

and the propagation constant of the Test Structure be given by,

$$\gamma_2(\omega) = \sqrt{[R_2(\omega) + j\omega L_2(\omega)][G_2(\omega) + j\omega C_2(\omega)]}. \tag{4-8}$$

It has been shown that for quasi-TEM lines, the resistance and inductance are primarily functions of the metal thickness and conductivity, while the capacitance and conductance are primarily functions of the dielectrics and line geometry [88]. Because the thickness and conductivity of the metal effect the ohmic loss, skin depth regions and overall charge distribution, the dispersion of the line can be seen in the resistance and inductance. The capacitance of the structure depends on its geometry of the structure and is relatively independent of frequency. Assuming a lossless dielectric, the conductance is negligible.

The measured propagation constants of the structures are both complex and dispersive. The technique for determining the dielectric properties of the thin film assumes that the measured dispersion of the Reference Structure is due to the resistance and inductance and that the capacitance and conductance are frequency independent. Because the Test Structure has the same metalization as the Reference Structure, the resistance and inductance are identical for both structures. In addition, the capacitance and conductance change due to the presence of the top dielectric layer. By comparing the measured propagation constants of the Reference Structure and the Test Structure, the dispersion due to the metalization and the top dielectric layer can be distinguished.

Assuming the substrate in the Reference Structure is lossless and that the capacitance is independent of frequency, the propagation constant can be written as,

$$\gamma_1(\omega) = \sqrt{[R_1(\omega) + j\omega L_1(\omega)][j\omega C_o]} \tag{4-9}$$

The first step in determining the resistance and inductance of the line is to determine the capacitance (C_O) of the Reference Structure. Two techniques can be used to determine C_O. The first technique uses a method developed at NIST [89] and requires a measurement of the DC resistance per unit length of the lines. The low frequency limit of the propagation constant, assuming a lossless dielectric, is given by,

$$\gamma_1(\omega) = \sqrt{j\omega C_L(\omega) R_{dc}} \tag{4-10}$$

where,

$$\lim_{\omega \to 0} R_1(\omega) = R_{DC} \text{ and } \lim_{\omega \to 0} C_1(\omega) = C_L(\omega).$$

The low frequency (C_L) capacitance of the Reference Structure in terms of the measured DC resistance and propagation constant is,

$$C_L(\omega) = \frac{1}{R_{dc}} \mathrm{Re}\left\{\frac{\gamma_1^2(\omega)}{j\omega}\right\} = \frac{2\alpha_1(\omega)\beta_1(\omega)}{\omega R_{dc}} \tag{4-11}$$

This capacitance is calculated over the measurement frequency range. To determine the frequency independent capacitance (C_O) of the line, C_L is extrapolated down to DC using a least squares fit.

The frequency independent capacitance (C_O) can also be determined using closed-form approximations. W. Heinrich has developed a quasi-TEM model of coplanar structures taking into account the effects of non-ideal conductors, finite

metallization thickness and substrate loss [90], [91]. From the model, the elements of the distributed equivalent circuit can be determined for a given coplanar waveguide structure.

From C_o and the measured propagation constant, the frequency dependent parameters $L_1(\omega)$ and $R_1(\omega)$ can be determined from,

$$R_1(\omega) = \mathrm{Re}\left\{\frac{\gamma_1^2(\omega)}{j\omega C_o}\right\} = \frac{2\alpha_1(\omega)\beta_1(\omega)}{C_o\omega} \tag{4-12}$$

$$L_1(\omega) = \frac{1}{j\omega}\mathrm{Im}\left\{\frac{\gamma_1^2(\omega)}{j\omega C_o}\right\} = \frac{\left[\beta_1^2(\omega) - \alpha_1^2(\omega)\right]}{C_o\omega^2}. \tag{4-13}$$

Because the same waveguide is used for the Reference Structure and the Test Structure, the resistance and inductance are identical and $R_2(\omega) = R_1(\omega)$, $L_2(\omega) = L_1(\omega)$. The capacitance and conductance of the Test Structure can now be determined from $R_1(\omega)$ and $L_1(\omega)$ and the measured propagation constant of the Test Structure by,

$$C_2(\omega) = \frac{1}{j\omega}\mathrm{Im}\left\{\frac{\gamma_2^2(\omega)}{R_1(\omega) + j\omega L_1(\omega)}\right\} \tag{4-14}$$

$$G_2(\omega) = \mathrm{Re}\left\{\frac{\gamma_2^2(\omega)}{R_1(\omega) + j\omega L_1(\omega)}\right\} \tag{4-15}$$

The final step in determining the dielectric constant of the thin dielectric is to compare the capacitance of the Reference Structure (C_o) and the Test Structure (C_2). Without loss of generality, the capacitance of the Test Structure can be related to the

dielectric constant of the substrate (ε_s) and the dielectric constant of the polymer (ε_p) by the relation,

$$C_2(\omega) = k_1\varepsilon_s + k_2\varepsilon_p(\omega) + k_3. \tag{4-16}$$

Similarly, the capacitance of the Reference Structure can be related to the dielectric constant of the substrate (ε_s) with ε_p=1 by,

$$C_o = k_1\varepsilon_s + k_2 + k_3. \tag{4-17}$$

By combining the relations for C_o and C_2 in Equations (4-16) and (4-17) and solving for the dielectric constant of the polymer, the dielectric constant of the polymer is given by,

$$\varepsilon_p(\omega) = \frac{C_2(\omega) - C_o}{k_2} + 1 \quad . \tag{4-18}$$

From the program developed to model the capacitance of a multi-layered structure with thick electrodes (Chapter 3), the DC capacitance of the Test Structure as a function of the dielectric constant of the top polymer layer for the given geometry can be determined. The result is an approximately linear relation between the capacitance and the dielectric constant. From Equation (4-16) it is seen that k_2 is the derivative of this relation and hence the slope of the line describing the capacitance as a function of the dielectric constant of the top layer,

$$k_2 = \frac{\partial C_2}{\partial \omega}. \tag{4-19}$$

The loss tangent of the dielectric thin film can be determined from the real and

imaginary parts of the dielectric constant by,

$$\tan\delta = \frac{\varepsilon_i}{\varepsilon_r} \tag{4-20}$$

from the calculated dielectric constant εp and the circuit parameters by,

$$\tan\delta = \frac{L_2(\omega)G_2(\omega) + R_2(\omega)C_2(\omega)}{\varepsilon_o\, Re(\varepsilon_p)\mu_o\omega} \tag{4-21}$$

or in terms of the propagation parameters as,

$$\tan\delta = \frac{2\alpha_2(\omega)\beta_2(\omega)}{\varepsilon_o\, Re(\varepsilon_p)\mu_o\omega}. \tag{4-22}$$

Thus, by measuring the propagation constants of the Reference Structure and the Test Structure, the complex dielectric constant of the thin film can be determined.

4.5 Measurements

The dielectric properties of several polymers were measured over the frequency range of 0.5 GHz to 40 GHz by patterning the TRL calibration standard shown in Figure 4-6 onto quartz wafers. The quartz wafers were 25 mils thick and the dielectric constant was assumed to be 3.85. The metallization consisted of 50 Å of tantalum and 1200 Å of titanium followed by a thick layer of aluminum. Three different aluminum thicknesses were fabricated (1.2 μm, 1.8 μm and 2.2 μm) to verify the validity of this technique in extracting the dielectric properties. The 50 Ω TRL standards on the Reference Structure were designed to have a center conductor width (S) of 100 μm, a gap width (W) of 10 μm, and a ground conductor width (G) of

2000 μm. After processing, the actual center conductor width was 110 μm and the gap was 17.5 μm. The length of the THRU was 0.5 cm. In order to cover the frequency range of 0.5 GHz to 40 GHz three LINEs were required, as shown in Table 4-1.

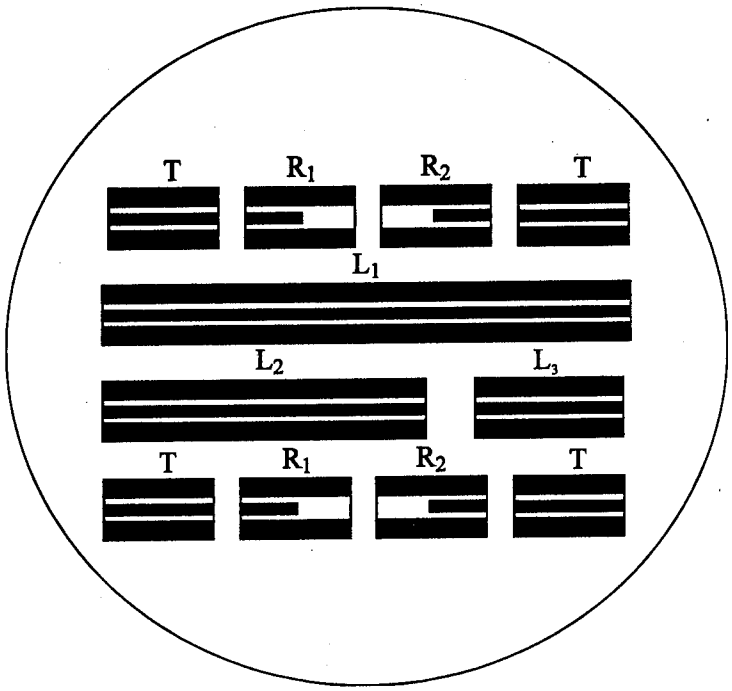

Figure 4-6 TRL Layout on a 3 inch wafer

Table 4-1 Lengths of lines used in TRL standard for quartz for 0.5 GHz to 40 GHz.

Line Type	Length (cm)
THRU	0.5
LINE 1	2.641
LINE 2	0.844
LINE 3	0.709
REFLECT	0.250

The complex propagation constant of the Reference Structure was measured from 0.5 GHz to 40 GHz using the setup shown in Figure 4-4. A 1/4" thick plate of plexiglass was placed between the sample and the wafer chuck to prevent additional modes being set up between the waveguide structure and the metal wafer chuck. The Test Structure was fabricated by spinning a 2.2 μm thick layer of polymer (PMMA-DR1 10 mer%) on top of the Reference Structure. Small areas at the ends of each coplanar line were masked off before spinning to provide clear areas for the probe contact. The S-parameters were measured for each transmission line in the TRL calibration. Figure 4-7 shows the uncalibrated and calibrated S-parameters for the THRU. When the calibration is applied to the THRU, S_{12} and S_{21} are flat at 0 dB and the reflection parameters, S_{12} and S_{21} are less than -40 dB.

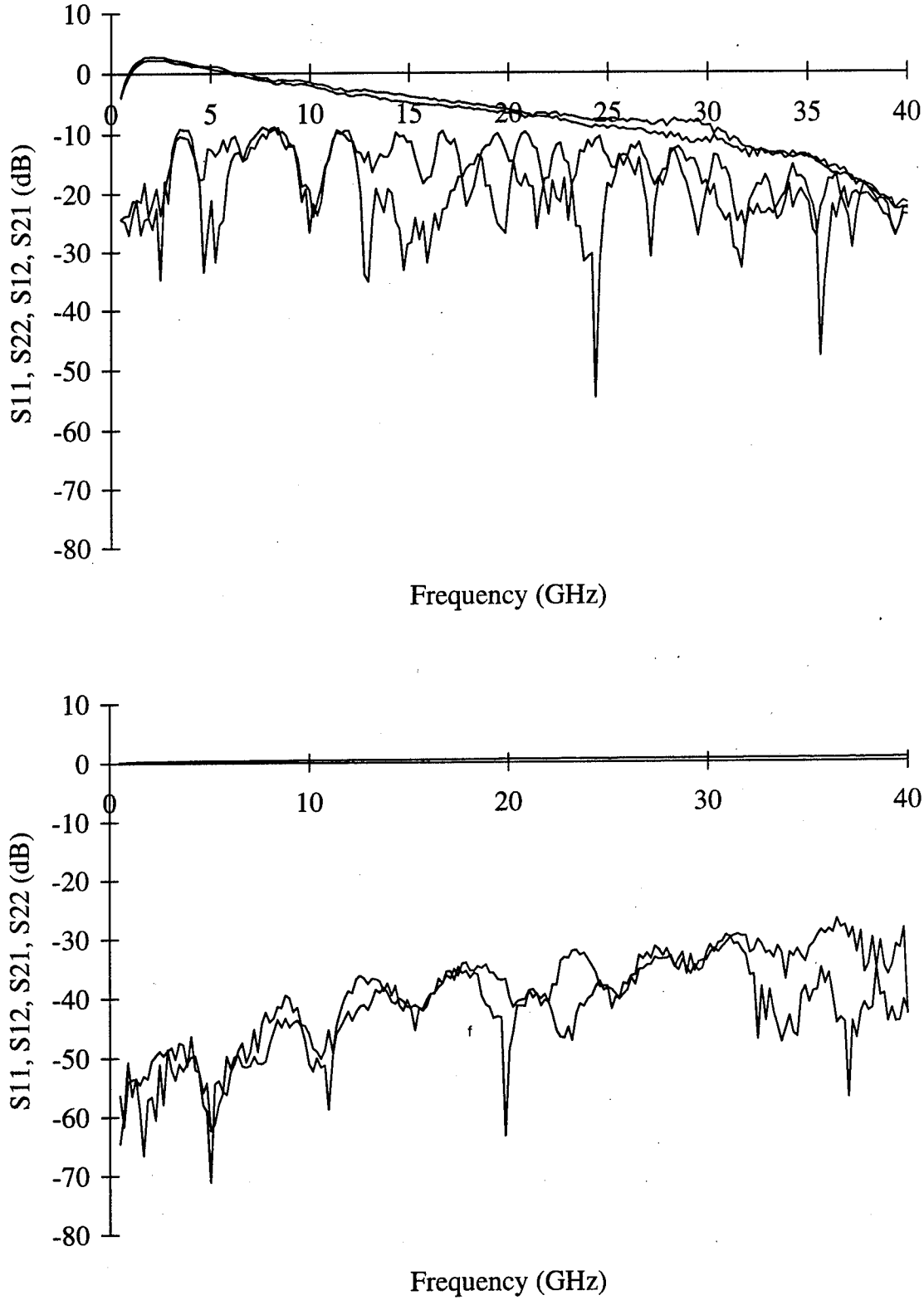

Figure 4-7 Measured S-parameters for the uncalibrated and calibrated THRU.

4.6 Results

The complex propagation constants of the Test Structure and Reference Structure were determined from the measured S-parameters of each line using DEEMBED. Figure 4-8 shows the attenuation of Reference Structure and the Test Structure calculated from the measured propagation constants, along with the attenuation predicted by W. Heinrich for this geometry. The attenuation of the Test Structure is slightly greater than the attenuation of the Reference Structure due to the presence of the top dielectric layer. The low frequency attenuation is due to the resistive losses of the metal, while the high frequency attenuation is due to skin depth effects. For low loss lines at low frequencies, the loss is related to the DC resistance and the impedance by,

$$\alpha\left(\frac{\Omega}{m}\right) = \frac{R_{DC}}{2Z_o} \tag{4-23}$$

where,

$$\alpha\left(\frac{dB}{m}\right) = 20\left[\log\left(e^{\alpha\left(\frac{1}{m}\right)}\right)\right].$$

The DC resistance of this 50 Ω line was measured to be 329.1 (Ω/m), resulting in a loss

of 3.291 (1/m) or 0.285 dB/cm. This attenuation agrees well with the measured and attenuation predicted by W. Heinrich.

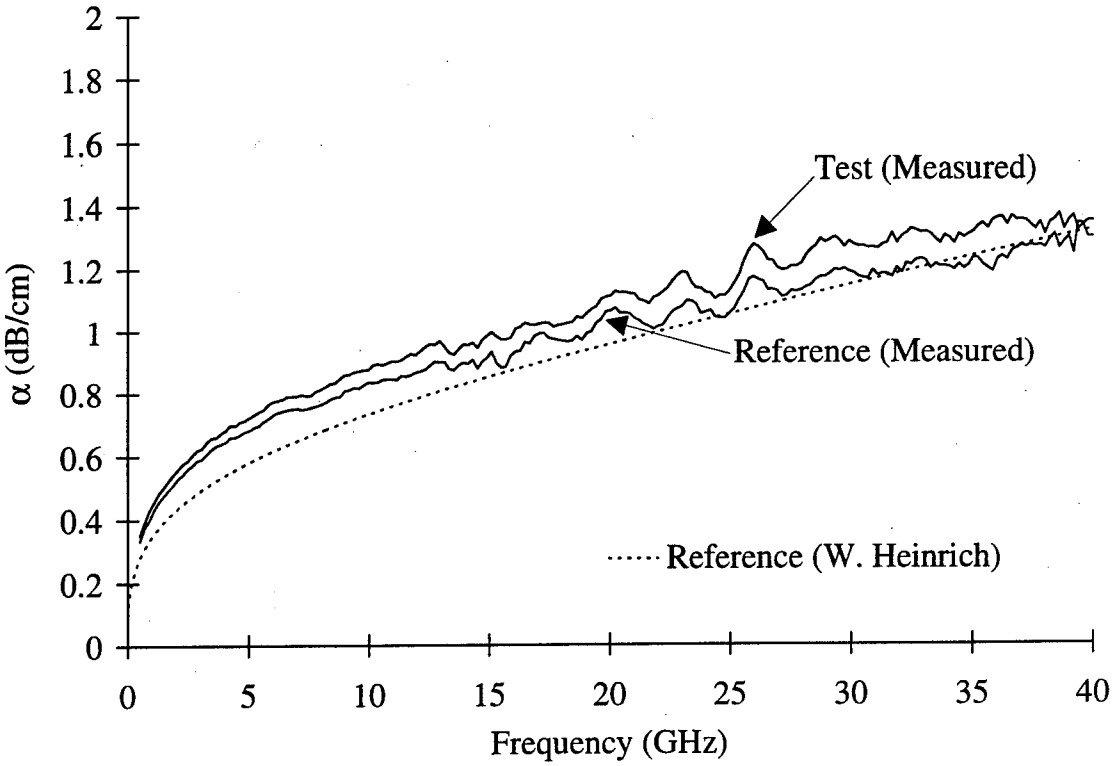

Figure 4-8 Attenuation of the Reference Structure and Test Structure for a CPW with 110 μm center conductor, 17.5 μm gap, 1.2 μm thick Al electrodes and 2.2 μm thick polymer layer.

Figure 4-9 shows the normalized phase constant of the Reference Structure and the Test Structure along with that predicted by W. Heinrich for this geometry where,

$$\beta = \omega\sqrt{LC} = \omega\sqrt{\mu_o \varepsilon_o \varepsilon_{eff}}$$

$$\beta_o = \omega\sqrt{\mu_o \varepsilon_o} \qquad (4\text{-}24)$$

$$\frac{\beta}{\beta_o} = \sqrt{\varepsilon_{eff}} \cong \sqrt{\frac{1+\varepsilon_s}{2}}.$$

The phase constant is also increased slightly due to the top dielectric layer. The dielectric constant of quartz is 3.85, resulting in a $\beta/\beta o$ of 1.557 (1/m), which also agrees with the measured and predicted values.

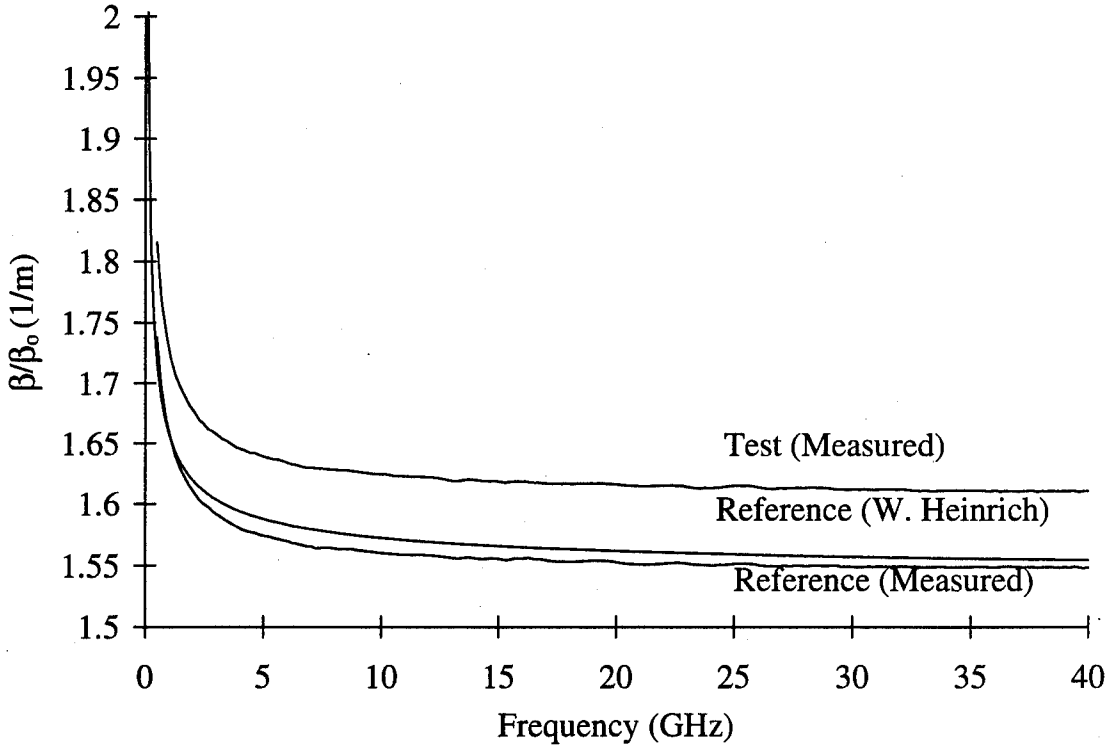

Figure 4-9 Normalized phase constant of the Reference Structure and Test Structure for a CPW with 110 μm center conductor, 17.5 μm gap, 1.2 μm thick Al electrodes and 2.2 μm thick polymer layer.

The capacitance C_o was determined using W. Heinrich's program, resulting in a value of 93.684 pF/m. The technique of extrapolating to find C_o could not be used because the lowest frequency that could be measured in our system was 0.5 GHz. From C_o and the measured propagation constants, the resistance (R_1) and inductance (L_1) were calculated. The resistance is shown in Figure 4-10.

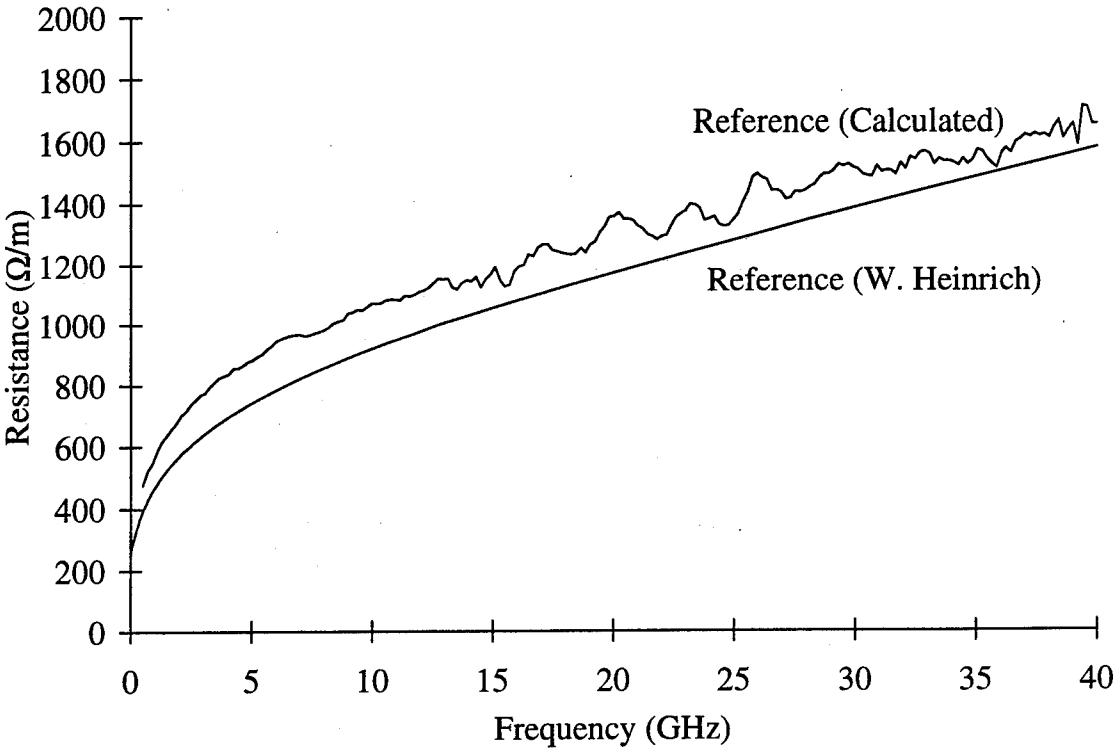

Figure 4-10 Resistance calculated from the measured propagation constants and C_o and the resistance predicted by W. Heinrich.

The DC resistance of the line can be approximated by,

$$R\left(\frac{\Omega}{m}\right) \cong \frac{1}{\sigma T}\left[\frac{1}{S}+\frac{1}{2G}\right]. \tag{4-25}$$

For the dimensions used in these measurements, this corresponds to a resistance of 321.9 Ω/m. The high frequency resistance is due to the skin depth effect. The resistance due to the skin depth can be approximated by,

$$R\left(\frac{\Omega}{m}\right) \cong \frac{2}{\delta \sigma S} \tag{4-26}$$

where the skin depth is given by,

$$\delta = \frac{1}{\sqrt{\pi f \mu_o \sigma}}. \qquad (4\text{-}27)$$

For the aluminum electrodes, the skin depth at 40 GHz is 0.459 μm, resulting in a resistance per unit length of 1319.1 Ω/m.

The resulting measured inductance and predicted inductance are shown in Figure 4-11.

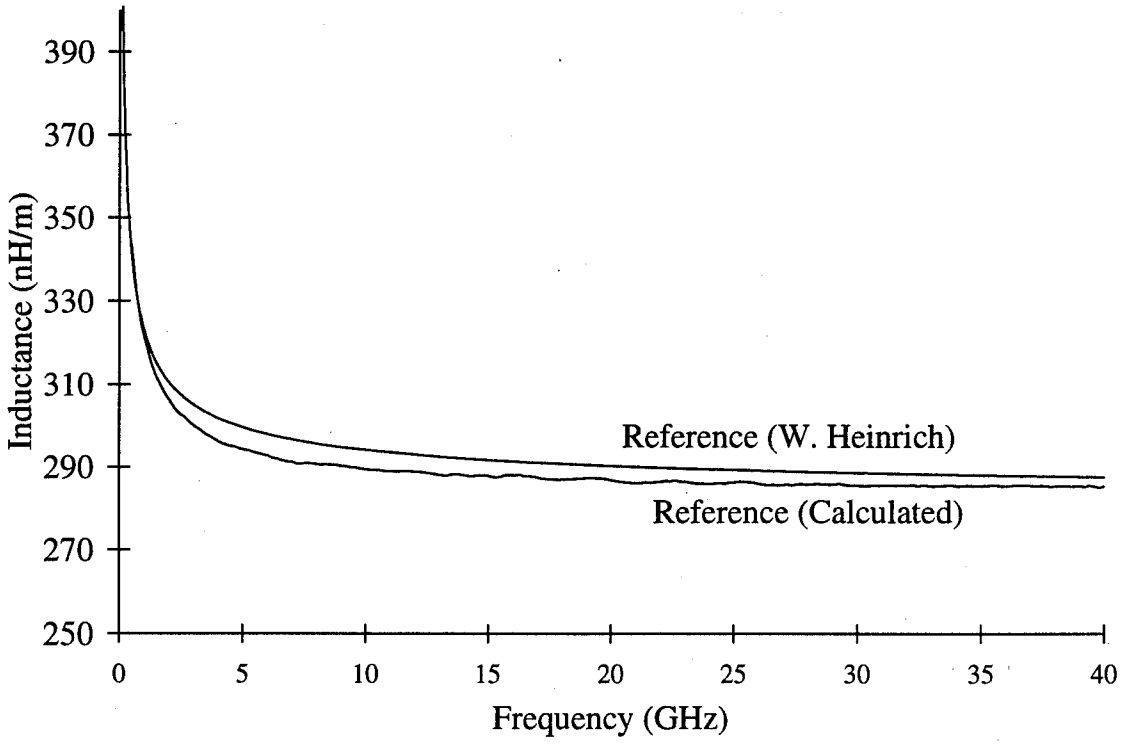

Figure 4-11 Resistance calculated from the measured propagation constants and C_o and the resistance predicted by W. Heinrich.

With the measured propagation constant of the Test Structure, the calculated resistance ($R_2 = R_1$) and the calculated inductance ($L_2 = L_1$), the capacitance (C_2) and conductance (G_2) of the Test Structure could be determined (Figure 4-12 and Figure 4-13).

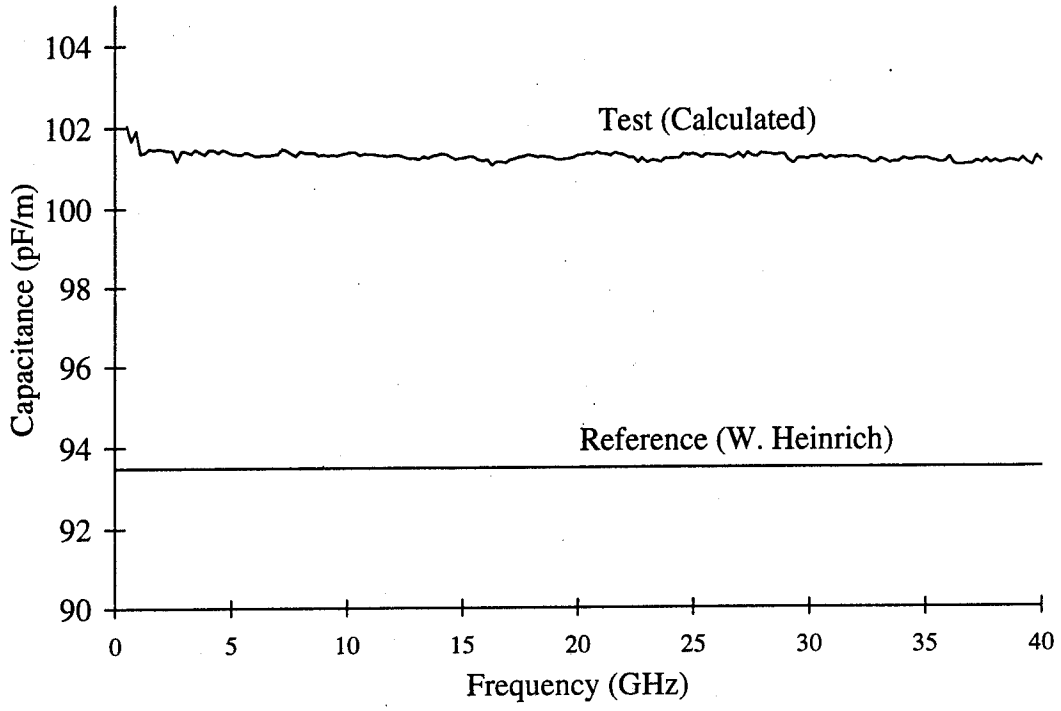

Figure 4-12 Capacitance of Reference and Test Structure

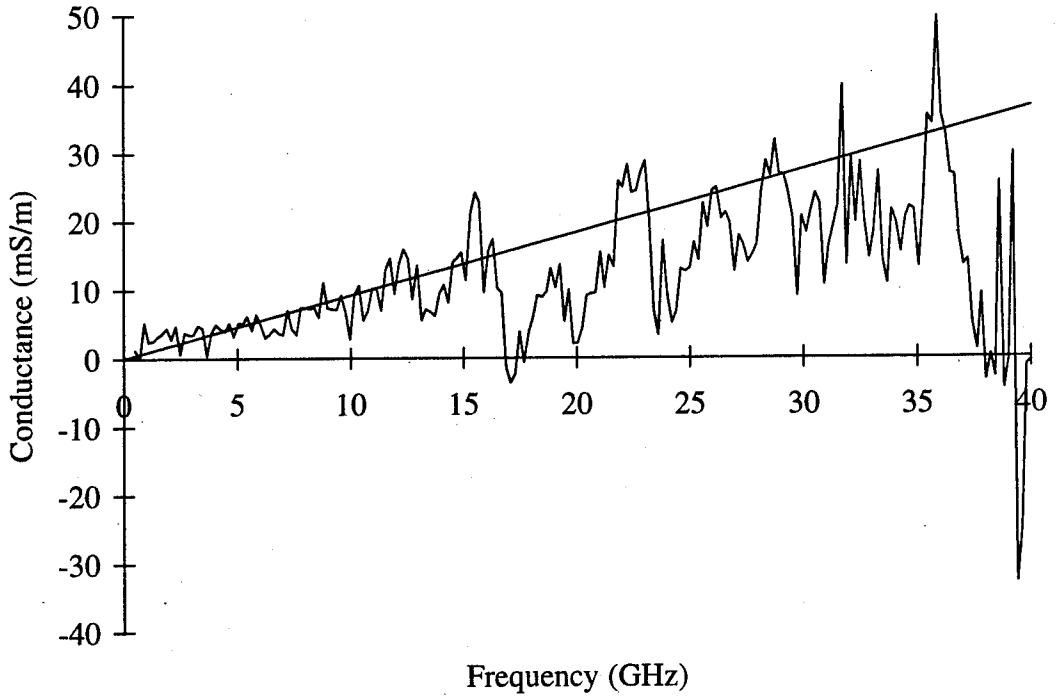

Figure 4-13 Conductance of Test Structure

As shown in Figures 4-10 through 4-13, the dispersion of the lines shows up in the resistance and inductance as expected and the capacitance is increased due to the dielectric layer, but is flat with frequency. The high frequency fluctuations in the conductance are exaggerated because the conductance is so small.

The next step was to determine the proportionality constant k_2 for a 2.2 μm thick layer of polymer above the electrodes that are 1.2 μm thick. The model presented in Chapter 3 was used to determine the effect of the dielectric material on the capacitance of the structure. The capacitance was calculated for different thickness of dielectric having dielectric constants ranging from 1 to 4, as shown in Figure 4-14.

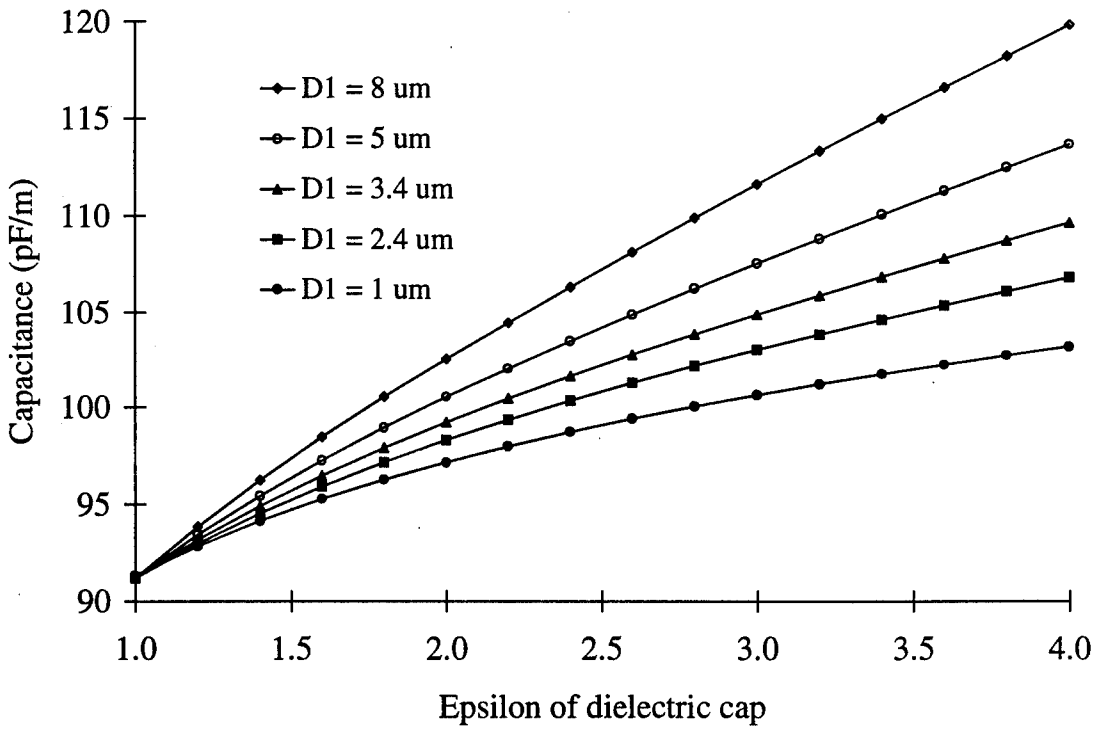

Figure 4-14 Capacitance of the Reference Structure for different dielectric materials and thicknesses on top of the electrodes.

Because the dielectric constant of the polymer known apriori to be between 3 and 4, the slope of the capacitance curve over this range was determined for several different polymer thicknesses. This data was compiled for two different metal thicknesses and is shown in Figure 4-15.

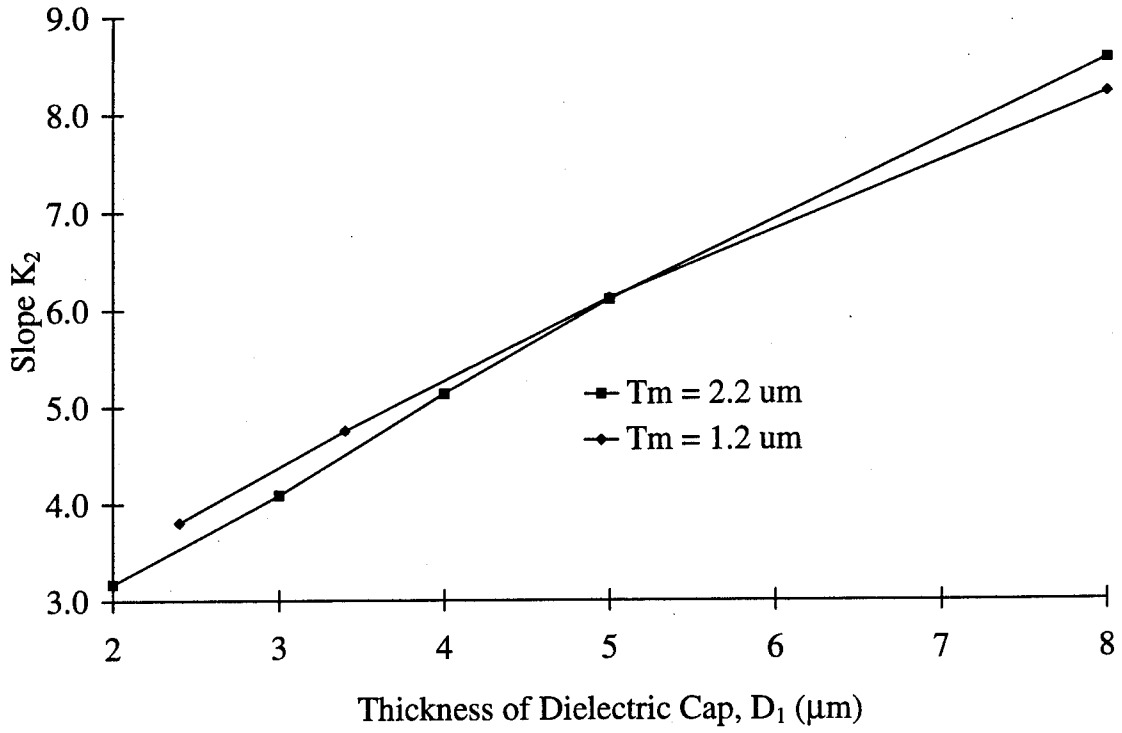

Figure 4-15 Slope of the capacitance verses dielectric constant for εp between 3 and 4.

From Figure 4-15, k_2 was determined to be 3.4 pF/m for a polymer thickness of 2.2 μm. The dielectric constant of the polymer could then be extracted from the capacitance measurements. A plot showing the effective dielectric constant of the Reference Structure and Test Structure is shown in Figure 4-16.

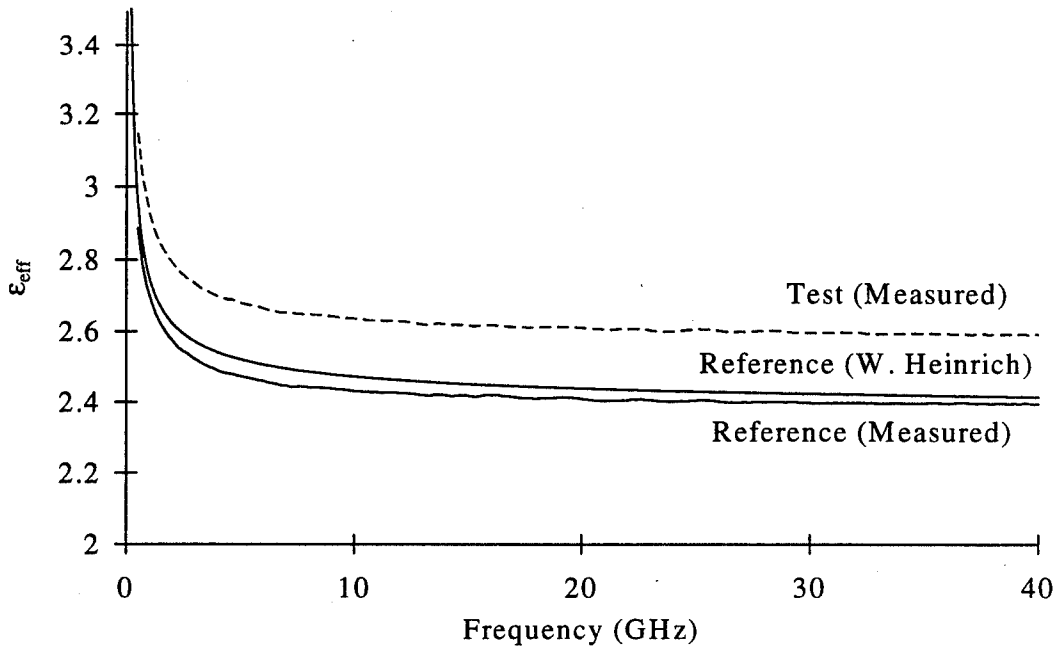

Figure 4-16 Epsilon effective of the Reference and Test Structure and ε of the polymer

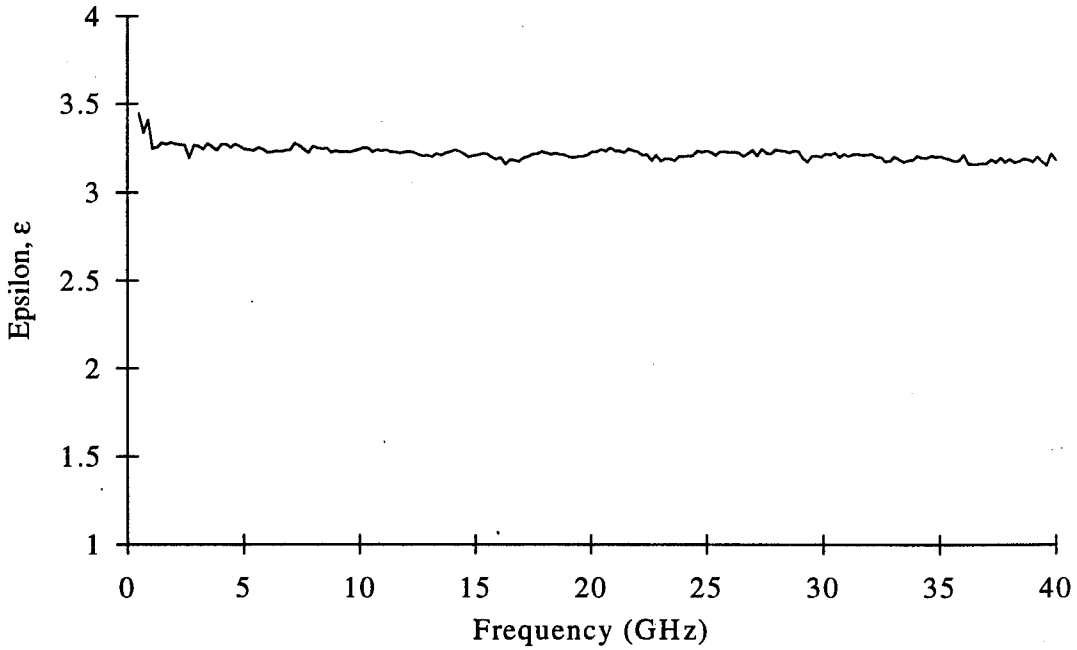

Figure 4-17 Dielectric constant of a 2.2 μm layer of PMMA/DR1 from 0.5 to 40 GHz.

The dielectric constant of the polymer was determined to be flat out to 40 GHz and had a value of 3.3. The loss tangent of the material was determined to be less than 0.05. These measurements show that the dielectric constant of the polymer is very flat out to frequencies of 40 GHz and that the loss is very low. The low dielectric constant and low loss make this material ideal for high-speed electro-optic applications. Several measurements were made on the same polymer, but with different thickness electrodes, and the dielectric constant was extracted to the same value.

4.7 Conclusion

A technique has been developed for determining the dielectric constant of a thin layer of optical polymer for electro-optic applications. The technique extracts the dielectric constant of the thin film from the propagation constant of a coplanar waveguide structure, before and after it is coated with a dielectric layer. The effect of the electrode thickness on these propagation constant can be taken into account. From this technique, a data base of the dielectric properties of NLO materials can be constructed. The technique can also be used to characterize the polymers after bleaching and poling. Although these measurements were made from 0.5 GHz to 40 GHz, they can be made at higher frequencies depending on the measurement system. The technique is very general, and can be used to characterize any thin dielectric material at microwave frequencies.

Chapter 5

ELECTRO-OPTIC PROPERTIES OF POLED POLYMER WAVEGUIDES

5.1 Introduction

In order for NLO polymers to be used for electro-optic applications, they must be efficiently and completely poled. The electro-optic coefficient is strongly dependent on the configuration used for poling. The poling process consists of heating the sample up to a temperature near the glass transition temperature of the material, applying a strong electric field (10 - 100 V/μm), maintaining that field for a sustained period of time, cooling the material back down to room temperature with the poling field still present and then removing the field when the material has cooled back down to room temperature. This process is shown in Figure 5-1. The resulting molecular alignment makes the material noncentrosymmetric.

This chapter will begin with a comparison of various electrode configurations used for poling. A discussion of some of the factors that can influence the strength and distribution of the poling field will then be presented. Depending on the configuration used, the conductivity of the buffer relative to the conductivity of the polymer can change the effective field across the polymer. A brief description of the techniques currently used to measure the electro-optic coefficient of a poled polymer will be presented, followed by a description of the technique used in this work. This

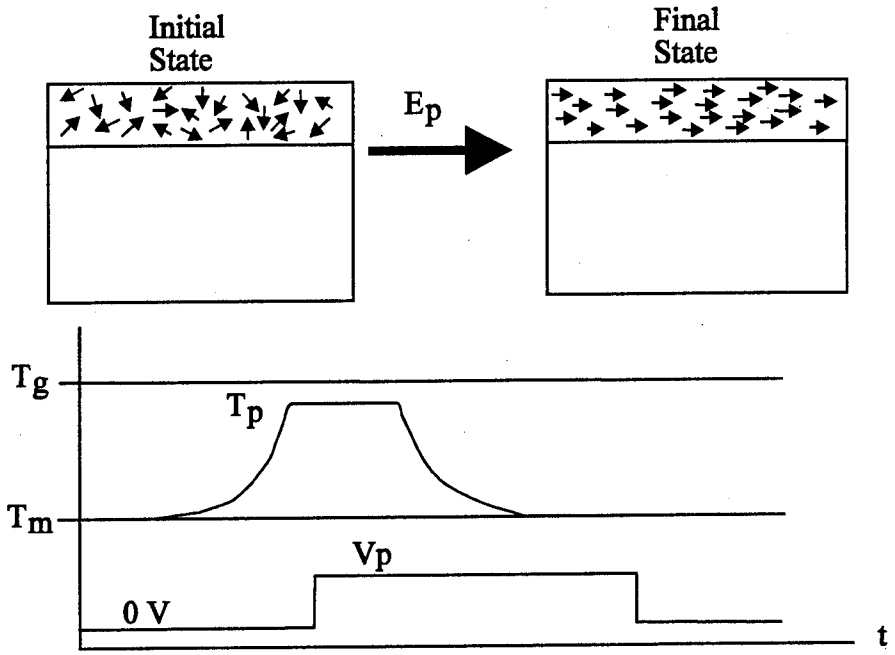

Figure 5-1 Process of poling a thin polymer film.

technique is based on an all fiber Mach-Zehnder interferometer and has been tested on transversely poled polymer waveguides.

The measurement setup for this fiber Mach-Zehnder is unique in that the sample can be poled and the resulting electro-optic coefficient monitored at the same time. By monitoring the electro-optic coefficient during the poling process, the dynamics of poling can be studied, including the time necessary to complete the molecular alignment and the effect of the poling temperature relative to the glass transition temperature of the polymer on the alignment. As with the characterization of the dielectric constants of polymers presented in Chapter 4, an emphasis is placed on doing the electro-optic characterization of the materials as they will be used in multi-layered devices that can be coupled to optical fibers.

5.2 Poling Configurations

The four most common configurations used for poling polymers are corona, parallel plate, vertical electrode and transverse electrode. The configurations vary depending on whether the bulk properties of the poled polymer layer are of interest or the properties specific to a poled optical waveguide. Electrode poling is compatible with poled optical channels. In some cases one configuration is used for poling and another is used for the actual device modulation or switching. When considering different device configurations, the buffer layers surrounding the polymer layer must also be characterized. The poling electrode configuration determines which polarization of light, either TE or TM, the guide will support and which types of switching devices can be formed.

In corona poling, shown in Figure 5-2, a metal electrode is placed on the bottom of a substrate and then the polymer layer is spun on top of the substrate [92], [93], [94].

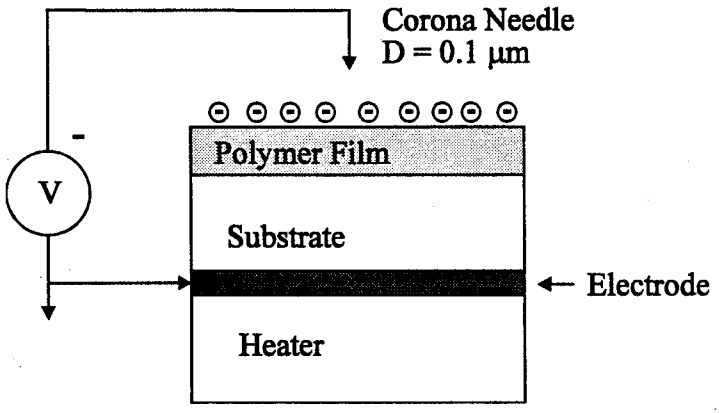

Figure 5-2 Setup for corona poling.

The lower electrode is grounded and a corona-needle, usually made of tungsten, is placed above the sample and raised to the poling potential. Once there has been discharge, ions are created and form on the top of the polymer structure. A fairly uniform electric field is then produced across the polymer.

Parallel plate poling is very similar to corona poling, as shown in Figure 5-3.

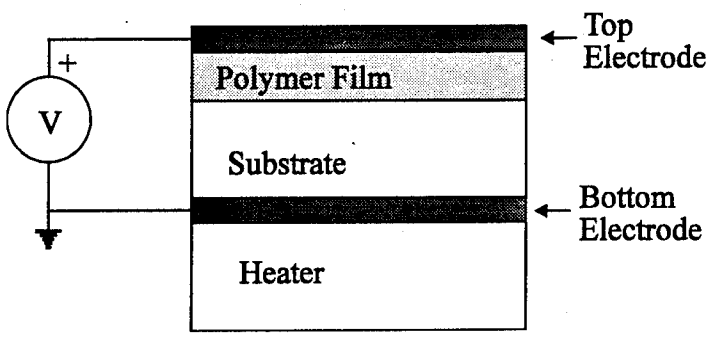

Figure 5-3 Parallel plate poling setup.

In this configuration, a top electrode is placed directly on the polymer. The poling potential is applied to this top electrode [95], [96]. Any pinholes or defects in the metal can cause high current concentrations and lead to dielectric breakdown across the material. In both corona poling and parallel plate poling, the entire surface is poled including both the bleached and unbleached areas. The top metal layer is typically removed after poling and separate switching electrodes can be fabricated above the optical channels.

When using electrode poling, rather than corona or parallel plate poling, areas can be selectively poled according to the pattern of the poling electrodes [97]. In

vertical poling, shown in Figure 5-4, a microstrip electrode is used as the poling electrode and placed directly over the optical guide.

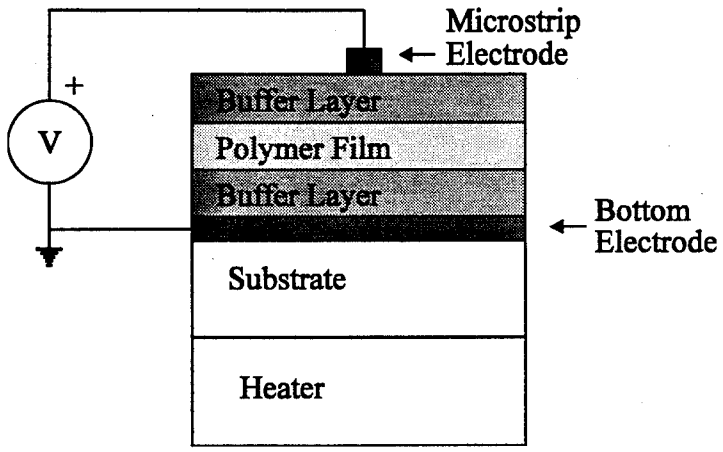

Figure 5-4 Microstrip poling configuration.

As mentioned earlier, the impedance of a microstrip waveguide is a function of the dielectric constants of the materials and the thicknesses of the substrate and dielectric layers. Therefore, the width of the center electrode cannot be varied to match the width of the optical guide without altering the impedance of the line. In microstrip poling, the molecules are aligned vertically under the microstrip electrode, causing the channel to support TM polarized light (perpendicular to the surface of the polymer). Because the electrodes are placed directly over the channels, the overlap of the optical fields and switching fields can be close to 100%.

In transverse electrode poling, two electrodes are placed parallel to each other either above or below the polymer layers. If the electrodes are placed on top of the

polymer layers, a material with a high dielectric strength must be placed over the electrodes during poling so that the electric field won't break down in the air (V_b = 3 V/μm) between the center electrode and the ground electrode. By placing the electrodes beneath the polymers, which have breakdown strengths around 100 V/μm, a high poling field can be applied, Figure 5-5.

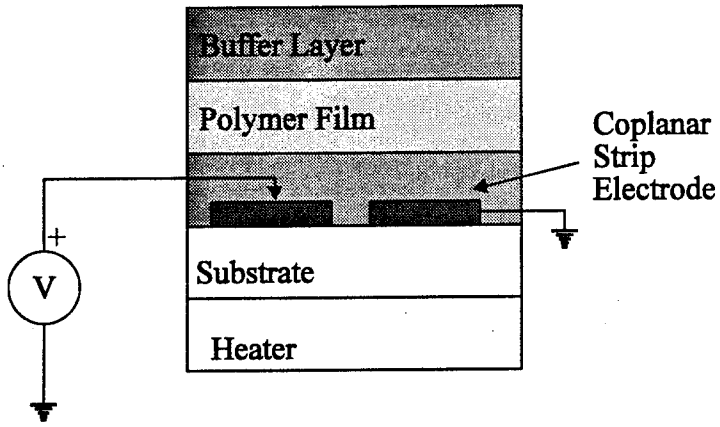

Figure 5-5 Buried coplanar strip electrode poling.

The channels poled by transverse electrodes will support TE polarized light (parallel to the surface of the polymer).

By using coplanar waveguide electrodes, two parallel optical channels can be poled in the opposite direction by putting a positive voltage on the left electrode, grounding the center electrode and putting a negative voltage on the right electrode, as shown in Figure 5-6.

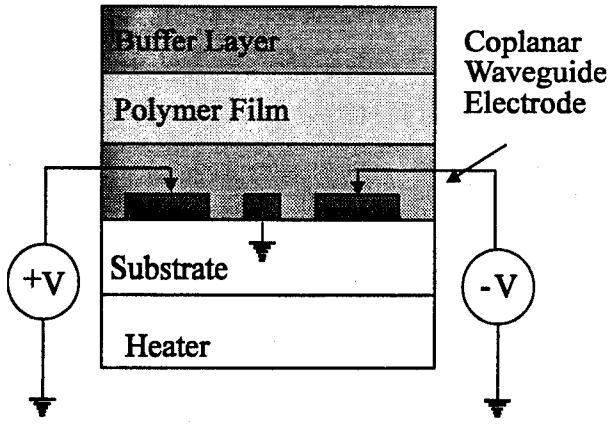

Figure 5-6 Configuration used to pole to parallel optical waveguides with the opposite voltage.

Then by applying the switching voltage to the center electrode and grounding the two outer electrodes, the channels can be modulated in a push/pull configuration.

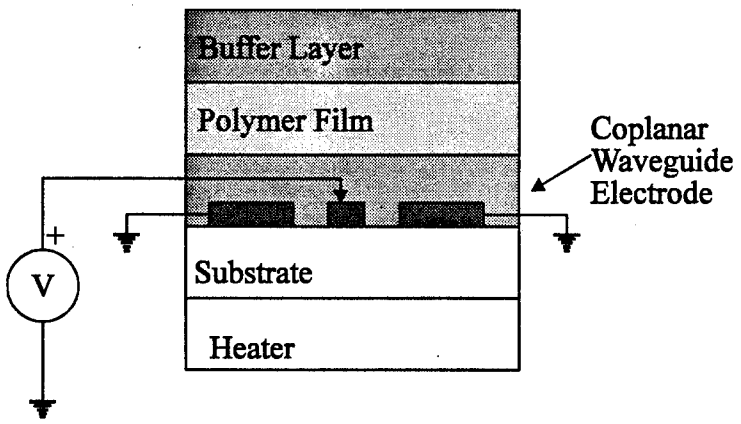

Figure 5-7 Configuration used for push/pull modulation.

When these channels are modulated, the index change increases in one arm and decreases in the other, resulting in a larger electro-optic effect. The coplanar waveguide electrodes can be used for both poling and modulation, reducing the

processing steps involved in the fabrication of polymeric devices. Depending on the configuration and electro-optic coefficient of the material, the optical channels can be formed by poling alone, eliminating the fabrication step of bleaching the optical waveguide.

In polymeric devices, a buffer layer is usually placed above and below the polymer layer, and the entire structure is poled. Depending on the poling configuration, the conductivity difference between the buffer material and the polymer material can alter the effective poling field. Ideally the conductivity of the polymer and the buffer should be identical and very small. If the polymer is poled using parallel plate electrodes, and the conductivity of the buffer is greater than the conductivity of the polymer, the entire voltage will be dropped across the polymer, resulting in a much larger effective poling field [98].

It has been reported that, depending on the geometry, charge may be injected into the polymer, effecting the measured electro-optic coefficients [99], [100], [101]. The trapped charges have an internal field that may oppose the applied field and reduce the measured electro-optic effect.

5.3 Device Configuration

As has been emphasized throughout this dissertation, coplanar waveguide electrodes are used because they maintain a planar surface and can be designed for the desired impedance. The efficiency of the poling process depends on many parameters including the thicknesses of the buffer and polymer layers and the electrode spacing.

Buried coplanar waveguide electrodes were used as the poling electrodes in the experiments described here, Figure 5-8.

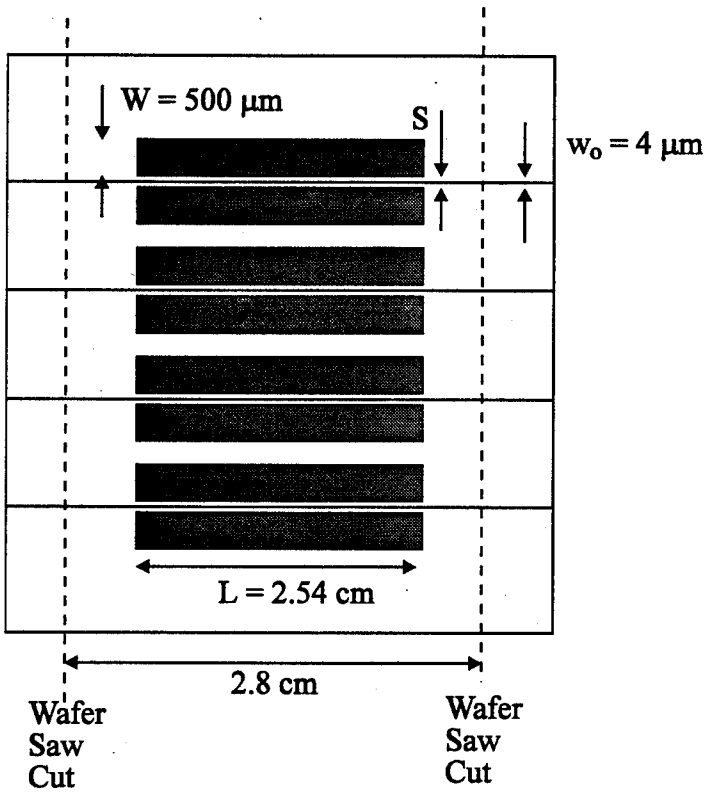

Figure 5-8 Configuration of sample used in poling experiments.

The samples used in this work were prepared by spin coating a buffer layer (5 μm) and polymer layer (2.2 μm) on top of coplanar strip electrodes. The aluminum electrodes were 0.5 μm thick and 500 μm wide with gap widths (S) of 10, 20, 30, 60 and 100 μm. Optical channels, 4 μm wide, were formed in the polymer by bleaching.

After the top buffer layer was spun on, the endfaces of the samples were prepared by sawing the ends off with a wafer saw. The resulting surface roughness was less than 0.1 μm.

5.4 Poling Considerations

The overlap of the optical fields and the electric fields in an anisotropic medium must be determined for electro-optic devices made from polymers [102], [103]. The model presented in Chapter 3 was used to determine the electric field distribution as a function of the thickness and dielectric constant of the top dielectric layers. This information can then be used in optimizing the poling process and in determining the best position for the optical guides relative to the gaps in the electrodes. The magnitude of the x-component of a 50 V/μm electric field applied across two different gap widths was computed from y = T to y = 20 μm. As shown in Figure 5-9, the electric field across the 10 μm gap decays faster in the y direction than it does for 50 μm gap.

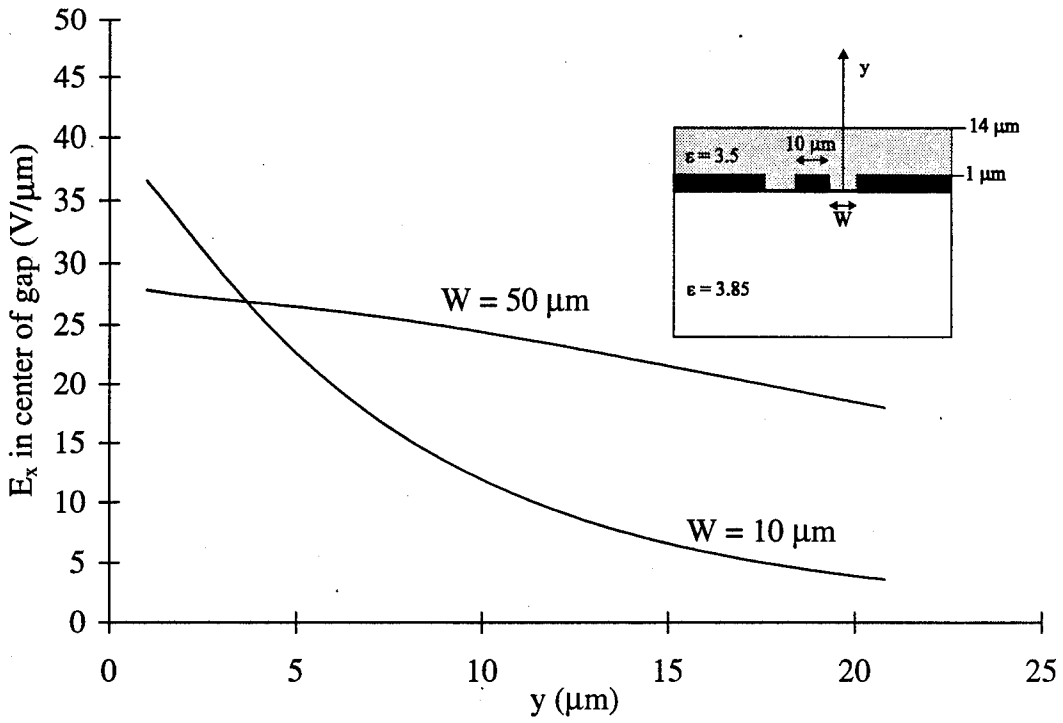

Figure 5-9 Magnitude of the x component of the electric field in the center of a 50 μm gap and a 10 μm gap for an applied field strength of 50 V/μm.

There is a tradeoff between how quickly the electric field drops off and how much voltage is needed across the gap to get the required field strength.

For maximum switching, the electric field should completely overlap the optical fields in the guide and be uniform throughout the guide. Figure 5-10 shows the electric field distribution for a 50 μm gap over the region defined by the optical guide. The optical guide is 4 μm wide and 2 μm thick and is centered directly over the gap in the electrodes.

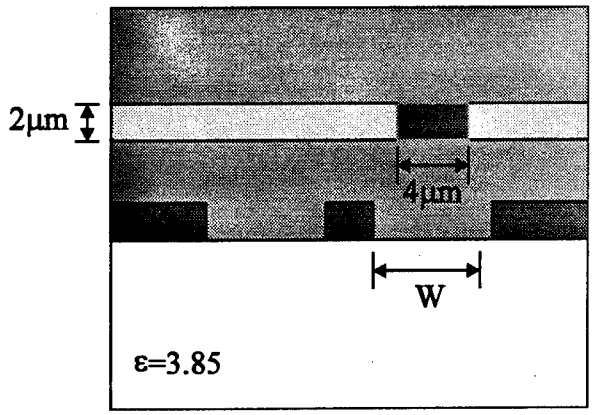

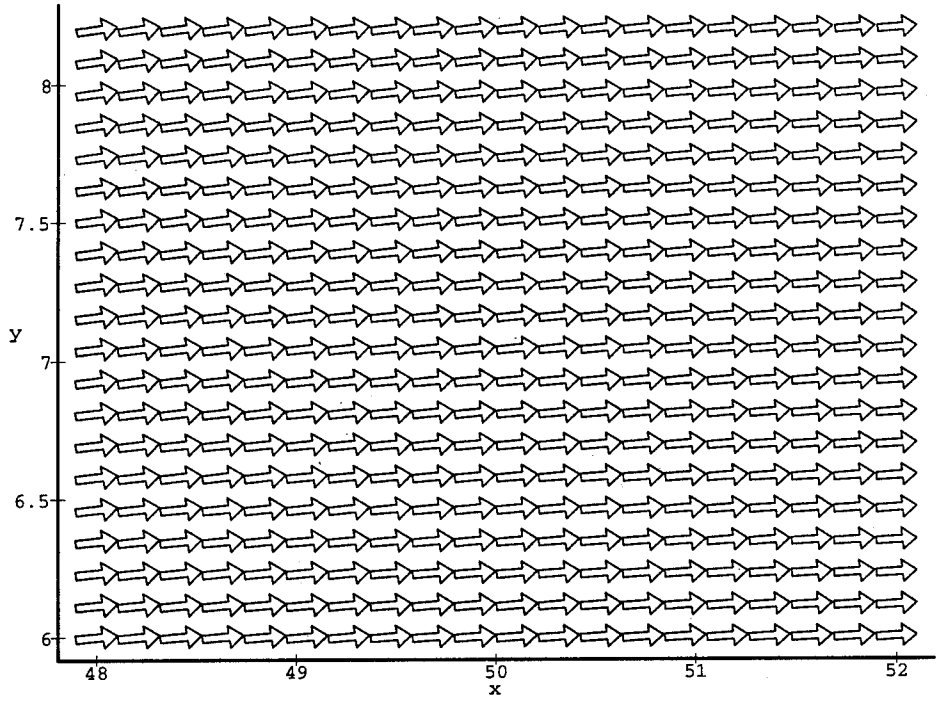

Figure 5-10 Vector field plot of electric field within the optical guide (4 μm x 2.2 μm) for an electrode gap of 50 μm. The CPW electrodes are coated with a 13 μm thick layer of dielectric with ε = 3.5.

Because the poling is done at temperatures near the glass transition temperature of the polymer, the conductivity of the materials as a function of temperature is important. The conductivity of the buffer/polymer/buffer structure coating coplanar electrodes was measured using an HP 4145B Semiconductor Parameter Analyzer. In this measurement, the voltage applied to one electrode was swept from 0 to 50 volts while the other electrode was grounded and the resulting current was measured (Figure 5-11).

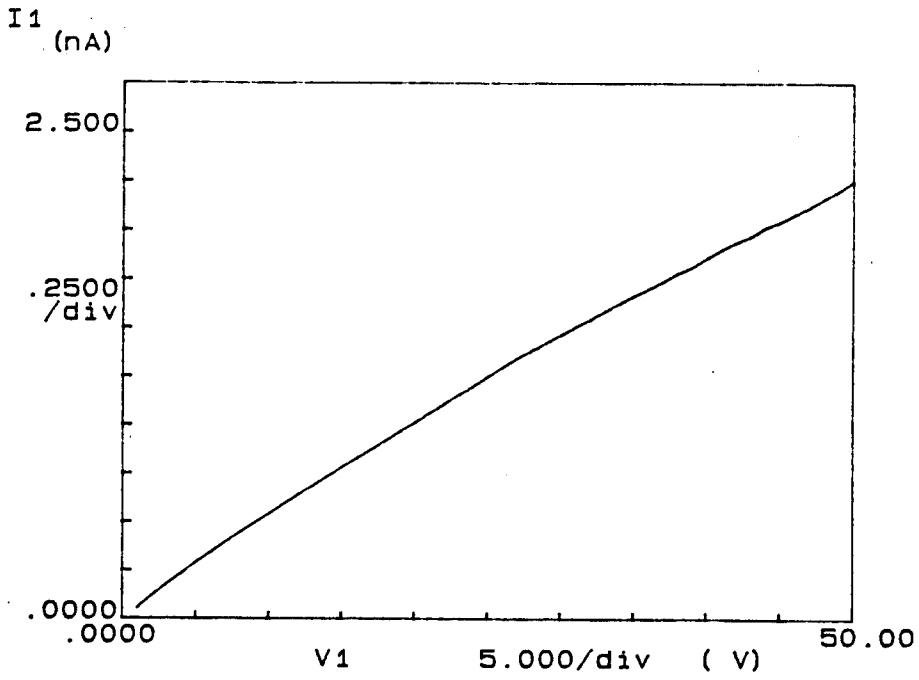

Figure 5-11 Example IV curve used to measure effective resistance of polymer.

The effective resistance of the structure was determined by finding the slope of the IV curve as the sample was heated. The resistance as a function of temperature is shown in Figure 5-12.

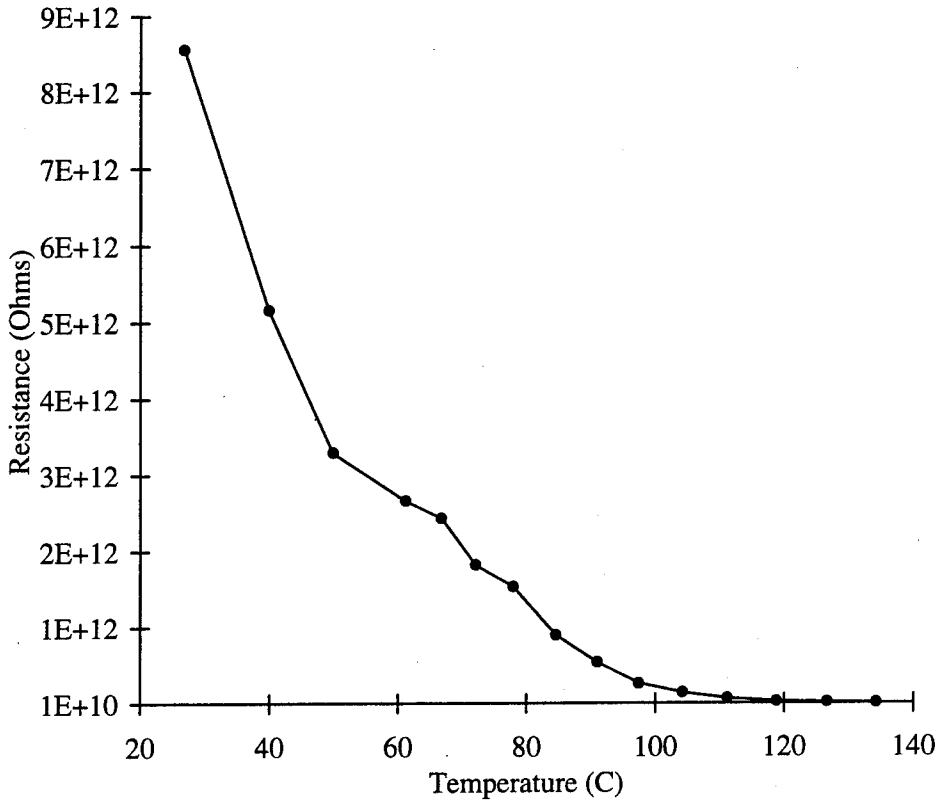

Figure 5-12 Effective resistance of a CPW structure as the sample is heated.

As shown in Figure 5-12, the effective resistance of the structure decreases dramatically at temperatures near the glass transition temperature of the polymer. Because the effective resistance decreases, or the conductivity increases, the applied electric field strength may be limited at temperatures near the poling temperature.

5.5 Electro-Optic Coefficient Measurement Technique

There are several different techniques used for measuring the electro-optic coefficient of a poled polymer [104], [105]. The electro-optic coefficient can be determined indirectly by measuring the second-order susceptibility in a Maker fringe second-harmonic generation technique [106]. The attenuated total reflection (ATR) technique can be used to determine the electro-optic coefficient directly [107], [108]. This technique is similar to the M-line measurements, in that the reflectivity minima are monitored as the index is modulated. Interferometric techniques are also very effective for these measurements. The most common technique is to place the sample in one arm of a free space Mach-Zehnder interferometer [109], [110], [111], [112].

The measurement setup developed for this work is an all fiber optic Mach-Zehnder interferometer (Figure 5-13). This measurement system has three unique features. The first is that it is an all fiber Mach-Zehnder interferometer. All the components can be purchased with fiber pigtails previously attached and then fusion spliced together. The light can then be coupled into and out of the single mode channel in the sample by butt coupling to an optical fiber. Additional free space optical components are not needed. An electronic stabilization circuit was added to the Mach-Zehnder interferometer to eliminate the random fluctuation in the intensity interference due to slow phase drifts in either arm. This allows the detection of modulation signals with large dynamic range to be distinguished from random phase fluctuations. It also keeps the phase in the two arms in quadrature, eliminating the "fading" problem that occurs if the signals aren't in quadrature. The third unique

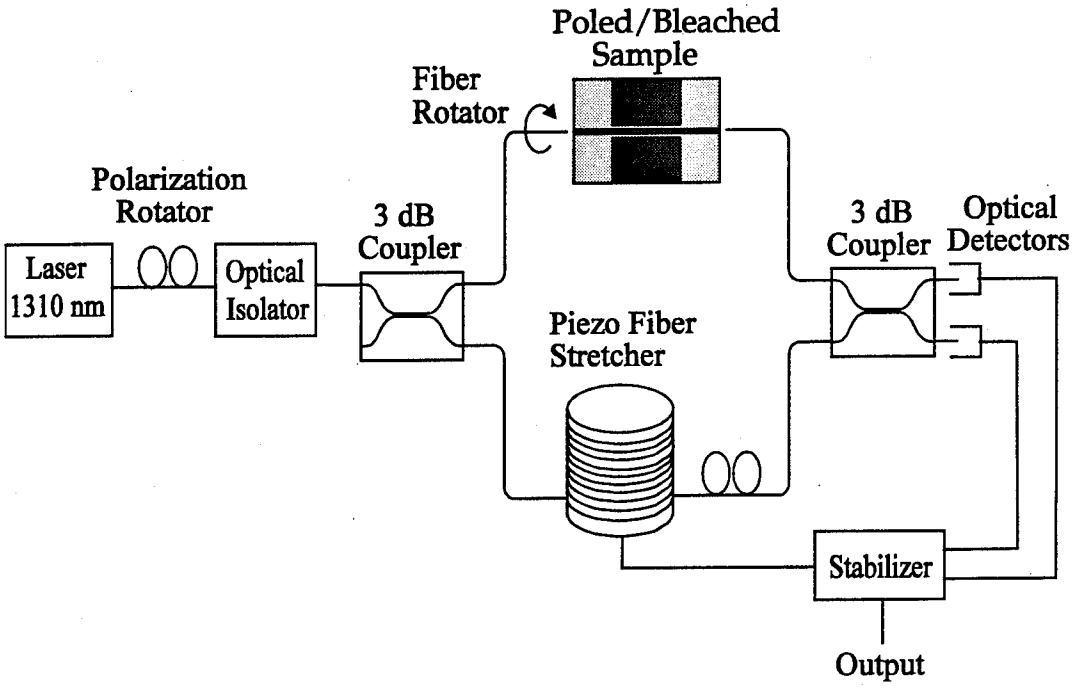

Figure 5-13 Fiber Mach-Zehnder interferometer used to measure the electro-optic coefficient of a poled polymer waveguide.

feature of this measurement system is that the poling apparatus is included in the sample arm of the Mach-Zehnder. It is a compact setup, consisting of a thermoelectric cooler/heater, micropositioners to align the fiber to the sample and probes that can be used to pole the sample and modulate it.

The fiber optic Mach-Zehnder consists of a fiber pigtailed DFB laser operating at 1310 nm connected to an optical isolator. A polarization rotator is placed between the laser and the optical isolator to align the polarization of the light from the laser to the input polarizer of the isolator [113]. The signal out of the isolator is split by a 3 dB coupler. One arm of the Mach-Zehnder contains a piezo fiber stretcher. The

piezo fiber stretcher is a device consisting of two plexiglass cylinders and a piezo element. The fiber is wound around the cylinders and attached to the piezo element. When a voltage is applied to the piezo, the fiber is stretched, causing an effective phase delay in the signal. The sample to be measured is placed in the other arm of the Mach-Zehnder interferometer. The test sample is a straight optical channel with electrodes on either side of the channel. A fiber rotator is used to align the polarization of the light from the laser with the preferred polarization of the optical guides. Since the field is applied parallel to the surface, the guide will support TE polarization. Any voltage applied to the electrodes, modulates the phase of the light propagating through the waveguide. The two arms of the Mach-Zehnder are recombined again using another 3 dB coupler. A polarization rotator is placed in the arm with the piezo fibers stretcher so that the two polarizations entering the second coupler can be matched. Two fiber pigtailed optical detectors are used to detect the intensity out of the Mach-Zehnder. All devices where attached by fusion splicing the fibers together. The specific components used in this work are listed in Appendix C.

The coherence length of the laser had to be determined so that the lengths of fibers in the two arms could be matched to within a coherence length. An optical spectrum analyzer with resolution of 0.08 $\mathring{A}$ was used to measure the linewidth, but the linewidth was smaller than 0.08 $\mathring{A}$. In order to measure the linewidth of the laser, a 2 km length of fiber was placed in one arm of the Mach Zehnder. This length of fiber added a delay which was longer than the phase coherence time of the laser field, making the signals in both arms uncorrelated. The spectrum of the laser was

measured with a spectrum analyzer to be 40 MHz (Figure 5-14).

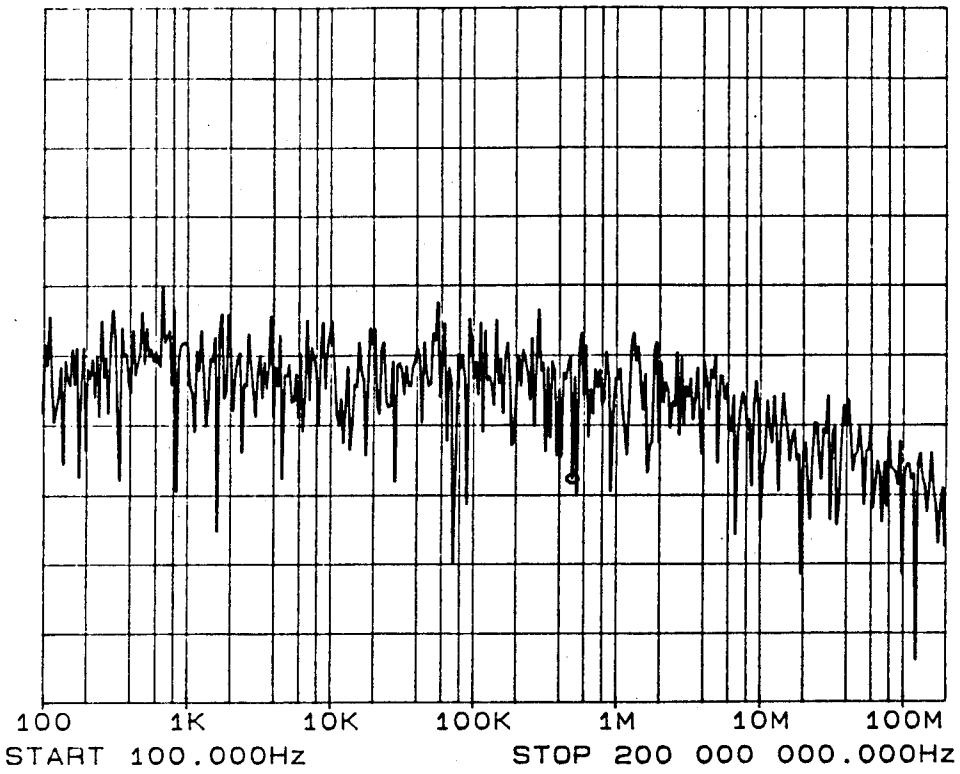

Figure 5-14 Spectrum of light measured with a 2 km length of fiber in one arm of the Mach-Zehnder.

The coherence length is related to the bandwidth by,

$$L_c = \frac{\lambda^2}{\Delta\lambda} = \frac{c}{\Delta f} \tag{5-1}$$

resulting in a coherence length of 7.5 meters for this laser. The difference in length of fiber between the two arms had to be less than 7.5 meters for the two signals to be coherent and interfere. A section of fiber 811 meters long had to be placed in the sample arm to equalize the lengths. If the signals from each arm aren't coherent, due

to path length differences greater than the coherence length of the laser, the modulation can't be 100% and a smaller output signal will result.

The outputs from the two detectors are combined in a stabilization circuit [114]. The stabilization circuit was used to compensate for phase drifts within the system and keep the phase of the two arms in quadrature. The stabilization circuit is shown in Figure 5-15.

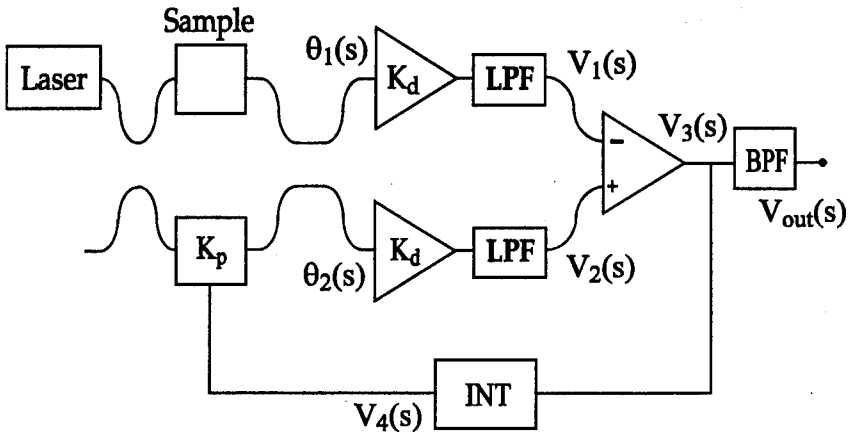

Figure 5-15 Feedback stabilization circuit

The currents out of the detectors are converted to voltages and filtered in low pass filters. The two voltages are then differenced in a diff-amp. This signal is split into two, with part of it going to the output stage and the other part being used as the correction signal. The correction signal is integrated and used to drive the piezo. The voltage on the piezo creates a phase change equal and opposite to the phase change caused by drifts in either arm. The closed loop response of this correction circuit is 300 Hz. The output signal is picked off before the integrator and passed

through a band pass filter. The output signal contains the modulation signal and is measured with an oscilloscope.

The feedback analysis of this circuit begins with the voltage out of the detectors relative to the phase of the light wave in each arm,

$$V_1(s) = k_d\theta_1(s) \quad \text{and} \quad V_2(s) = k_d\theta_2(s), \tag{5-2}$$

where k_d is the gain of the detectors in V/rad. The voltage out of the diff-amp with the low pass filters on the input is given by,

$$V_3(s) = \frac{k_1\omega_1^2[V_2(s) - V_1(s)]}{s^2 + 2\zeta\omega_1 s + \omega_1^2}. \tag{5-3}$$

The response of the integrator is given by,

$$V_4(s) = \frac{-k_2 V_3(s)}{S}, \tag{5-4}$$

and the response of the output bandpass filter is given by,

$$V_{out} = \frac{k_3 s V_3(s)}{(s+\omega_2)(s+\omega_3)}. \tag{5-5}$$

Combining Equations (5-2) through (5-5) results in the closed loop response of the circuit and for $\omega < \omega_1$ is given by,

$$\frac{V_{out}(s)}{\theta_1(s)} = \frac{2k_1k_dk_3}{(s+\omega_1)(s+\omega_2)}. \tag{5-6}$$

The feedback forces $\theta_2(s) = -\theta_1(s)$, making the two signals in the two arms conjugate. The gain of the piezo was measured to be $\pi/2$ (rad/v) (or 1 fringe at 1310

nm per volt). The gain of the detectors was measured to be 1.9 (V/rad). The low pass filters at the detectors were designed to have a 100 kHz bandwidth. The closed loop bandwidth was designed to be 300 Hz, which is a high enough frequency to correct for phase drifts, but won't effect typical modulation signals. The output bandpass filter was designed to pass 1 kHz to 100 kHz. Figure 5-16 shows the predicted response of the stabilization circuit, including the diff-amp, integrator, closed loop and band pass filter.

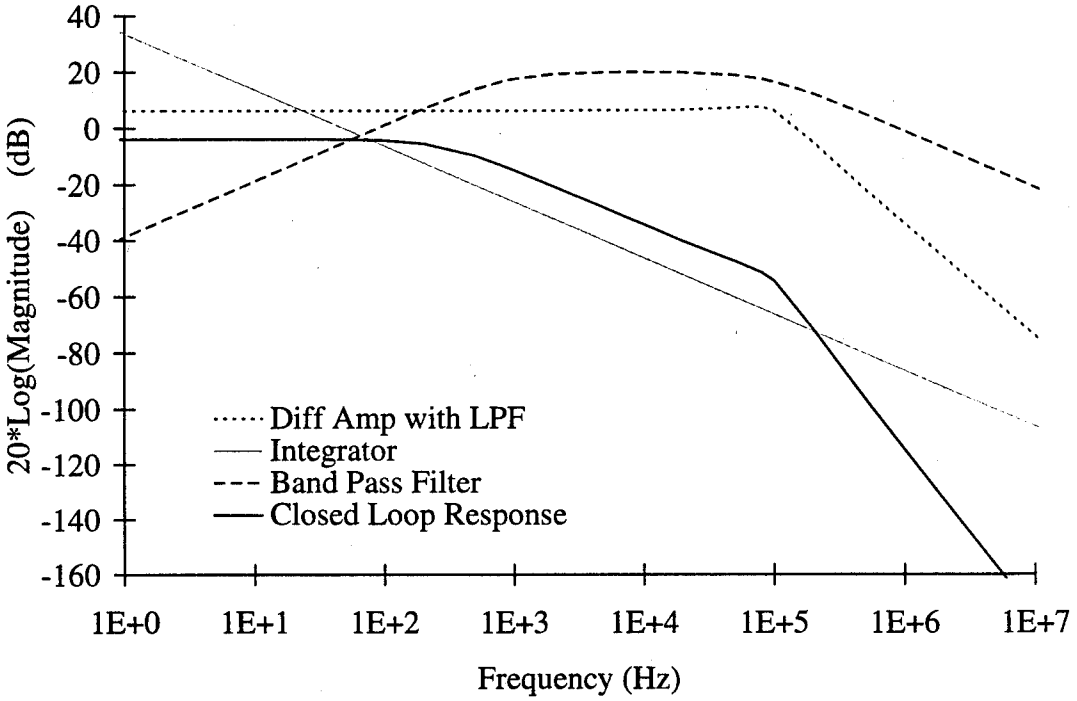

Figure 5-16 Frequency response at various points in the stabilization circuit.

The response of the circuit at different points was measured on an HP3577A network analyzer and matched the theoretical curves very closely.

The sample was mounted directly on a thermoelectric cooler/heater. This

peltier device can heat and cool over the range of -40 °C to 150 °C and is only 1.5 " by 1.5". The sample can be placed directly on the heater during poling. At a bias voltage of 10.7 volts and a current of 1.5 A, the sample can be heated to 113°C, Figure 5-17.

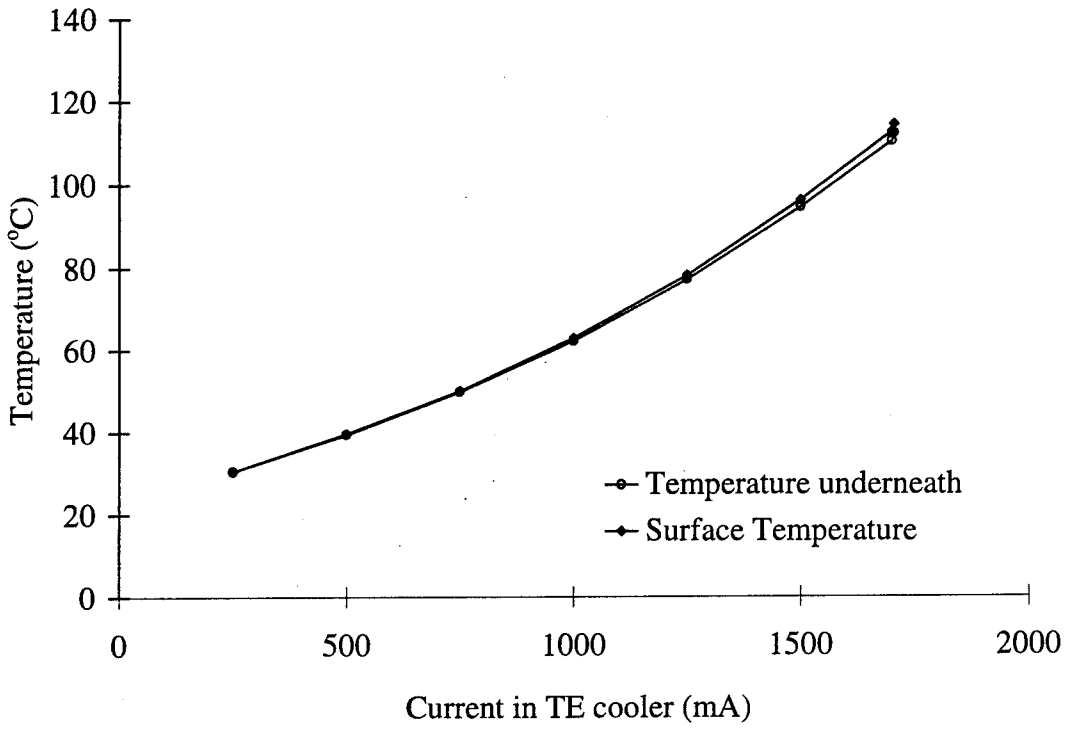

Figure 5-17 Current through thermoelectric cooler/heater and the resulting temperature change.

The electro-optic coefficient can be determined from the output intensity response. If the couplers have a 3 dB splitting ratio and the loss (α) in each arm is identical, the optical signals at each detector are complimentary and given by,

$$I = \frac{I_o \alpha}{2}(1 + \cos \Delta\phi) \qquad (5\text{-}7)$$

$$I' = \frac{I_o \alpha}{2}(1 - \cos \Delta\phi).$$

The detected output voltage is proportional to difference in intensities at each detector by,

$$V_{out} = k \cdot \cos \Delta\phi \tag{5-8}$$

The phase change ($\Delta\phi$) is due to the phase modulation of the optical channel, where the slow phase drifts have been removed by the feedback stabilizer. The poled sample becomes a phase modulator when a modulation signal is applied to the electrodes. The phase change across the device is given by,

$$\Delta\phi = \frac{2\pi \Delta n L \Gamma}{\lambda}. \tag{5-9}$$

The change in index resulting from the applied electric field is given by,

$$\Delta n(t) = \frac{n^3 r E(t)}{2} = \frac{n^3 r V(t)}{2d}. \tag{5-10}$$

Combining Equations (5-9) and (5-10), the phase change due to the modulation signal is given by,

$$\Delta\phi(t) = \frac{\pi n^3 r V(t) L \Gamma}{\lambda d}. \tag{5-11}$$

When a large sawtooth is applied to the modulation electrodes, the phase change over the device changes by many cycles and V_π can be determined. The voltage required to change the phase by π is known as $V\pi$ and is given by,

$$V_{\pi} = \frac{\lambda d}{n^3 r \Gamma L}. \qquad (5\text{-}12)$$

This provides a very direct measurement of the electro-optic coefficient. By measuring Vπ and knowing the waveguide dimensions, the electro-optic coefficient of a poled sample can be determined. A small signal sine wave can also be applied as the modulation signal, but the gain of the detection circuit would have to be calibrated in order to determine the electro-optic coefficient.

5.6 Monitoring While Poling

By monitoring while poling, the processes that effect the electric field induced alignment can be studied. A photo of the configuration used for poling and monitoring is shown in Figure 5-18. Two probes (Micromanipulator) were used to penetrate the polymers and provide the poling voltage to the electrodes. These same probes were also used to apply the modulation signal. The input and output fibers were coupled to the sample while it was on the heater. Because the heating stage is mounted in one arm of the Mach- Zehnder, the setup can be used for poling only, monitoring only or poling and monitoring. This measurement setup is ideal for monitoring the electro-optic coefficient while the sample is being poled. The configuration of the power supplies used for this setup is shown in Figure 5-19.

Figure 5-18 Photo showing sample on top of thermoelectric heater with fibers butt coupled to the edge of the sample

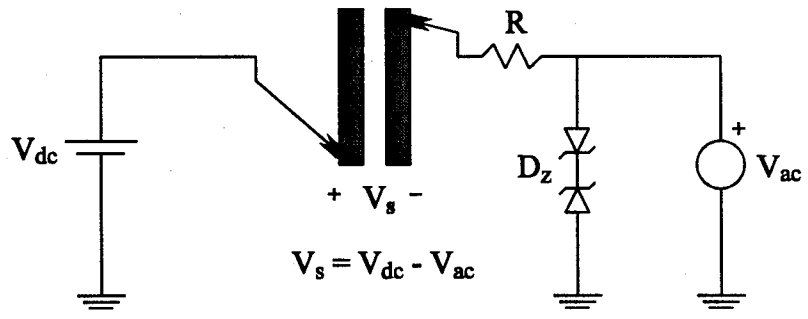

Figure 5-19 Configuration used for poling and monitoring.

The modulation signal, which is usually less than 20 V peak-to-peak is summed with the high poling voltage. Therefore, by monitoring the fringes at the output, the poling can be monitored. The fringe visibility will increase as the sample is poled. There is some adjustment necessary in the fiber coupling due to the thermal expansion of the sample during heating, but once the sample has reached the poling temperature, the alignment is fixed.

5.7 Results

A sample was fabricated as described earlier and mounted in the measurement setup. Light was coupled into and out of the waveguide with single mode fibers. The current through the thermoelectric cooler was increased until the sample reached 113 ^{o}C. A poling voltage of 2000 V was placed across the 60 μm gap resulting in a poling field of 33 V/μm. The field was applied for 20 min. and then the sample was cooled back down to room temperature. During poling, a sawtooth signal was placed on the piezo so that the poling could be monitored (with the stabilization circuit off). When the poling procedure was completed, a large sawtooth was placed on the sample electrodes (with the stabilization circuit on) and the Vπ was measured. The switching voltage for this sample was determined to be 325 V. The field strength was determined to be 90 % at the optical waveguides, resulting in an electro-optic coefficient of 3 pm/V. This value is smaller than expected, but could be due to poling in the bleached regions as well as the unbleached regions. The measured electro-optic coefficient is actually an effective electro-optic coefficient for the poled waveguide.

When a modulation signal is applied to the electrodes, the index of the polymer in the channel is changed, but the index of the buffer isn't. This causes the effective index of the structure to be altered. Therefore, the optical path length is also a function of the modulation voltage. The effective electro-optic coefficient can be used to characterize a poled optical channel. For device design, the effect of the poling parameters on the optical modulation resulting from an applied modulation signal can be used to optimize the performance of the device.

5.8 Conclusion

A unique measurement setup for determining the electro-optic coefficient of a poled polymer waveguide has been configured and tested. The measurement setup consists of an all fiber Mach-Zehnder interferometer. An electronic stabilization circuit was incorporated into the setup to compensate for random phase drifts. In this setup the electro-optic coefficient can be monitored while the sample is being poled. The poling apparatus is placed in one arm of the Mach-Zehnder interferometer. A thermoelectric heater/cooler provides a quick and controllable way to heat the sample for poling. The fringe visibility can be monitored while the sample is heated and poled. The resulting effective electro-optic coefficient of a poled optical channel can be characterized in terms of the poling parameters and configuration.

Chapter 6

CONCLUSION

Nonlinear optical polymers have the potential of being accepted as viable materials for electro-optic applications. Both passive and active devices can be easily fabricated using standard semiconductor processing techniques and can be extended to multiple layered applications. NLO polymers offer a great deal of flexibility due both to the material properties and the fabrication techniques. This flexibility leads to novel device designs and applications, but can't be fully utilized unless the materials are completely characterized. Both the fabrication processes and the configuration of the device can effect the properties of the device. Once the material is characterized as it will be used, the device design can be optimized.

This dissertation describes several techniques that were developed to characterize NLO polymers. The structure used for this work consisted of coplanar waveguide electrodes, coated with a lower buffer layer, a polymer layer and a top buffer layer. Optical waveguides were formed by UV bleaching. This configuration was chosen because it maintains a planar technology, allowing the structure to be extended vertically. The design of electro-optic devices should be optimized for high frequency response, low switching voltages and discrete devices that can be coupled to optical fibers. By preparing the endface with a wafer saw, light can be easily

coupled into and out of the waveguide with an optical fiber. This procedure has been optimized resulting in a surface roughness of less than 0.1 μm. As new materials are developed and placed on different substrates, the cutting parameters can be varied to produce the best endface.

The outcome of the work described in this dissertation has been several tools that can be used to characterize NLO polymers and multi-layered structures for use in integrated electro-optic devices. The material, electrical, optical and electro-optic properties of the device all effect the device performance. The techniques for device characterization developed in this work are very general and can be extended to different device configurations.

A model was developed to determine the electrical properties of a multi-layered structure of coplanar waveguide electrodes buried beneath three dielectric layers. All layers, including the substrate, could be modeled as anisotropic materials to account for inorganic crystalline substrates and poled polymers. Because the polymer layers are 1-5 μm thick and the electrodes are 0.5-2 μm thick, the analysis included the effect of the metallization thickness. The results of this model included the electric field distribution of a multi-layered structure. From the electric field distribution, the capacitance, impedance and effective dielectric constant of the structure were determined. The effect of the metal thickness, dielectric constants and thicknesses of the dielectric materials on these parameters were examined. In general, the three dielectric layers over the coplanar waveguide electrodes, tend to increase the

capacitance and decrease the impedance of the structure without significantly altering the electric field distribution.

Before the model could be used to determine the effective dielectric constant of the structure, the dielectric constant of the thin polymer layer had to be determined. A technique was developed to measure the dielectric constant of a thin dielectric film from 0.5 GHz to 50 GHz. The technique is based on measuring the propagation constants of a coplanar waveguide with and without a top dielectric layer. The propagation constants are easily obtained by doing a multi-line TRL calibration. A software package called DEEMBED, developed at NIST, is ideal for extracting the propagation constants from the measured S-parameters of the TRL calibration standards. Because the same electrode structure was used for both measurements, the resistance and inductance per unit length of the line were not altered by the top dielectric layer, but the capacitance and inductance were altered. By comparing the change in capacitance and using the model to relate the change in capacitance to the dielectric constant of the top layer, the dielectric constant could be extracted from the effective dielectric constant of the structure. This technique can be used to characterize the dielectric constant after various fabrication steps. The dielectric constant can also be used in the model to predict the waveguide parameters of the structure.

A unique measurement apparatus was designed and built for measuring the electro-optic coefficient of a poled polymer channel. This setup incorporated an all fiber Mach-Zehnder interferometer. A poled channel is placed in one arm of the

Mach-Zehnder. By placing a modulation signal on the electrodes, the Mach-Zehnder converts the phase fluctuation to intensity fluctuations. A stabilization circuit was designed and implemented in this setup to compensate for temperature drifts and random phase fluctuations. The setup is unique in that the light can be coupled into and out of the channel using optical fibers. The poling apparatus consists of a thermoelectric cooler/heater that is used to heat the sample during poling. This poling apparatus was included in one arm of the Mach-Zehnder interferometer. The electro-optic coefficient can be monitored during the poling using the same electrodes for poling and monitoring. While the sample is heated, a small AC voltage is superimposed on the poling voltage and applied to the electrodes. The fringe visibility increases as the sample is poled.

The techniques developed in this work are general and can be used to characterize new polymeric materials as they are developed. The information gained from this characterization can be used to extend the use of polymers in electro-optic applications.

BIBLIOGRAPHY

[1] S.T. Vohra and A.R. Mickelson, "Diffusion Characteristics and Waveguiding Properties of Proton-Exchanged and Annealed $LiNbO_3$ Channel Waveguides," *Journal of Applied Physics*, vol. 66, no. 11, pp. 5161-5174, December 1, 1989.

[2] R.R. Tummala, "Multichip Packaging - A Tutorial," *Proceedings of the IEEE*, vol. 80, no. 12, pp. 1924-1941, December 1992.

[3] P. Garrou, "Polymer Dielectrics for Multichip Module Packaging," *Proceedings of the IEEE*, vol. 80, no. 12, pp. 1942-1954, December 1992.

[4] M.M. Zurenda, "Base Materials: Meeting The Challenge of High Density Packaging," *Electronic Packaging and Production*, vol. 36, pp. 11-14, May 1993.

[5] C.P. Wong, Editor, *Polymers for Electronic and Photonic Applications*, Academic Press, Inc., San Diego, CA, 1993.

[6] K.W. Jelley, G.T. Valliath and J.W. Stafford, "High-Speed Chip-to-Chip Optical Interconnect," *IEEE Photonics Technology Letters*, vol. 4, no. 10, pp. 1157-1159, October 1992.

[7] K. Candela, "Photonic Interconnects Promise Computing Breakthrough," *Photonics Spectra*, pp. 83-88, February 1993.

[8] B. Reck, M. Eich, D. Jungbauer, R.J. Twieg, C.G. Willson, D.Y. Yoon and G.C. Bjorklund, "Crosslinked Epoxy Polymers With Large and Stable Nonlinear Optical Susceptibilities," *SPIE Nonlinear Optical Properties of Organic Materials II*, vol. 1147, pp. 74-83, 1989.

[9] J. Simon, P. Bassoul and S. Norvez, "Molecular Materials. III. Towards Opto-Electronics Finalities," *New Journal of Chemistry*, vol. 13, no. 1, pp. 13-31, 1989.

[10] K. Stewart, "Organic Crystals Give Optoelectronics a Boost," *Photonics Spectra*, pp. 104-108, July 1994.

[11] W. Charczenko, M. Surette, P. Matthews, H. Klotz and A.R. Mickelson, "Integrated Optical Butler Matrix for Beam Forming In Phased Array

Antennas," *SPIE Optoelectronic Signal Processing for Phased-Array Antennas II*, vol. 1217, January 1990.

[12] W. Charczenko, H. Klotz, P. Matthews and A.R. Mickelson, "Integrated Optics For Microwave and Millimeter Wave Detection and Signal Processing," *SPIE Integrated Optics and Optoelectronics*, vol. 1177, pp. 133-141, 1989.

[13] P. Liu, "Electrooptic Phase Modulator for Phased Array Applications," Optoelectronic Signal Processing for Phased-Array Antennas II, pp. 36-45, 1990.

[14] M.G. Armendariz, V.M. Hietala and D.R. Myers, "High Speed Optoelectronics," *Microwave Journal*, pp. 64-80, June 1994.

[15] G.F. Lipscomb, R.S. Lytel, A.J. Ticknor, T.E. Van Eck, D.G. Girton, S.P. Ermer, J.F. Valley, J. Kenney and E. Binkley, "Organic Electro-Optic Devices for Optical Interconnection," *SPIE Nonlinear Optical Properties of Organic Materials IV*, vol. 1560, pp. 388-399, 1991.

[16] T. Tumolillo, Jr., P.R. Ashley, "Fabrication Techniques of Photopolymer Clad Waveguides for Nonlinear Polymeric Modulators," *SPIE Photopolymer Device Physics, Chemistry and Applications II*, vol. 1559, pp. 65-73, 1991.

[17] E.Van Tomme, P.P. Van Daele, R.G. Baets and P.E. Lagasse, "Integrated Optic Devices Based on Nonlinear Optical Polymers," *IEEE Journal of Quantum Electronics*, vol. 27, no. 3, pp. 778-787, March 1991.

[18] D. Burland, R. Miller and C. Walsh, "Second-Order Nonlinearity in Poled-Polymer Systems," *Chem. Rev.*, vol. 94, pp. 31-75, 1994.

[19] G.T. Boyd, "Applications Requirements for Nonlinear-Optical Devices and the Status of Organic Materials," *J. Opt. Soc. Am. B*, vol. 6, no. 4, pp. 685-692, April 1989.

[20] M. A. Hubbard, T.J. Marks, J. Yang and G.K. Wong, "Poled Polymer Nonlinear Materials. Enhanced Second Harmonic Generation Stability of Cross-Linkable Matrix/Chromophore Ensembles," *Chemistry of Materials*, vol. 1, no. 2, pp. 167-169, March/April 1989.

[21] P.A. Cahill, C.H. Seager, M.B. Meinhardt, A.J. Beuhler, D.A. Wargowski, K.D. Singer, T.C. Kowalczyk and T.Z. Kosc, "Polyimide-based Electrooptic materials," *SPIE Nonlinear Optical Properties of Organic Materials VI,* vol. 2025, pp. 48-55, July 1993.

[22] J.I. Thackara, G.F. Lipscomb, M.A. Stiller, A.J. Ticknor and R. Lytel, "Poled Electro-Optic Waveguide Formation In Thin Film Organic Media," *Applied Physics Letters*, vol. 52, no. 13, pp. 1031-1033, 1988.

[23] C.C. Teng, "Traveling-Wave Polymeric Optical Intensity Modulator With More Than 40 GHz of 3-dB Electrical Bandwidth," *Applied Physics Letters*, vol. 60, no. 13, pp. 1538-1540, March 30, 1992.

[24] D.G. Girton, S.L. Kwiatkowski, G.F. Lipscomb and R.S. Lytel, "20 GHz Electro-Optic Polymer Mach-Zehnder Modulator," *Applied Physics Letters,* vol. 58, no. 16, pp. 1730-1732, April 22, 1991.

[25] G.R. Mohlmann, W.H.G. Horsthuis, A. Mc Donach, M.J. Copeland, C. Duchet, P. Fabre, M.B.J. Diemeer, E.S. Trommel, F.M.M. Suyten, E. Van Tomme, P. Baquero and P. Van Daele, "Optically Nonlinear Polymeric Switches and Modulators," *SPIE Nonlinear Optical Properties of Organic Materials III* , vol. 1337, pp. 215-225, 1990.

[26] P. Singer, "Flat Panel Displays: An Interesting Test Case for the U.S.," *Semiconductor International*, pp. 78-88, July 1994.

[27] S. Ura, T. Suhara, and H. Nishihara, "An Integrated-Optic Device Using Electrooptic Polymer Waveguide on Si Substrate for Modulating Focus Spot Intensity Distribution," *IEEE Photonics Technology Letters*, vol. 5, no. 11, pp. 1291-1293, November 1993.

[28] R. Chen, M. Lee, S. Natarajan, C.Lin, Z.Z. Ho and D. Robinson, "Single-Mode Nd^{3+}-Doped Graded-Index Polymer Waveguide Amplifier," *IEEE Photonics Technology Letters*, vol. 5, no. 11, pp. 1328-1331, November 1993.

[29] J.D. Swalen, R. Santo, M.Tacke and J. Fischer, "Properties of Polymeric Thin Films by Integrated Optical Techniques," *IBM J. Res. Develop.*, pp. 2168-2629, March, 1977.

[30] K.D. Singer, "Molecular Polymeric Materials for Nonlinear Materials," *Polymers for Lightwave and Integrated Optics, Technology and Applications*, L. A. Hornak, Editor, Marcel Dekker, Inc. New York, pp. 322-333, 1991.

[31] C.P.J.M. van der Vorst, W.H.G. Horsthuis and G.R. Mohlmann, "Nonlinear Optical Side-Chain Polymers and Electro-Optic Test Devices," *Polymers for Lightwave and Integrated Optics, Technology and Applications*, L. A. Hornak, Editor, Marcel Dekker, Inc. New York, pp. 322-333, 1991.

[32] A. Yariv and P. Yeh, *Optical Waves in Crystals*, John Wiley & Sons, New York, pp. 220-275, 1984.

[33] R.C. Alferness, "Waveguide Electrooptic Modulators," *IEEE Transactions on Microwave Theory and Techniques*, MTT-30, pp. 1121-1137, August 1982.

[34] R. Goldstein, "Electro-Optic Devices in Review," *Lasers and Applications*, pp. 67-73, April, 1986.

[35] A. Skumanich, M. Jurich and J.D. Swalen, "Absorption and Scattering In Nonlinear Optical Polymeric Systems," *Applied Physics Letters*, vol. 62, no. 5, pp. 446-448, February 1, 1993.

[36] K. Al-hemyari, G. F. Doughty, C.D.W. Wilkinson, A.H, Kean, and C.R. Stanley, "Optical Loss Measurements on GaAs/GaAlAs Single-Mode Waveguide Y-junctions and Waveguide Bends," *Journal of Lightwave Technology*, vol. 11, no. 2, pp. 272-276, February 1993.

[37] I. P. Januar, Characteristics of Integrated Optical Devices and Structures, Ph.D. Thesis, University of Colorado, Boulder, pp. 37-49, November 1992.

[38] A.R. Mickelson, *Guided Wave Optics*, Van Nostrand Reinhold, New York, pp. 224-241, 1993.

[39] R.C. Alferness, C.H. Joyner, L.L. Buhl and S.K. Korotky, "High-Speed Traveling-Wave Directional Coupler Switch/Modulator for λ = 1.32 μm," *IEEE Journal of Quantum Electronics*, vol. QE-19, no. 9, pp. 1339-1341, September 1983.

[40] S.K. Korotky and R.C. Alferness, "Time- and Frequency-Domain Response of Directional-Coupler Traveling-Wave Optical Modulators," *Journal of Lightwave Technology*, vol. LT-1, no. 1, pp. 244-251, March 1993.

[41] D. M. Burland, R.D. Miller and C.A. Walsh, "Second-Order Nonlinearity in Poled-Polymer Systems," *Chem. Rev.*, vol. 94, pp. 31-75, 1994.

[42] P.N. Prasad, D. J. Williams, *Introduction to Nonlinear Optical Effect in Molecules and Polymers*, John Wiley & Sons, Inc., New York, pp. 122-128, 1991.

[43] S. Wolf, *Silicon Processing for The VLSI Era, Volume 2: Process Integration*, Lattice Press, Sunset Beach, California, pp. 195, 1990.

[44] M. Haruna, Y. Segawa and H. Nishihara, "Nondestructive and Simple Method of Optical-Waveguide Loss Measurement with Optimization of End-Fire Coupling," *Electronics Letters*, vol. 28, no. 17, pp. 1612-1613, August 13, 1992.

[45] P. J. Brannon, "Improved Method of Measuring Optical Waveguide Propagation Losses," *Applied Optics*, vol. 25, no. 20, pp. 3596-3597, October 15, 1986.

[46] Monk and D.S. Soane, "Interconnect Dielectrics," *Polymers for Electronic and Photonic Applications*, C.P. Wong, editor, D.J. Academic Press, Boston, pp. 131, 1993.

[47] Superstrate 996, Coors Ceramics Company, Electronics, 17750 W. 32nd Avenue, Golden, CO 80401.

[48] S. Ermer, J.F. Valley, R. Lytel, G. F. Lipscomb, T.E. Van Eck, and D.G. Girton, "DCM-Polyimide System for Triple-Stack Poled Polymer Electro-Optic Devices," *Applied Physics Letters*, vol. 61, no. 19, pp. 2272-2274, November 9, 1992.

[49] J.C. Chon, J.I. Thackara, P.B. Comita, M.C. Jurich, and J.D. Swalen, "Characterization of Low Loss Polymer Modulators Fabricated By Laser Ablation," to be published.

[50] J.C. Chon and P.B. Comita, "Laser Ablation of Nonlinear Optical Polymers to Define Low Loss Optical Channel Waveguides," accepted for publication in Optics Letters (1994).

[51] A. Brauer, J.Gehler, M. Jager, E.B. Kley, C. Wachter, "Antiresonant Reflecting Optical Waveguides (ARROW) in Polymer Multilayer Structures and With Lateral Confinement," *SPIE Nonconducting Photopolymers and Applications*, vol. 1774, pp. 295-307, 1992.

[52] L. Thylen, "Integrated Optics In $LiNbO_3$: Recent Developments In Devices for Telecommunications," *IEEE Journal of Lightwave Technology*, vol. 6, no. 6, pp. 847-861, June 1988.

[53] I.P. Januar, "Characteristics of Integrated Optical Devices and Structures," Ph.D. Thesis, University of Colorado, Boulder, 1992.

[54] P.J. Matthews, "Proton Exchange in Lithium Niobate and Lithium Tantalate", Ph.D. Thesis, University of Colorado, Boulder, 1991.

[55] C.P. Wen, "Coplanar Waveguide: A Surface Strip Transmission Line Suitable for Nonreciprocal Gyromagnetic Device Applications," *IEEE Transactions on Microwave Theory and Techniques*, vol. MTT-17, no. 12, pp. 1087-1090, December 1969.

[56] O.G. Ramer, "Integrated Optic Electrooptic Modulator Electrode Analysis," *IEEE Journal of Quantum Electronics*," vol. QE-18, no. 3, pp. 386-392, March 1982.

[57] K.C. Gupta, R. Garg, and I.J. Bahl, *Microstrip Lines and Slotlines*, Dedham, MA, Artech House, pp. 258-301.

[58] D. Marcuse, "Optimal Electrode Design for Integrated Optics Modulators," *IEEE Journal of Quantum Electronics*, vol. QE-18, no. 3, pp. 393-398, March 1982.

[59] M. Gillick, I.D. Robertson and J.S. Joshi, "Direct Analytical Solution for the Electric Field Distribution at the Conductor Surfaces of Coplanar Waveguides," *IEEE Transactions on Microwave Theory and Techniques*, vol. 41, no. 1, pp. 129-135, January 1993.

[60] F. Bogelsack and I. Wolff, "Application of a Projection Method to a Mode-Matching Solution for Microstrip Lines with Finite Metallization Thickness," *IEEE Transactions on Microwave Theory and Techniques*, vol. MTT-35, no. 10, pp. 918-921, October 1987.

[61] J. Gerdes, K. H. Helf, and R. Pregla, "Full Wave Analysis of Traveling-Wave Electrodes with Finite Thickness for Electro-Optic Modulators by the Method of Lines," *Journal of Lightwave Technology*, vol. 9, Nno. 4, pp. 461-467, April 1991.

[62] D. Marcuse, "Electrostatic Field of Coplanar Lines Computed with the Point Matching Method", *IEEE Journal of Quantum Electronics*, vol. 25, no. 5. May 1989.

[63] W. Charczenko. P.S. Weitzman, H. Klotz, M. Surette, J.M. Dunn and A. R. Mickelson,, "Characterization and Simulation of Proton Exchanged Integrated Optical Modulators With Various Dielectric Buffer Layers, *Journal of Lightwave Technology*, vol. 9, pp. 92-100, 1991.

[64] M. Horno, F. Mesa, F. Medina and R. Marques, "Quasi-TEM Analysis of Multilayered, Multiconductor Coplanar Structures with Dielectric and Magnetic Anisotropy Including Substrate Losses," *IEEE Transactions on Microwave Theory and Techniques*, vol. 38, no. 8, pp. 1059-1068, August 1990.

[65] T. Kitazawa and T. Itoh, "Asymmetrical Coplanar Waveguide with Finite Metallization Thickness Containing Anisotropic Media," *IEEE Transactions on Microwave Theory and Techniques*, vol. 39, no. 8, pp. 1426-1433, August 1991.

[66] T. Kitazawa, D. Polifko and H. Ogawa, "Analysis of CPW for $LiNbO_3$ Optical Modulator by Extended Spectral-Domain Approach," *IEEE Microwave and Guided Wave Letters*, vol., 2, no. 8, pp. 313-315, August 1992.

[67] K. Kawano, T. Kitoh, H. Jumonji, T. Nozawa, M. Yanaagibashi and T. Suzuki, "Spectral-Domain Analysis of Coplanar Waveguide Traveling-Wave Electrodes and Their Applications to Ti:$LiNbO_3$ Mach-Zehnder Optical Modulators," *IEEE Transactions on Microwave Theory and Techniques*, vol. 39, no. 9, pp. 1595-1601, September 1991.

[68] H. Jin and M. Belanger, "General Analysis of Electrodes in Integrated-Optic Electrooptic Devices", *IEEE Journal of Quantum Electronics*, vol. 27, no. 2. February 1991.

[69] Hang Jin and Ruediger Vahldieck, "A Mode Projecting Method for the Quasi-Static Analysis of Electrooptic Device Electrodes Considering Finite Metalization Thickness and Anisotropic Substrate", *IEEE Journal of Quantum Electronics*, vol. 27, no. 10, October 1991.

[70] G. L. Matthaei, K. Kiziloglu, N. Dagli and S. Long, "The Nature of the Charges, Currents, and Fields in and About Conductors Having Cross-Sectional Dimensions of the Order of a Skin Depth," *IEEE Transactions on Microwave Theory and Techniques*, vol. 38, no. 8, pp. 1031-1036, August 1990.

[71] P. Waldow and I. Wolff, "The Skin-Effect at High Frequencies," *IEEE Transactions on Microwave Theory Techniques*," vol. MTT-33, no. 10, pp. 1076-1082, October 1985.

[72] W. Heinrich, "Quasi-TEM Description of MMIC Coplanar Lines Including Conductor-Loss Effect," *IEEE Transactions on Microwave Theory and Techniques*," vol. 41, no. 1, pp. 45-52, January 1993.

[73] V. Radisic, D.R. Hjelme, A. Horrigan, Z.B. Popovic and A.R. Mickelson, "Experimentally Verifiable Modeling of Coplanar Waveguide Discontinuities," *IEEE Transactions on Microwave Theory and Techniques*, vol. 41, no. 9, pp. 1542-1533, September, 1993.

[74] P. Garrou, "Polymer Dielectrics for Multichip Module Packaging," *Proceedings of the IEEE*, vol. 80, no. 12, pp. 1942-1954, Dec. 1992.

[75] H. Jin, M. Belanger, and Z. Jakubczyk, "General Analysis of Electrodes in Integrated-Optics Electrooptic Devices," *IEEE Journal of Quantum Electronics*, vol. 26, no.2, pp. 243-251, Feb. 1991.

[76] O.G. Ramer, "Integrated Optic Electrooptic Modulator Electrode Analysis", *IEEE Journal of Quantum Electronics*, vol. QE-18, no. 3, pp. 386-392, March 1982.

[77] HP 85070A Dielectric Probe Kit, 200 MHz to 20 GHz (Application Note).

[78] E.J. Vanzura, C.M. Weil and D.F. Williams, "Complex Permittivity Measurements of Gallium Arsenide Using a High-Precision Resonant Cavity," *Digest of the Conference on Precision Electromagnetic Measurements*, pp. 103-104, 1992.

[79] R.G. Geyer, C. M. Weil and W.A. Kissick, "Precision Dielectric Measurements Using a Mode-Filtered Cylindrical Cavity Resonator, *Digest of the Conference on Precision Electromagnetic Measurements*, pp. 174-175, 1990.

[80] D. J. Monk and D. S. Soane, "Interconnect Dielectrics," *Polymers for Electronic and Photonic Applications*, Editor, C. P. Wong, pp. 147, Academic Press, Inc. New York.

[81] S.K. Mohapatra , C.V. Francis, K. Hahn and D.W. Dolfi, "Microwave Loss In Nonlinear Optical Polymers", *Journal of Applied Physics*, vol. 73, no. 5, pp. 2569-2572, March 1, 1993.

[82] Product Note 8510-3, "Materials Measurement, Measuring the Dielectric Constant of Solids With the HP 8510 Network Analyzer," August, 1985.

[83] G.F. Engen, C.A. Hoer, "'Thru-Reflect-Line': An Improved Technique for Calibrating the Dual Six-Port Automatic Network Analyzer," *IEEE Transactions Microwave Theory and Techniques*, vol. MTT-27, no. 12, pp. 987-993, Dec. 1979.

[84] R.B. Marks, "A Multiline Method of Network Analyzer Calibration," *IEEE Transactions on Microwave Theory and Techniques*, vol. 39, no. 7, pp. 1205-1215, July 1991.

[85] HP Product Note 8510-8, Network Analysis, "Applying the HP 8510B TRL Calibration for Non-Coaxial Measurements.

[86] J. Baker-Jarvis, E.J. Vanzura and W.A. Kissick, "Improved Technique for Determining Complex Permittivity with the Transmission/Reflection Method," IEEE Transactions on Microwave Theory and Techniques," vol. 38, no. 8, pp. 1096-1103, August, 1990.

[87] R.B. Marks, "A Multiline Method of Network Analyzer Calibration," *IEEE Transactions on Microwave Theory and Techniques*, vol. 39. no. 7, pp. 1205-1215, July 1991.

[88] R.B. Marks and D.F. Williams, "Characteristic Impedance Determination Using Propagation Constant Measurement," *IEEE Microwave and Guided Wave Letters*, vol. 1, no. 6, pp. 141-143, June 1991.

[89] D.F. Williams and R.B. Marks, "Transmission Line Capacitance Measurement," *IEEE Microwave and Guided Wave Letters*, vol. 1, no. 9, pp. 243, pp. 243-245.

[90] W. Heinrich, "Quasi-TEM Description of MMIC Coplanar Lines Including Conductor-Loss Effects," *IEEE Transactions on Microwave Theory and Techniques*, vol. 41, no. 1., pp. 45-52, Jan.1993.

[91] W. Heinrich, "Full-Wave Analysis of Conductor Losses on MMIC Transmission Lines," *IEEE Transactions on Microwave Theory and Techniques*, vol. 38, no. 10., pp. 1468-1472, Oct. 1990.

[92] M. Eich, A. Sen, H. Looser, G. Bjorklund, J.D. Swalen, R. Twieg and D.Y. Toon, "Corona Poling and Real-Time Second-Harmonic Generation Study of a Novel Covalently Functionalized Amorphous Nonlinear Optical Polymer," *Journal of Applied Physics*, vol. 66, no. 6, pp. 2559-2567, September 15, 1989.

[93] R.H. Page, M.C. Jurich, B. Reck, A. Sen, R.J. Twieg, J.D. Swalen, G.C. Bjorklund and C.G. Willson, "Electrochromic and Optical Waveguide Studies of Corona-Poled Electro-Optic Polymer Films," *Journal of the Optical Society of America B*, vol. 7, no. 7, pp. 1239-1250, July1, 1990.

[94] S. J. Bethke and S. G. Grubb, "Atmospheric Effects on Corona Poling of Nonlinear Optical Doped Polymer Films," *SPIE Nonlinear Optical Materials and Devices for Photonic Switching*, vol. 1216, pp. 260-271, 1990.

[95] J.F. Valley, J.W. Wu, S. Ermer, M. Stiller, E.S. Binkley, J.T. Kenney, G.F. Lipscomb and R. Lytel, "Thermoplasticity and Parallel-Plate Poling of Electro-Optic Polyimide Host Thin Films," *Applied Physics Letters*, vol. 60, no. 2, pp. 160-162, January 13, 1992.

[96] S. Yitzchaik, G. Berkovic and V. Krongauz, "Two-Dimensional Poling of Organic and Polymer Films for Improved Nonlinear-Optical Properties," *Optics Letters*, vol. 15, no. 20, pp. 1120-1122, October 15, 1990.

[97] J.I. Thackara, G.F. Lipscomb, M.A. Stiller, A.J. Ticknor and R. Lytel, "Poled Electro-Optic Waveguide Formation in Thin -Film Organic Media," *Applied Physics Letters*, vol. 52, no. 13, pp. 1031-1033, March 28, 1988.

[98] P.R. Ashley and E.A. Sornsin, "Doped Optical Claddings for Waveguide Devices with Electrooptical Polymers," *IEEE Photonics Technology Letters*, vol. 4, no. 9, pp. 1026-2040, September 1992.

[99] G. Berkovic, S. Yitzchaik and V. Krongauz, "In-Plane Poling of Doped Polymer Films: Creation of Two Asymmetric Directions for Second Order Optical Nonlinearity", pp. 238-242, *SPIE Nonlinear Optical Properties of Organic Materials IV*, vol. 1560, 1991.

[100] S. Yitzchaik, G. Berkovic and V. Krongauz, "Charge Injection Asymmetry: A New Route to Strong Optical Nonlinearity In Poled Polymers," *Journal of Applied Physics*, vol. 70, no. 7, pp. 3949-3951, October 1, 1991.

[101] M.G. Kuzyk and J.E. Sohn, "Mechanisms of Quadratic Electro-Optic Modulation of Dye-Doped Polymer Systems," *Journal of the Optical Society of America B*, vol. 7, no. 5, pp. 842-858, May 1990.

[102] R. V. Mustacich, "Scalar Finite Element Analysis of Electrooptic Modulation In Diffused Channel Waveguides and Poled Waveguides in Polymer Thin Films," *Applied Optics*, vol. 27, no. 17, pp. 3732-3737, September 1, 1988.

[103] R. Mustiacich, M. Gilbet, R. Finn, and C. Swann, "Analysis and Fabrication of Overlapping-Electrode Designs for Poling and Modulating Channels in Polymer Thin Films," *Applied Optics*, vol. 31, no. 15, pp. 2800-2806, May 20, 1992.

[104] J.T. Gallo, T. Kimura, S. Ura, T. Suhara, and H. Nishihara, "Method for Characterizing Poled-Polymer Waveguides for Electro-Optic Integrated-Optical-Circuit Applications", *Optics Letters*, vol. 18, no. 5, pp. 349-351, March 1, 1993.

[105] T. Tumolillo, Jr. and P.R. Ashley, "A Novel Pulse-Poling Technique for EO Polymer Waveguide Devices Using Device Electrode Poling," *IEEE Photonics Technology Letters*, vol. 4, no. 2, pp. 142-145, February 1992.

[106] M. Eich, B. Reck, D.Y. Yoon, C.G. Willson, and G. Bjorklund, "Novel Second-Order Nonlinear Optical Polymers via Chemical Cross-Linking-Induced Vitrification Under Electric Field", *Journal of Applied Physics*, vol. 66, no. 7, pp. 3241-3247, October 1, 1989.

[107] S. Herminghaus, B.A. Smith, and J.D. Swalen, "Electro-Optic Coefficients in Electric-Field-Poled Polymer Waveguides," *Journal of the Optical Society of America B*, vol. 8, no. 11, pp. 2311-2317, Novermber 1991.

[108] P. Rohl, B. Andress, and J. Nordmann, "Electro-Otpic Determination of Second and Third-Order Susceptibilities in Poled Polymer Films," *Applied Physics Letters*, vol. 59, no. 22, pp. 2793-2795, November 25, 1991.

[109] K.D. Singer, W.R. Holland, M.GT. Kuzyk, G.L. Wolk, H.E. Katz, M.L. Schilling, P.A. Cahill, "Second-Order Nonlinear Optical Devices in Poled Polymers," *SPIE Nonlinear Optical Properties of Organic Materials II*, vol. 1147, pp. 233-244, 1989.

[110] T. Suzuki, O. Eknoyan, and H.F. Taylor, "Electrooptic Coefficient Measurements in $LiTaO_3$ and $LiNbO_3$ Waveguides," *Journal of Lightwave Technology*, vol. 11, no 2, pp. 285-289, February 1993.

[111] C.H. Wang, H.W. Guan and J.F. Zhang, "Electro-optic Measurements of Dye/Polymer Systems," *SPIE Photopolymer Device Physics, Chemistry, and Applications II* , vol. 1559, pp. 39-48, 1991.

[112] J.F. Valley and J.W. Wu, "Measurement of Electro-Optic Poling Transient Effects In Polymer Thin Films," *SPIE Nonlinear Optical Properties of Organic Materials III* , vol. 1337, pp. 226-233, 1990.

[113] D. B. Sarrazin, "Behavior of Miniaturized Polarization Controllers," *OCS Technical Report*, no. 89-49, Optoelectronic Computing Systems Center, University of Colorado, Boulder, CO, December, 1989.

[114] K. Fritsch and G. Adamovsky, "Simple Circuit for Feedback Stabilization of a Single-Mode Optical Fiber Interferometer," *Rev. Sci. Instrum.* vol. 52, no. 7, pp. 996-1000, July 1981.

Appendix A

PROCESSING INFORMATION FOR POLYMERIC DEVICES

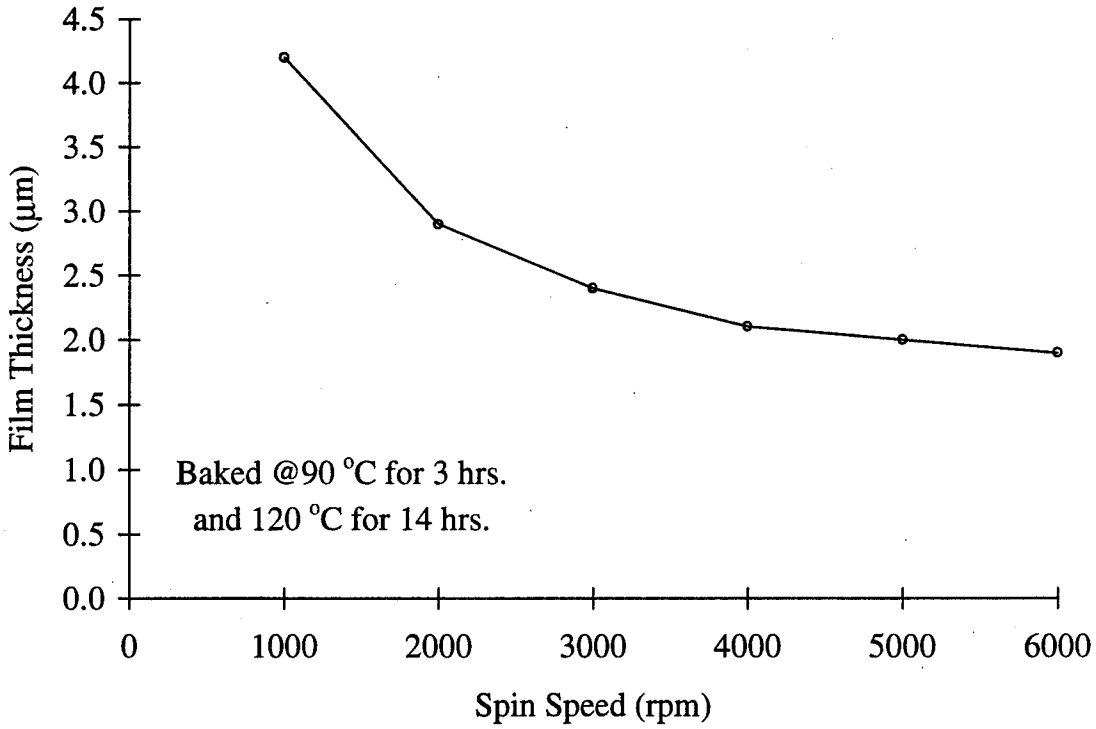

Figure A-1 Spin curve for PMMA/DR1.

Table A-1 Wafer saw cutting parameters for the Model 1006 wafer saw from Assembly Technologies.

Wafer Saw Cutting Parameters	
Forward Cut Speed	25 mil/sec.
Spindle Speed	16,000 rpm
Blade Type	102DK10-101312EGA Assembly Technology Mutli-composite resin blade

Table A-2 Fabrication steps used for the work described in this thesis.

Clean Substrate (Quartz 1"square h = 0.025" +/-0.002")	1. Rinse: Acetone, Methanol, De-ionized water 2. 4 - 30 sec. dips in $HF:H_2O$ (1:10) 3. Bake quartz at 110 °C for 30 min.
Metal Evaporation (Ti:Al)	1. 50-100 A Titanium 2. 0.5 µm Aluminum
Photolithography Photoresist : HPR 504 Developer: HPRD 426	1. Spin: 4000 rpm /27sec. (1.2 µm) 2. Prebake: 25 min. / 100 °C 3. Expose: 11 sec. (w/450nm filter) 4. Develop: 50 sec. 5. Postbake: 30 min. at 90 °C
Metal etching Al etchant: Ti etchant: $HF:H_2O$ (1:10)	1. Etch Aluminum Al etch rate: 80 A/sec. 2. Etch Titanium Ti etch rate: 50 A/sec.
Lower Buffer Layer (UV cured acrylate)	1. Spin: 3000 rpm / 30 sec. (5 µm) (Buffer at room temperature) 2. Purge in 5 psi of N_2 3. Expose: 1 min. in N_2 (w/out UV filter) 4. Soft Bake: 90 °C /3 hours 5. Hard Bake: 120 °C / 24 hours
Phase I Material (PMMA/DR1)	1. Prebake:100 °C / 5min. 2. Spin: 3000 rpm /60 sec. (2.2µm) With acceleration of spinner at 3-5 sec. 3. Soft Bake in air: 90 °C/ 3 hours 4. Hard Bake in air: 110°C/12hours
Bleach channels	No UV filter 50 hours at 140 °C 72 hours at room temp.
Upper Buffer Layer (UV cured acrylate)	1. Spin: 3000 rpm / 30 sec. (5 µm) (Buffer at room temperature) 2. Purge in 5 psi of N_2 3. Expose: 1 min. in N_2 (w/out UV filter) 4. Soft Bake: 90 °C /3 hours 5. Hard Bake: 120 °C / 24 hours
Prepare endface with wafer saw	1. Mount sample to cutting substrate with tape or wax 2. Saw endface perpendicular to channels 3. Remove sample
Pole channels	1. Heat sample to 113 °C 2. Apply field of > 50 V/µm for 30 min. 3. Cool sample with field still present

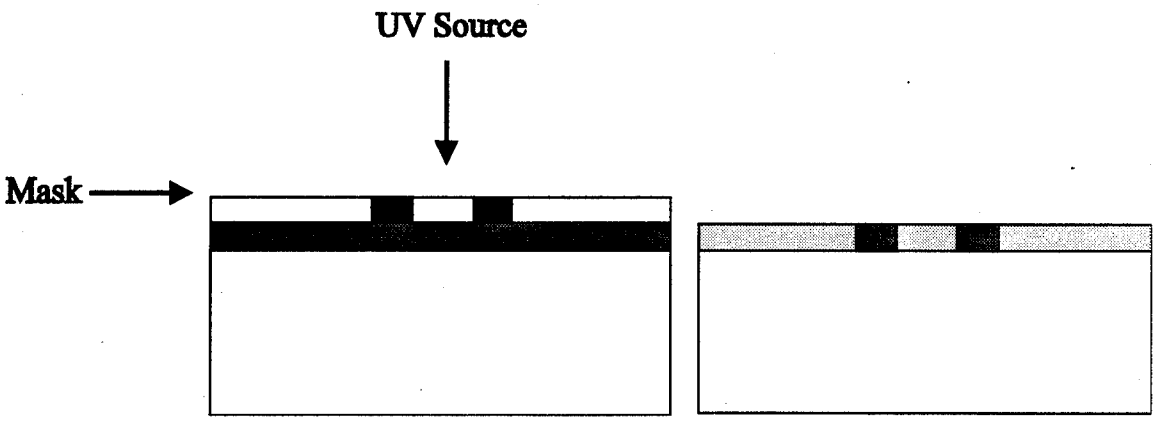

Figure A-2 Procedure used to UV bleach optical channels in a polymer.

Table A-3 The index change resulting from UV bleaching with an Oriel flood exposure unit with 10.7 mW/cm^2 @ 300 nm, 25 mW/cm^2 @ 365 nm, 37.4 mW/cm^2 @ 400 nm and 23.8 mW/cm^2 @ 435 nm.

	Index of Refraction of PMMA/DR1			
	λ=0.83 μm		λ=1.3 μm	
	n_{TE}	n_{TM}	n_{TE}	n_{TM}
Unbleached	1.556	1.554	1.536	1.533
Bleached for 48 hours	1.547	1.548	1.526	1.525
Δn	0.009	0.006	0.010	0.008

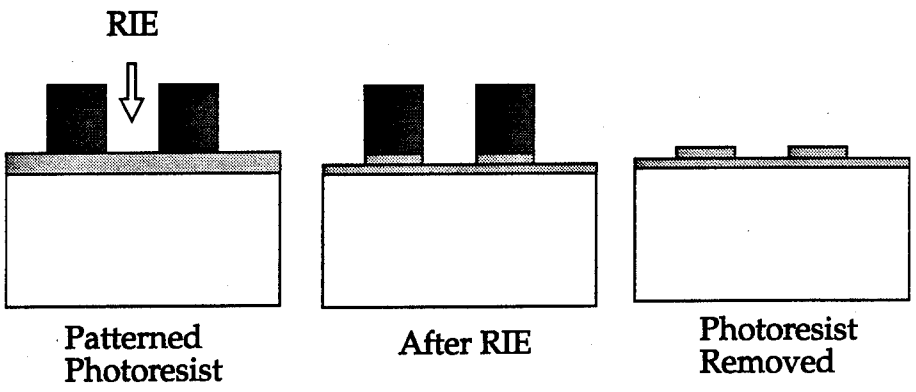

Figure A-3 Processing steps for etching waveguide by RIE

Table A-4 Parameters used for reactive ion etching of optical waveguides in polymers.

Parameters for Reactive Ion Etching of Polymers	
Type of photoresist Exposure time of photoresist Develop time of photoresist	Need thick photoresist for vertical walls
RF Power	50 Watts
Throttle Valve Position	35 %
RF Voltage	-77 V
DC Bias	-1.3 DCV
Gas O_2	1 cc/min.
Gas Ar	40 cc/min.
Etch Rate	90 nm/min.
Surface plate in chamber	Quartz or carbon

Appendix B

IMPEDANCE OF A COPLANAR WAVEGUIDE ELECTRODES

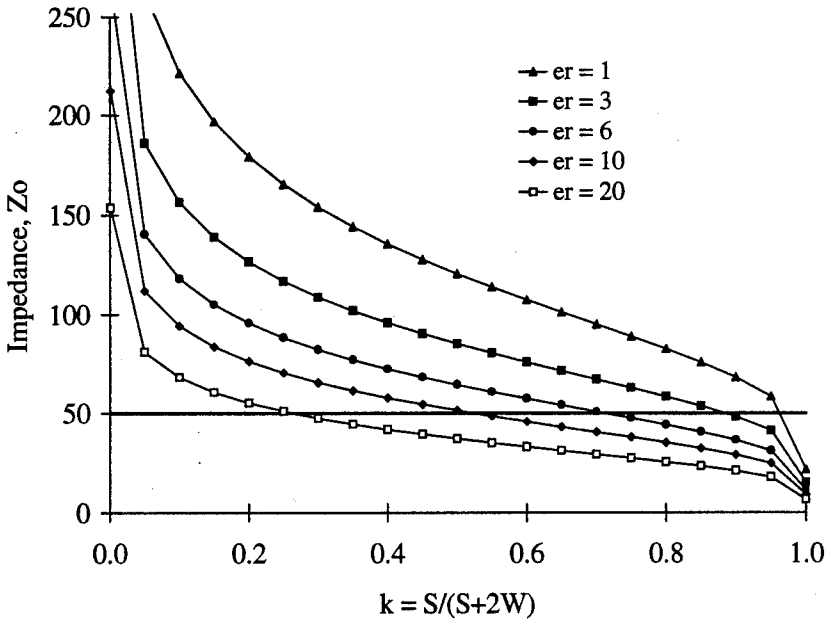

Figure B-1 Impedance of a coplanar waveguide electrode as a function of the dimensions of the waveguide, where S is the width of the center conductor and W is the width of the gap.

The general design rules for CPW electrodes are:

$$S + 2W \leq 0.25h \tag{B-1}$$

where h is the thickness of the substrate and

$$G \geq 5(S + 2W) \tag{B-2}$$

where G is the width of the ground plane.

An approximate for the impedance of a coplanar waveguide is given by,

$$Z_0 = \frac{30\pi}{\sqrt{\frac{\varepsilon_s + 1}{2}}} \frac{K(k')}{K(k)}, \tag{B-3}$$

where, K(k) is the complete elliptic integral of the first kind and is defined by,

$$K(k) = \int_0^{\frac{\pi}{2}} \frac{d\theta}{\sqrt{1 - k^2 \sin^2 \theta}} \tag{B-4}$$

and,

$$\frac{K(k)}{K(k')} \cong \frac{1}{\pi} \ln\left(2\frac{1+\sqrt{k}}{1-\sqrt{k}}\right) \quad \text{for} \quad \frac{1}{2} \le k^2 \le 1$$

$$\frac{K(k)}{K(k')} \cong \frac{\pi}{\ln\left(2\frac{1+\sqrt{k}}{1-\sqrt{k}}\right)} \quad \text{for} \quad 0 \le k^2 \le \frac{1}{2}$$

$$k = \frac{\sinh\left(\frac{\pi S}{4h}\right)}{\sinh\left(\frac{\pi(S+2W)}{4h}\right)} = \frac{S}{S+2W}.$$

Appendix C

COMPONENTS USED FOR THE FIBER OPTIC MACH-ZEHNDER INTERFEROMETER

1. Fiber pigtailed distributed feedback (DFB) laser*
   Philips Optoelectronics Centre
   Model No. CQG 62/D
   Operating wavelength = λ = 1310 nm
   Minimum rated optical power = P_o = 2 mW
   Threshold current = I_{th} = 25 mA

2. Fiber pigtailed optical isolator
   MP World Manufacturing, Inc.
   Model No. IUA13-B
   Operating wavelength = λ = 1310 nm
   Isolation = 55 dB
   Insertion loss = 0.8 dB
   Return loss = 60 dB
   Bandwidth > 40 nm

3. Fiber optic 3dB coupler
   Sifam Limited
   Model No. P22513AA50
   Operating wavelength = λ = 1300 nm
   Coupling ratio = 50/50
   Excess losses < 0.1 dB

4. Piezo fiber assembly
   Canadian Instrumentation and Research Limited
   Number of fiber turns = 25
   Gain = 1 Fringe/Volt
   Driver board has built in oscillator

5. Fiber pigtailed optical detectors
   Epitaxx
   Model No. ETX 75 FC
   Active diameter = 75 μm

Responsivity = R = 0.85 A/W
Dark current = 0.15 nA
Total capacitance (measured with case grounded) = 0.55 pF
Bandwidth (-3 dB into 50 Ω load) = 2 GHz
Rise time (R_{load} = 50 O) = 180 psec.

* ILX temperature controller LDT-5412
Melles Griot 06 DLD 301 Laser driver

All components were connected by fusion splicing the fiber pigtails together.